Novel nanomechanical property instrumentation development and its application to surface engineered systems

by

GERARD ANTHONY BELL

A thesis submitted to the

University of Birmingham

For the degree of

Engineering Doctorate

School of Metallurgy and Materials

University of Birmingham

April 2012

Abstract

Surface engineered systems for industrial applications must be able to withstand the harsh in-service environments that they will be operated under. Localised testing on the nanoscale is a method commonly used to probe such systems at very high temperatures, varying humidity and even under liquid environments. However little or no research has been directed towards investigating their behaviour under low temperature conditions.

In this study a novel sub-ambient temperature nanomechanical testing instrument has been designed and developed. It allows testing of materials under the temperature range from 20 ^{o}C to minus 30 ^{o}C. The instrument employs peltier coolers to provide vibration free measurements and a custom purging chamber has been designed to prevent condensation of water vapour on the sample surface during the sub-ambient testing. The study demonstrated the need for dual cooling of both the sample and indenter to ensure drift free measurements are obtained under sub-ambient regimes.

A section of the research is dedicated to the testing of polymeric materials. A range of tests were performed from nanoindentation through to probing of time and environmental dependence parameters. In particular creep was studied at ambient temperatures on a range of engineering polymers and also on Nylon's which were submerged in a fluid cell.

The prototype was constructed and validation tests carried out to ensure its performance on standard samples. Next the mechanical properties and creep behaviour of an atactic-polypropylene through its glass transition temperature was examined. Further experiments were

carried out focusing on tribological testing of surface engineered systems with the new prototype providing interesting results on DLC's when tested under below ambient temperatures.

Based on the outcomes of this research, a few papers have been published in peer-reviewed technical journals and it is envisaged that the novel sub-ambient instrumentation will be used for the design, charaterisation and optimization of novel engineered surfaces for various environmental applications.

Dedication

My Late Father, teacher, mentor and friend. Forever influencing and always guiding never forgotten.

Acknowledgments

I owe a deep gratitude to supervisors Professor Hanshan Dong and Professor Ben Beake for helping me along this journey.

Professor Paul Bowen for guidance and support through difficult times.

The Birmingham surface engineering group and extended network especially the time devoted by Dr J Chen, Dr X Li and Miss Teresa Wall.

The Micro Materials Ltd Team past and present. Micro Materials Founder Dr Jim Smith for encouragement and hours of discussion and deliberation, his knowledge and expertise knows no bounds.

I must thank my Mother, Sisters and Brothers for their continued love and support.

Table of Contents

List of figures

Chapter 1 Overview

1.1 Main achievements of the doctorate

8 Scientific papers:

1. Chen J, Bell GA, Dong H, Smith JF, Beake BD. A study of low temperature mechanical properties and creep behaviour of polypropylene using a new sub-ambient temperature nanoindentation test platform. Journal of Physics D: Applied Physics. 2010;43(42):425404.

2. Beake BD, Bell GA, Goodes SR, Pickford NJ, Smith JF. Improved nanomechanical test techniques for surface engineered materials. Surface Engineering. 2010 Feb 1;26(1):37–49.

3. Bell GA, Bieliński DM, Beake BD. Influence of water on the nanoindentation creep response of nylon 6. Journal of Applied Polymer Science. 2008 Jan 5;107(1):577–82.

4. Beake BD, Bell GA, Brostow W, Chonkaew W. Nanoindentation creep and glass transition temperatures in polymers. Polymer International. 2007 Jun;56(6):773–8.

5. Chen J, Bell GA, Beake BD, Dong H. Nano-mechanical and tribological properties of a multilayered DLC coating under sub-ambient temperatures. International Journal of Engineering Systems Modelling and Simulation. 2010;2(4):199.

6. Bell GA, Chen J, Dong HS, Beake BD, Smith JF. The design of a novel cryogenic nanomechanical and tribological properties instrumentation. International Heat Treatment & Surface Engineering. 2011;5(1):21–5.

7. Chen J, Bell GA, Beake BD, Dong H. Low Temperature Nano-Tribological Study on a Functionally Graded Tribological Coating Using Nanoscratch Tests. Tribology Letters. 2011 Jun 25;43(3):351–60.

8. Bell GA, Chen J, Dong HS, Beake BD, Smith JF in preparation 2011

Design, development and commissioning of below ambient temperature nanomechanics instrumentation

Technology Transfer

1.2 Business context

This thesis is based on the research of novel nanomechanical property instrumentation. The sponsor company for this Engineering Doctorate (EngD) is Micro Materials Ltd (MML).

MML is a small medium enterprise (SME). The company designs and develops and manufactures nanomechanical property instrumentation for research in the worlds of both industry and academia. The company has developed a world leading materials characterisation platform called the NanoTest. The NanoTest has evolved over the years through collaboration with Universities, the University of Birmingham to name just one of many and establishments such as the National Physics Laboratory (NPL) to ensure it has the most advanced and forefront capabilities required by researchers.

Formerly a subsidiary of the Millbrook Scientific Instruments PLC group which specialised in instrumentation for surface science and surface engineering applications. MML went through a shareholder buyout and is now an independent limited company.

In order to continue to grow as one of the five world leaders in nanomechanical measurements and instrumentation design, MML must be at the leading edge, and be able to offer advanced capabilities so research can continue as scientists need and focus change with industry. MML continues to develop the electronics and physics behind the system as data acquisition techniques advance with new computer power becoming available and affordable to desktop computer users.

MML's ethos is to have the NanoTest system, which is a platform to fit the needs of the researcher. As the scope of a particular researcher changes, because the system is modular, it can

be upgraded to provide additional functions, as the researcher requires them.

The NanoTest system covers a wide load range, it is fitted with dual loading heads. A Micro Indentation head [1], capable of delivering depth load sensing measurements on the micro scale. A surface engineer also requires being able to characterise surfaces of materials rather than the bulk and the Nano Indentation head for the NanoTest system enables these experiments to be performed.

Research grew in the field of nanomechanical measurements, and scientists wanted to be able to find out the wear and fatigue properties of materials on the nanoscale. These were then developed, adhesion – scratch testing[2]; more recently fretting[3]. The impact/wear [4] and fretting can be considered a suite of nanotribological test techniques see

Figure 1.1.

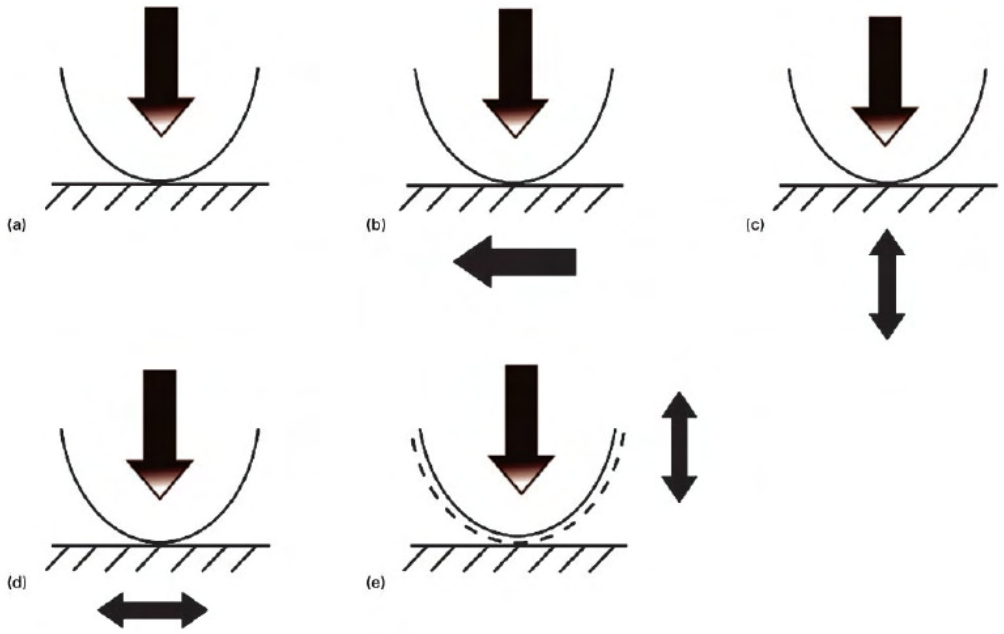

Figure 1.1 Contact geometries in nanomechanical testing (a) indentation, (b) scratch/wear, (c) impact/contact fatigue, (d) fretting and reciprocating wear and (e) impulse impact.

MML reputation and market lead increased as they strived towards environmental nanoindentation. 1) Their new hot stage option. They were the first company to produce a commercial nanoindentation system to be capable of testing materials at high temperatures. The Hot stage is continued to be developed to meet the ever demanding needs of the research community[5]. 2) Samples can be tested and the levels of humidity can be varied between tests[6]. 3) It is also possible to test materials in a liquid environment.

It was envisaged that a below ambient temperature capability would be required for future research and MML embarked on a collaboration with the University of Birmingham to design a cold stage for the NanoTest System.

A research engineer was chosen to develop the novel nanomechanical instrumentation

capabilities. This was not only to develop a new option for the NanoTest but also to look into the capabilities of the existing options that were being developed for the NanoTest and realise the potential for surface engineered systems.

1.3 Motivation

Materials and their properties have been tested and evaluated for centuries. There is a good understanding of materials when it comes to the bulk properties; however, research is advancing and becoming more focused towards coatings and micro-electromechanical systems and surface engineered systems. Appropriate tools are required so that materials' properties can be probed and extracted on a localised scale; this has led scientists to look for new methods to be able to characterise these novel materials.

There is an array of testing machines for the macro- and microscale, which can test a variety of materials' mechanical properties at ambient and in service temperature conditions. This was an important step forward; however, for probing on the localised scale, there has been a lack of commercial equipment for testing under in-service conditions.

1.4 Thesis aims and objectives

The approach to this thesis is to test existing technology and hardware for robustness in the aim to continue on and develop a cold stage instrument to be able to test materials at below ambient temperatures.

Nanomechanical and creep experiments on polymers were performed at ambient conditions and in non-ambient environments, to test the techniques and ensure they were robust[7,8]. Once it

was established that they could stand up to ambient and non-ambient conditions the research could progress into developing the instrumentation to assist researches in testing materials at below ambient temperatures, therefore being able to test the materials at their true in-service temperatures.

The nanomechanical tests and creep tests would be carried out first on a range of polymers, at ambient temperatures and also in a liquid environment.

The aim of the research is to design and manufacture a novel nanomechanical instrument for below ambient in-service temperature materials testing. At present the testing range is limited to ambient and elevated temperatures up to 700 ^{o}C.

1. Test existing hardware which the new instrumentation will be based on.
2. Design a prototype to be able to cool samples to below ambient temperatures.
3. Manufacture and develop the prototype so that it can be used to test materials from 20 ^{o}C to -30 ^{o}C
4. Perform experiments on a range of materials to test the capability of the new instrumentation.

1.5 Research background

Over the past decade, commercial nanoindentation equipment has been developed to test materials designed for high temperature service conditions. It is now a rule of thumb that it is critical among researches to have a good understanding of materials at the in service conditions. Material scientists empower engineers with the expertise to be able to design machinery, and

coatings that will perform in all environments. Equipment for testing at sub-ambient temperatures is still not commercially available which include both tip and sample cooling even though many applications exist which require materials to withstand service conditions well below ambient temperature. Polymer thin films, diamond-like carbon coatings, lead free solders, cryogenic machining and pharmaceutical products for example drugs in the form of tablets are just a handful of applications, which would require testing at below ambient temperatures.

1.6 Thesis organisation

In this section a brief overview of the structure of the thesis is presented. Chapter 2 provides an overall view of the classical research of nanoindentation and a detailed literature review of the field where the nanoindentation technique can be applied.

Chapter 3 explores nanopolymeric materials using nanomechanical probing techniques. Focusing on hardness and young's modulus data and going further into exploring elastic properties as well as the more complex area of viscoelastic properties studying Youngs modulus versus the depth of the material as well as looking at creep cycles by placing dwell periods in the traditional nanoindentation experiment. This provides a comprehensive overview of recent research and illuminates areas with open issues which lay the foundation for further study.

Detailed information of the investigations into a number of polymers both amorphous and semi - crystalline. Nanomechanical and creep data are extracted from the materials using the existing hardware. The data was collected at ambient and aqueous conditions.

In chapter 4 the main design and development of the sub-ambient nanomechanical instrumentation is provided in detail, going through the rational for the cooling design and covering each of the steps in reaching the final prototype instrumentation.

Chapter 5 concludes the thesis, examining the overall contribution of the research in context of related work in the area. In addition the limitations and future work are also highlighted.

Finally, the Appendices presents a management chapter where the research engineer undertook dissemination of the project and other e-learning projects promoting surface engineering.

Chapter 2 Literature survey

2.1 Introduction

The characterisation of mechanical properties of bulk and surface engineered materials is a fundamental task in research and development and the drive for application of surface engineering technologies. In this thesis nanoindentation is the key methodology used to gather these crucial properties and will be discussed further below. It is therefore obvious that the testing techniques and methods to be employed are crucial for this purpose. These include the principle of depth-sensing indentation and obtaining force-displacement hysteresis curves, the models and procedures for the load-depth data processing and the calculation of mechanical property parameters. Some examples are shown in employing this unique and powerful testing technique to characterise the mechanical properties of surface engineered and other engineering materials.

2.2 Testing methods and instruments

For traditional hardness testing the measurement relies on the size of indents left on the specimen surface after the indenter and load have been retracted. Typical examples of this are Brinell and Vickers hardness. In order to eliminate the substrate affect, very low indentation load must be used. This allows measurement of thin surface layers and coatings. The problem faced with traditional techniques is that at low loads a very small indent impression is created. The accuracy of measurement of the indent size becomes low or even impossible under microscope. This problem is overcome using the nanoindentation method, where the depth-sensing indentation techniques are used. During the nanoindentation test, the indent sizes and relevant mechanical properties are calculated, instead of being directly measured, using force-displacement curve

recording.

Early reports in the 1950s demonstrated the use of measuring the depth of an indentation impression during the microindentation hardness testing [9]. The important finding from these initial observation is the appreciably difference between the size measured of the unloaded indentation and the indentation while the load is applied. For low load indentations and especially on non-metallic materials, e.g. rubbers and polymers, there is a marked elastic recovery which occurs. The only dimension that can be conventionally measured as the test is being carried out is in fact the indentation depth. These early machines focused merely on microindentation testing technique and only low resolution in force and displacement is required. There was also a lack of mechanics background to further process the data to obtain useful information now seen from the modern nanoindention instrument.

Starting in the late 1970s, several prototype nanoindentation tests have been developed across the world in several different research laboratories [10]. In principle, all these machines are quiet similar, measuring the load-depth relationship during indentation. High-resolution continuous depth recording techniques became possible through the use of computer controlled facilities. The nanoindentation machine used in this thesis is the NanoTest 600 machine developed and manufactured by Micromaterials Ltd. Wrexham, UK. An example is shown in Figure 2.1, the principle operation is as follows: a pendulum is pivoted on “frictionless” bearing and a coil is mounted at the top of the pendulum. With a coil current present, the coil is attracted towards a permanent magnet. This produces the motion of the indenter towards the specimen and eventually into the specimen surface. The displacement of indenter is measured by a parallel plate

capacitor. When the indenter moves, the capacitance changes, and this is measured by the capacitance bridge box. The specimen can be moved in the X- Y- Z- directions by means of three precision dc motors driving micrometer stages. These motors are controlled by a motor control unit link to a computer interface. Today's nanoindentation instrument can precisely measure the movement of a diamond indenter. Either a varying or constant load is applied to the indenter which is impressed into the specimen surface. The whole process of the indentation loading and unloading can be recorded as a force-displacement or depth-time relationship. After these measurement are recorded, the software package is used to analyse the date produced. Information as such as hardness, young's modulus, elasto-plastic deformation flow behaviour, creep and viscoelasticity, elastic and plastic work, friction and even film residual stress can be obtained directly and indirectly [11,12].

Figure 2.1 Nanotest Vantage latest Micro Materials Ltd instrument (Courtesy of Micro Materials Ltd)

In nanoindentation tests a Berkovich indenter is used Figure 2.2. This is a three face pyramid indenter which is different from a square based pyramid used for Vickers [13] measurements. It is very difficult to manufacture a four sided indenter with all four faces meeting in a common point, resulting in the so-called "chisel edge" effect. Hence the Berkovich pyramid indenter is easy to manufacture and produces reliable results. Spherical indenter tip of 5 μm is also used for the same reason. The geometrical parameters of the Berkovich [14] indenter are as follows. The angle at the apex between the normal and the sides β =65°02´, and the angle between the normal and edges γ = 76°54´. This results in the same projected area-to-depth function in a Berkovich indenter as in a Vickers indenter, i.e., $A = 24.5\ h^2$.

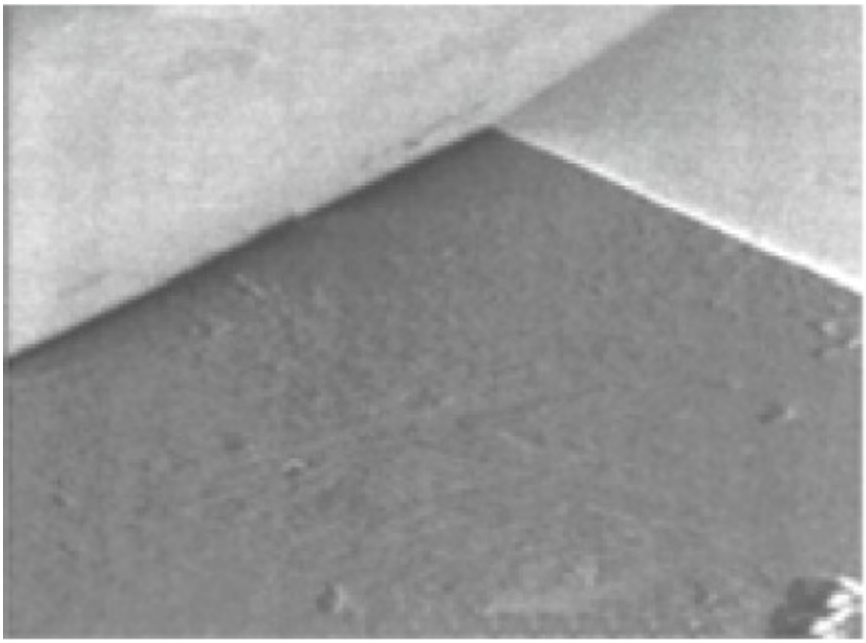

Figure 2.2 SEM image of Berkovich tip typically 100 nm sharp.[15]

2.3 Theory

2.3.1 Mechanical and models

2.3.1.1 Sneddon's theoretical solutions

Boussinesq [16] first considered the problem of determining the distribution of elastic stresses within an elastic half space when it is deformed by the normal pressure against its boundary of a rigid punch. Since those preliminary numerical results were derived, several alternative solutions have been put forward. Of these the most interesting was achieved by Sneddon [17] and his co-workers, which is now the theoretical background of contact mechanics involved in the indentation of materials. In that body of work, the solutions for some special shape of punch indenters were presented. They were a spherical punch, conical punch, flat ended cylindrical punch, a punch in form of paraboloid of revolution and a punch in the shape of ellipsoid of

evolution. The key findings are the relationship between the total load P and the penetration depth D for the different shapes of punch, where μ and η are the shear modulus and the Poisson ratio of the half space being indented, respectively, and a the radius of the circle of contact:

(1) Flat-ended cylindrical punch:

$$P = \frac{4\mu a}{1-\eta} D \qquad \text{Equation 2-1}$$

(2) Conical punch:

$$P = \frac{4\mu \cot \alpha}{\pi(1-\eta)} D^2 \qquad \text{Equation 2-2}$$

where α is the semi vertical angle of a cone.

(3) Punch in the form of a paraboloid of revolution:

$$P = \frac{8\mu}{3(1-\eta)} (2kD^3)^{\frac{1}{2}} \qquad \text{Equation 2-3}$$

where, k is the parameter in the equation $\rho^2 = 4kz$ for a paraboloid of revolution.

It was found that when applying the Sneddon's theoretical solution to real diamond indenters, the indenter itself was found to be not ideally rigid. Therefore the addition of the reduced modulus E_r was defined to take into account this effect. On the load-displacement behaviour, through the follow equation:

$$\frac{1}{E_r} = \frac{1-\upsilon_s^2}{E_S} + \frac{1-\upsilon_i^{\,2}}{E_i} \qquad \text{Equation 2-4}$$

where E_S and υ_s are Young's modulus and Poisson's ratio of the half space, E_i and υ_i are the same parameters of the diamond indenter, respectively.

2.3.1.2 Doerner-Nix method

In the early 1980s, Loubet et al [18,19] first evaluated the elastic moduli of materials using the load-displacement sensing indentation technique. However, it was Doerner and Nix who systematically studied and established a method and procedure for data interpretation of depth-sensing indentation instruments. Doerner and Nix [11] method are outlined as follows:

(A) The adoption of Sneddon's flat ended punch solution for elastic deformation of isotropic elastic materials was undertaken by equating projected area in contact under the indenter to the area of punch, and assuming that indenter had ideal pyramidal geometry and using the plastic depth h_p, giving the following equation:

$$\frac{dh}{dP} = \frac{1}{2h_p}\left(\frac{\pi}{24.5}\right)^{\frac{1}{2}}\frac{1}{E_r} \qquad \text{Equation 2-5}$$

where *dh/dP* is the reciprocal of the unloading slope, or the compliance.

(B) The compliance, *dh/dP*, and the plastic depth h_p, were determined in the following ways. For metals, a line is fit as tangent to the unloading curve as the maximum load and extrapolated at zero loads. The compliance is determined from a slope and the intercept on the depth axis is then a plastic depth. This assumes that during initial unloading, the area in contact with the indenter remains constant, which implies unlinear unloading. This relationship is observed for metals over most of the unloading range, while for materials with higher ratios of hardness and elastic modulus (e.g. silicon), where more curvature is observed in the unloading curve, a linear fitting is achieved using the first one third of data from the maximum load.

(C) When assuming that the diamond indenter is perfectly shape, the hardness at small depth is seriously over estimated. In reality, the geometry of the indenter is never ideal. Therefore, the shape of indenter must be calibrated. The method successfully used by Pethica et al [19] was adopted. Firstly, making an indentation in soft materials such as pure aluminium was followed secondly by producing carbon replicas of the indents and imaging them in the TEM. The area of indentation were measured and compared to the plastic depth as measured in the nanoindentation test. Finally a second order polynomial fit of the data was carried out to specify the diamond indenter shape.

(D) The effective depth h_{eff} was proposed for correcting imperfection inherent with the indenter tip geometry, as per the following equation:

$$h_{eff} = (\frac{A_c}{24.5})^{\frac{1}{2}} \qquad \text{Equation 2-6}$$

where the area, A_c is obtained from the indent shape calibration and the true plastic depth h_p. To obtain a projected contact area of a real indenter equivalent to that of the ideal indenter geometry, effective depth h_{eff} is used.

2.3.1.3 Oliver-Pharr method

Using their own work (1983, 1987, 1991) and combined with all the investigations such as Deorner and Nix [11] and others, Oliver and Pharr proposed an improved technique for determine hardness and elastic modulus using load and displacement-sensing indentation [12]. They argued that the flat punch approximation used so often in analysis of the unloading data was not entirely adequate, because the unloading part of the load-curve for most material tested were not linear. A physical adjustable data-processing procedure was established accounting for the curvature in unloading curve. This was used to determine the contact depth which should be used in conjunction with the indenter shape function in order to obtain the contact area at peak load. This methodology is outlined as follows.

The three key experimental parameters needed to calculate hardness *H* and elastic modulus *E* are the peak load $P_{\max}$, the contact depth at peak load h_c and the initial unloading contact stiffness *S*,

Using the equation

$$E_r = \frac{\sqrt{\pi}}{2}\frac{S}{\sqrt{A}} \qquad \text{Equation 2-7}$$

which relates the reduced modulus, E_r, to the indent contact area, A, and the unloading stiffness, S, and the equation

$$H = \frac{P_{\max}}{A} \qquad \text{Equation 2-8}$$

hardness H and elastic modulus E can thus be calculated.

The procedure for determining the contact depth (h_c) at peak load the projected contact area $A(h_c$), and the initial unloading contact stiffness (S) is summarized as follows, which is different from those used previously:

(A) At any time during loading, the total displacement h is written as

$$h = h_c + h_S \qquad \text{Equation 2-9}$$

where h_c is the vertical distance along which contact is made (hereafter called the contact depth), and h_s is the displacement of the surface at the perimeter of the contact. Thus, at a peak load, $P_{\max}$,

the contact depth, h_c, will be

$$h_c = h - h_S \qquad \text{Equation 2-10}$$

Considering the indenter tip geometry modelled by Sneddon [7], the following equation is obtained:

$$h_S = \varepsilon \frac{P_{maz}}{S} \qquad \text{Equation 2-11}$$

where ε is the geometric constant: ε=1.0 for a flat punch; ε=0.75 for an indenter of paraboloid of revolution; and ε=0.72 for a conical indenter. Comparing load-displacement characteristics of all the tested materials with Sneddon's analytical results, the unloading behaviours is best described by the paraboloid geometry, i.e., ε=0.75, which is used in the analysis procedure.

(B) In order to measure the initial unloading stiffness, *S*, a simple power law fit of the unloading data is done by the equation

$$P = A(h + h_f)^m \qquad \text{Equation 2-12}$$

where the constants *A*, *m*, and h_f are all determined by a least squares fitting procedure. The initial unloading stiffness, *S*, is then obtained by differentiating this regressive expression and evaluating the derivative at the peak load and displacement.

(C) Another practical consideration is how well the load frame compliance, C_f, and the diamond indenter area function, $A=F(h_C)$ are known. By modelling the load frame and the specimen as two springs in series, the total measured compliance can be expressed by

$$C = C_S + C_f \qquad \text{Equation 2-13}$$

where C_S is the specimen compliance and C_f is the frame compliance. Since the specimen compliance, C_S, during elastic contact is given by the inverse of the contact stiffness, S, then

$$C = C_f + \frac{\sqrt{\pi}}{2E_r}\frac{1}{\sqrt{A}} \qquad \text{Equation 2-14}$$

From the above equation, if the modulus is constant, a plot of C vs $A^{-1/2}$ is linear for a given material, and the intercept of the plot is the load frame compliance, C_f. The best values of C_f are obtained when the second term of the above equation is small, i.e., for large indentations.

Relatively large indentations were made in aluminium because of its of low hardness; while the area-to-depth function for a perfect Berkovich indenter

$$A(h_c) = 24.5h_c^2 \qquad \text{Equation 2-15}$$

was used to provide a first estimate of the contact area. Initial estimates of C_f and E_r were thus obtained by plotting C vs $A^{-1/2}$ for the two largest indentations in aluminium sample. Using these values, contact areas were then computed for all indentation sizes by equation

$$A = \frac{\pi}{4}\frac{1}{E_r^2}\frac{1}{(C - C_f)^2} \qquad \text{Equation 2-16}$$

from which, an initial guess at the area function was made by fitting the A vs h_c data to the relationship

$$A(h_c) = 24.5h_c^2 + C_1h_c^1 + C_2h_c^{1/2} + C_3h_c^{1/4} + \ldots + C_8h_c^{1/128} \qquad \text{Equation 2-17}$$

where C_1 through C_8 are constants. The leading term, $24.5\,h_c^2$, implies a geometrically-perfect Berkovich indenter; the others describe deviations from the Berkovich geometry due to the indenter tip bluntness.

The procedure is still incomplete because the exactly form of the area function influences the value of C_f and E_r subsequently. The procedure was applied again using the new area function and interacted several times until coverage was achieved. To check the validity of the constant modulus assumption and extend the area function to smaller depth, the procedure was subsequently applied to all other calibration materials. This allowed the load frame compliance C_f to be held as a constant value determined from the aluminium data since the largest contacts were made in this material.

2.3.1.4 A revised method

Oliver-Pharr method [12] is a more accurate method than original Deorner-Nix method [11] because it takes into account the effect of indenter geometry in determining the contact depth of indents as well as using iteration procedure to simultaneous calibrate machine compliance and the indenter area to depth function. However, the Oliver-Pharr method is complicated and time consuming. A revised method has been proposed [20] which combines the main points of Deorner-Nix method and Oliver-Pharr method. It is outlines as follows:

(A) Machine frame compliance determination:

Using single crystal tungsten (E=410 GPa and υ=0.28), therefore,

$$C[\frac{nm}{mN}] = C_f + \frac{2765}{\sqrt{A}} \qquad \text{Equation 2-18}$$

A series of relative high load indentation were made then the total compliance C and the contact depth h_c values were derived from the indentation hysteresis curves. Theoretical area function A=24.5 h_c^2 was used. Therefore, a linear fit curve through C vs $A^{-1/2}$ would determine C_f value from the intercept on the compliance axis. Optionally, a more rigorous and complicated procedure could be adopted, using isotropic sintered fused silica (SiO_2: E=72 GPa and υ=0.17), which the equation

$$C[\frac{nm}{mN}] = C_f + \frac{12726}{\sqrt{A}} \qquad \text{Equation 2-19}$$

Since h_c and thus $A^{1/2}$ depend on the load frame compliance C_f, a simple iterative procedure has to be used.

(B) Indenter shape (area function) determination:

Atomic force microscopy (AFM) is a recommended method for calibrating the shape of indenter directly. An indirect procedure can also be used and this assumes the reference material is isotropic and it is known that its elastic modulus is independent of the depth. In addition, it also requires calculation of the instrument frame compliance. The procedure involves making a series of indentation into reference materials: tungsten and fused silica. Tungsten is used at high loads to determine the overall diamond area function. Fused silica is much harder and therefore is used to define the tip region using low loads. The C_f value determined in the tungsten step will be used to computerise more realistic values of A_c at small indentation depth in fused silica. Using a elastic constants for the diamond indenter (E=1140 GPa and υ=0.07) and fused silica, re-arrangement of the former equation results in

$$A_c = \frac{12726^2}{(C - C_f)^2} = \frac{12726^2}{C_S^2} \qquad \text{Equation 2-20}$$

The area function for small contact depths can then be derived by fitting the A_c vs h_c data to a polynomial expression:

$$A_c = K_1 h_c^2 + K_2 h_c$$ Equation 2-21

The theoretical area function $A=24.5 h_c^2$ could be used for contact depths which is more than 800 nm.

(C) Analysis of indentation hysteresis curves:

The hardness and Young's modulus of materials to be tested can be measured once the load frame compliance C_f has been determined and the indenter area function $A=F(h_c)$ has been established. The indentation load-displacement hysteresis curve is obtained with frame compliance C_f corrected. The simple linear fitting through the upper 1/3 of the unloading data will intersect the depth axis at h_t. The stiffness $S(=1/C)$ is given by the slope of this line. The contact depth h_c is calculated by:

$$h_c = h_m - \varepsilon(h_m - h_t)$$ Equation 2-22

where ε depends on the investigated material: for metals, ε=1.0; for alloys and compounds (e.g., fused silica, TiN), ε=0.75. By using the following equations, hardness H and modulus E values will be obtained:

$$H = \frac{P_{\max}}{A_c}$$ Equation 2-23

$$E_r = \frac{\sqrt{\pi}}{2}\frac{1}{\sqrt{A_c}}\frac{1}{C_s}$$ Equation 2-24

$$\frac{1}{E_r} = \frac{1-\upsilon_s^2}{E_S} + \frac{1-\upsilon_i^{\,2}}{E_i}$$ Equation 2-25

2.4 Heating and cooling mechanisms for nanoindentation

There are many instruments commercially available that claim to be able to perform high temperature nanoindentation. However only Micro Materials ltd has dual heating.

Everitt et al have been using this approach. They have tried various methods turning off the tip heating for different samples. They found that if the sample is extremely conductive you have no choice but to heat both the indenter and the sample[5].

Schuh et al have also been performing high temperature nanoindentation, but they are restricted with their instrument manufactured by Hysiton, USA to only heat the sample. They have to rely on equilibrium of the tip and sample[21,22].

Both methods use resistive heating with PID control, however the NanoTest hot stage control uses a constant power in its indenter heating, after firstly controlling the temperature with a PID

feedback loop.

Cooling mechanisms on the other hand are all controlled with thermo electric coolers (TEC) until cryogenic levels are needed. CSM instruments, Switzerland claim to reach -40 ^{o}C and with liquid nitrogen stage in vacuum they claim to reach -150 ^{o}C[23]. Hysitron only claim to reach -10 ^{o}C[24]. CSM instruments have the advantage of using a small chamber purged with dry gas.

An independent company Surface also reaches -40 ^{o}C by circulating a cold liquid through a cooling block. They supply heating and cooling modules for Agilent / MTS[25]. There is little or no reported literature to-date on the cold stages from other manufactures and they do not claim to actively cool the indenter tip.

One conference paper by Syed Asif and Pethica exists using TEC's to cool both the indenter and the sample; they only reported cooling down to 17 ^{o}C[26].

Chapter 3 Nanoindentation of polymers

3.1 Introduction – polymers & need for nanoindentation

3.1.1 Time-dependent

Approaches to modelling the time-dependent deformation of polymeric systems in nanoindentation can assume constitutive models such as linear viscoelasticity with data fitted to 3-element (Maxwell or Voigt) or 4-element (combined Maxwell-Voigt) models [27,28]. These are standard elastic equations with time-dependent terms added to represent the fluid-like behaviour without necessarily any real physical significance [27]. Although values of fitting parameters can be obtained, it is not at all clear that the fitting is sufficiently robust so that these are really representative. Fits to these equations can be somewhat inexact in practice [28], questioning the reliability of the fitting parameters.

To study the time-dependent behaviour of aPP at different temperatures, the creep data were analysed and fitted using two approaches: (i) the logarithmic method discussed in Refs. [29] and [30], and (ii) the Boltzmann integral method discussed in Refs. [27,31–33]. The logarithmic equation can be expressed as

$$d = A\ln\left(\frac{t}{\tau_L}+1\right) \qquad \text{Equation 3-1}$$

where d is the increase in depth at maximum load, t is the time at peak load, A and τ_L are termed the extent parameter and the time constant, respectively. Equation 2-1 can also be expressed as the creep strain

$$\frac{d}{d(0)} = \frac{A}{d(0)} \ln\left(\frac{t}{\tau_L} + 1\right)$$ Equation 3-2

where d(0) is the initial penetration depth at the beginning of the hold (creep) period. A/d(0) (the dimensionless fractional increase in depth during creep) is known as the strain rate sensitivity parameter [29].

Although only two variables – measures of extent and rate - are used to describe the visco-deformation behaviour, in practice the creep curves normally show a quasi-logarithm feature [30], thus producing an excellent fit to the raw data. This method can be used not only for linear viscoelastic materials, but also non-linear viscoelastic materials, and with the quality of the fit it is possible to predict the creep response over a relatively long time. In the past, this method has been used for a range of polymer systems to identify changes in creep behaviour with density of cross-linking [34].

The major limitations of this method are that the equation is empirical and does not explicitly take into account differences in the time taken to reach the peak load, though the fitting parameters reflect this. It is not possible to deconvolute the particular contributions of elasticity, plasticity, viscoelasticity and visco-plasticity by this approach.

In other work [27,31–33,35], different combinations of springs and dashpots have been used to simulate the instantaneous elasticity, instantaneous plasticity, viscoelasticity and visco-plasticity. The creep compliance function is then deduced. The penetration depth can be calculated using the Boltzmann integral operator. This methodology has been successfully adapted by Oyen [33,35–

37] to simulate the whole loading and holding curve. However, a better fit required more variables, which can degrade the accuracy of the solution [37]. Compared to the logarithmic method, this needs more time and a careful selection of the initial value to make the iteration converge. In the present study, a free spring in series with a Kelvin parallel spring and dashpot element was used as the temperature effect can be studied using the time constant from the only dashpot. The background of this method is briefly described as follows.

For a conical-pyramidal indenter, the indentation depth can be expressed as

$$h^2 = m \cdot \int_0^t J(t-u)\frac{dP}{du}du \qquad \text{Equation 3-3}$$

where h is the penetration depth, m is constant, P is the load, t is the time, u is the dummy variable of integration for time and J(t) is the material's creep function. The creep function J(t) can be expressed as

$$J(t) = c_0 - c_1 \exp\left(\frac{-t}{\tau_B}\right) \qquad \text{Equation 3-4}$$

The solved Equation 3-4 using the creep function of Equation 3-5 gives

$$h^2 = m \cdot \left(c_0 k t_R - c_1 k \tau_1 \exp\left(\frac{-t}{\tau_B}\right)\left[\exp\left(\frac{t_R}{\tau_B}\right) - 1\right]\right) \qquad \text{Equation 3-5}$$

where t_R is the loading time. Assuming $c_0^{'} = mc_0$ and $c_1^{'} = mc_1$, Equation 3-5 can be simplified

into

$$h = \left(c_0' k t_R - c_1' k \tau_1 \exp\left(\frac{-t}{\tau_B}\right)\left[\exp\left(\frac{t_R}{\tau_B}\right) - 1\right]\right)^{\frac{1}{2}} \qquad \text{Equation 3-6}$$

3.2 Time dependence

3.2.1 Creep

3.2.1.1 INTRODUCTION

When materials are subjected to a constant load for a period of time, a time-dependent deformation - namely creep - is observed. Creep is an important phenomenon not only for describing viscoelasticity of polymeric materials (PMs) but also in the design of products made from PMs. Thus, creep affects significantly service performance and service life of PMs.[38–45] A better understanding of creep would clearly improve our capabilities to enhance the service performance of polymers, polymer-containing composites and hybrids.

Creep testing was performed on several polymeric materials using nanoindentation. The technique has been used to characterize mechanical properties such as hardness and elastic modulus of a wide variety of materials although there is still some debate about whether it is possible to determine hardness of strongly time-dependent materials meaningfully.[12,34,46–48] Results obtained from nanoindentation have an important advantage over those from conventional methods: they can separate creep from wear. The nanoindentation has been performed with a Micro Materials NanoTest system which allows for very high strain rate indentation in addition to more conventional quasi-static indentation, thus enabling comparison

between PM properties at high and low strain rates. Results to date have shown that it is not always possible to infer properties at high strain rates from slower measurements.[34,49,50]

3.2.1.2 EXPERIMENTAL

3.2.1.2.1 Materials

Polystyrene (PS) was purchased from Aldrich Chemicals Company. Santoprene® was supplied by Advanced Elastomer Systems, Houston, TX. Santoprene is a thermoplastic elastomer; it contains ethylene propylene diene monomer (EPDM) and polypropylene (PP) copolymer. Surlyn® 8140 was supplied by E. I. du Pont de Nemours, Wilmington, DE; it is a thermoplastic resin, an advanced ethylene/methacrylic acid (E/MAA) copolymer, in which the MAA acid groups have been partially neutralized with sodium ions. Polycarbonate (PC), acrylonitrile/butadiene/styrene (ABS) and polytetrafluoroethylene (PTFE) were supplied by the Dow Chemical Company. Polypropylene (PP) was supplied by Phillips. Low density polyethylene (LDPE) was supplied by Huntsman. Polyethersulphone (PES) was supplied by Solvay Engineered Plastics.

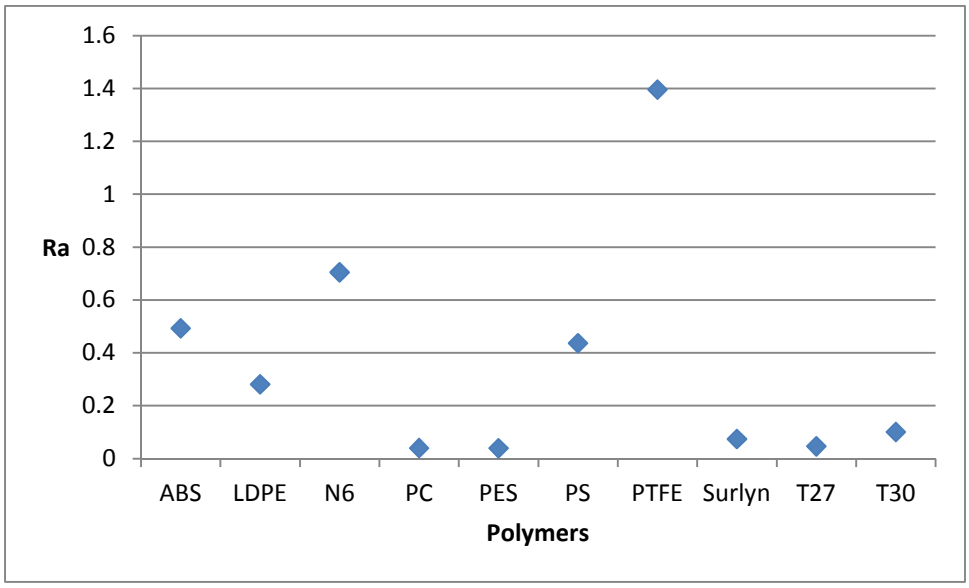

Figure 3.1 Surface Roughness

3.2.1.2.2 Nanoindentation testing

Indentations were load-controlled to 5 mN maximum load at 0.2 mN s^{-1} then there was a 60 s holding period at this peak load for creep testing. 20 tests were performed on each of the nine polymer samples at various locations on the surface of a given sample. A Berkovich type indenter was used to perform the measurements.

3.2.1.2.3 Analysis methodology

Equation 3-1 can be modified as (where $\tau = 1/B$ = creep time):

$$d = A\ln(Bt+1) \qquad \text{Equation 3-7}$$

As already mentioned, Equation 3-7 has been used previously [43,50–53] to fit the creep behaviour and found to indicate sometimes rather subtle differences in the rate and extent of the time-dependent deformation; A is interpreted as an extent term and B as a rate term. Normalizing, that is dividing A by the initial deformation at the first indentation d(0), provides a dimensionless parameter (A/d(0)) which enables comparison of different materials. In earlier work [49,54], the initial deformation was set equal by means of a depth-terminated load ramp, although values of A/d(0) [30] themselves were not explicitly quoted. Somewhat similarly, Berthoud, G'Sell and Hiver [55] have analysed the logarithmic behaviour by an Eyring-type creep law in terms of scalar stress and strain for a spherical indenter. According to them, the fractional increase in depth (i.e. strain) d/d(0) is

$$d/d(0) = [m_{eff}]\ln (t/\tau + 1) \qquad \text{Equation 3-8}$$

where $\tau = 1/B$ = creep time and $m_{eff} = A/d(0)$ = strain rate sensitivity. The first 60 s of experimental creep data was chosen to fit a modification of Equation 3-7 such that quantities on both sides are dimensionless:

$$d/d(0) = [A/d(0)]\ln (Bt + 1) \qquad \text{Equation 3-9}$$

3.2.1.3 EXPERIMENTAL RESULTS

Illustrative creep tests on PS, is shown in Figure 3.2. In this case the fit to Equation 3-9 is

excellent. The results are summarized in Table 3.1. By testing close to room temperature, on purpose some polymers studied are far above, some far below and some near the glass transition temperatures. Since large differences of behavior are expected far below and far above T_g, is defined by

$$y = T_g - T_{exper} \qquad \text{Equation 3-10}$$

to represent numerically the distance from the glass transition temperature. T_{exper} = Room temperature. Clearly negative y values correspond to rubber- or liquid-like behavior and positive y values to glassy behavior.

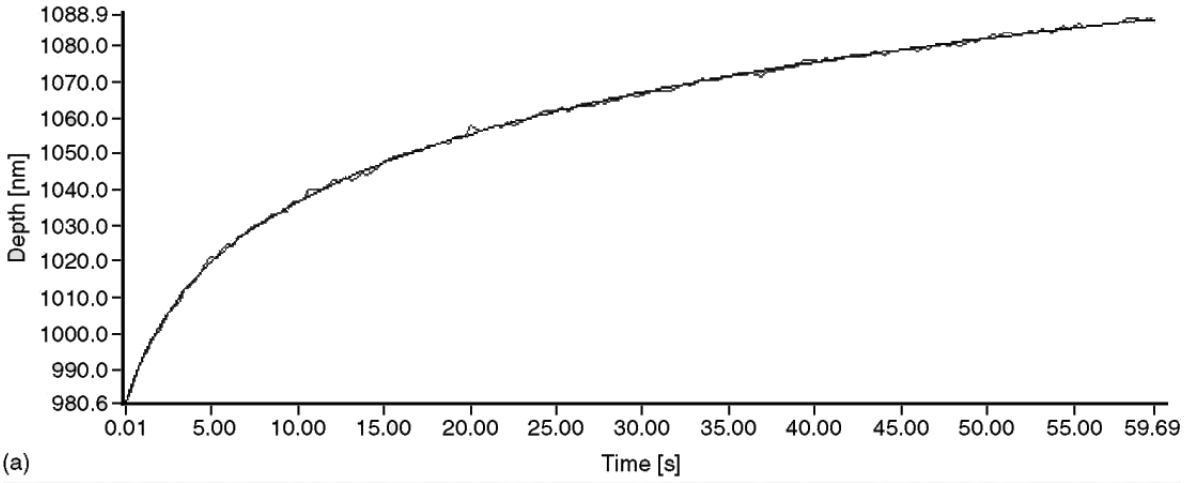

Figure 3.2 Illustrative creep results for PS

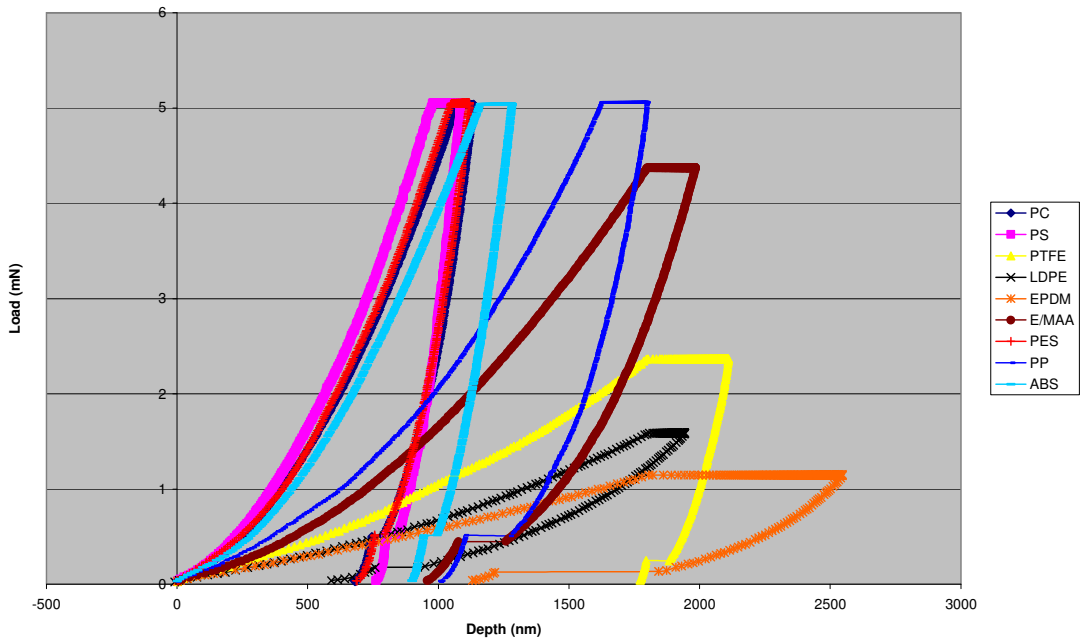

Figure 3.3 Tested polymers Load versus Depth

Table 3.1Summary of Hardness and Modulus values

Sample	H/GPa	Er/GPa	E/GPa
ABS	0.177 ± 0.042	3.97 ± 0.55	3.35
PC	0.229 ± 0.003	4.15 ± 0.04	3.50
PES	0.245 ± 0.014	4.39 ± 0.14	3.70
PP	0.083 ± 0.011	1.69 ± 0.16	1.42
PS	0.244 ± 0.012	5.52 ± 0.21	4.46
PTFE	0.0378 ± 0.0065	1.10 ± 0.19	0.92
LDPE	0.0364 ± 0.0057	0.281 ± 0.035	0.24
Santoprene	0.0151 ± 0.0062	0.254 ± 0.089	0.21
Surlyn	0.0726 ± 0.0012	1.043 ± 0.009	0.88

3.2.1.4 Discussion

Results of the first attempt to investigate the creep parameters are shown in Figure 3.4. The plot of A/d(0) as a function of y is fairly complex. A maximum seems to be present. Previously

Beake [30] has observed also a complex relationship between A/d(0) and T - T_g for a range of amorphous and semi-crystalline samples. In particular, ultra-high molecular weight PE (UHMWPE) showed large values of A/d(0) despite being far from T_g, in sharp contrast to LDPE which exhibits low A/d(0). Differences in crystallinity may be responsible for this.

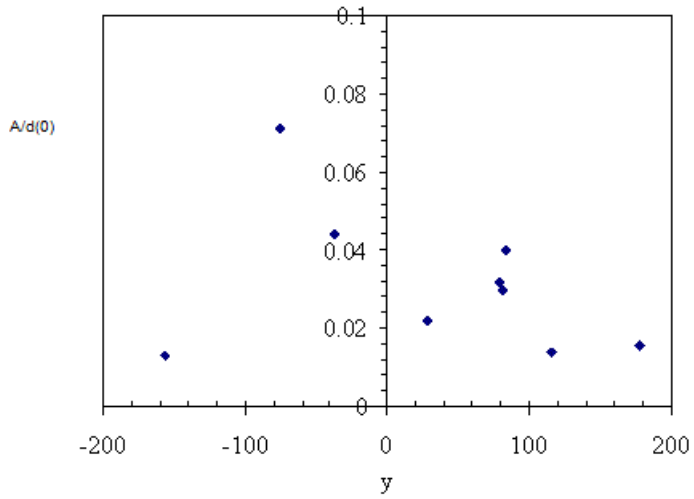

Figure 3.4 Strain rate sensitivity *A/d(0)* as a function of *y* as defined by Equation 3-10.

In turn, the strain rate sensitivity can be considered as a function of the creep time. Figure 3.5 shows such a plot. In this case a clear correlation is found. An inspection of earlier data indicates that this correlation applies to a variety of polymer systems.

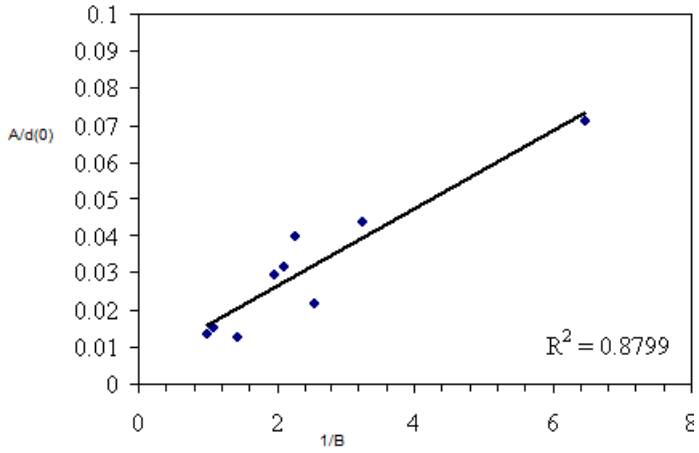

Figure 3.5 Strain rate sensitivity *A/d(0)* as a function of creep time 1/*B*. The perfect fit would correspond to *R*2 = 1.

From the viscoelasticity theory it is known that creep including its time dependence is controlled in polymeric materials by the free volume available for molecular (segmental) motions.[38–45] According to one explanation, around glass transition temperature T_g heating creates sufficient free volume v^f to allow molecules to move relative to one another.[56] As advocated by Flory [57] and others [58], the free volume can be calculated as

$$v^f = v - v^* \qquad \text{Equation 3-11}$$

where v is the specific volume (usually in cm^3g^{-1}) while v^* is the incompressible or hard core volume obtainable from v(T, P) results via an equation of the state such as that developed by Hartmann.[59] Considering a correlation between the parameters in Equation 3-7 and the glass transition temperature (a point representing the glass transition region) would exist. It is kept in mind that the location of T_g is determined by v^f changes. Large negative values of y

defined by Equation 3-10 mean that the PM is far above T_g in the liquid or rubbery region. This implies high v^f values, consequently large chain mobility, and thus high creep rate B. Ploting B = B(y) in

Figure 3.6.

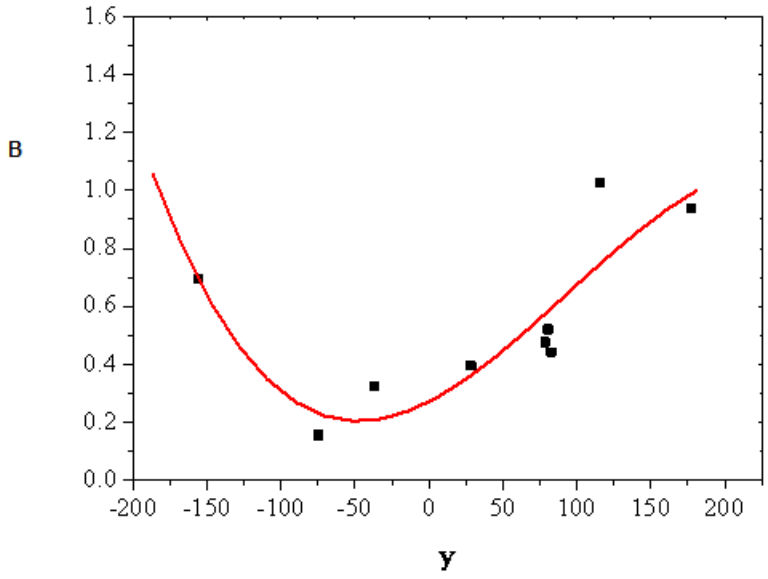

Figure 3.6 Creep rate *B* as a function of *y* defined by Equation 3-10.

The conclusions of this study are also supported by results of nanoindentation creep tests at elevated temperatures.[60]

3.2.1.5 Conclusion

A variety of PM's has been investigated, providing nanoindentation data and more importantly

creep data by placing holds at maximum load in the nanoindentation loading history. All the polymers were tested at room temperature and had various T_g. Values of y where obtained by using Equation 3-10. At large negative y values the creep rate is high due to the liquid like behaviour having past the T_g and are in the rubbery or liquid region.

Where A and B are constants, d(0) is the initial deformation at the beginning of the hold period at peak load in an indentation test, and d is the increase in depth during the hold period so that d/d(0) is the fractional increase in depth which occurs during this hold period. Values of A/d(0) for the range of PM's appear to correlate with tan delta and also with the distance from the test temperature to the glass transition temperature.[7].

The methods used and developed further in this investigation will be used to establish creep parameters under low temperatures. A polymer can be chosen with a T_g well below 0 ^oC, to see if the T_g can be pinpointed from creep analysis. It will also be interesting to see if high creep rates are noticeable when extremely large positive values of y are obtained as PMs become brittle.

3.3 Environmental dependence

3.3.1 Liquid cell

3.3.1.1 Introduction

Mechanical properties of biological and polymeric samples may vary considerably when in a fluid environment compared to the usual ambient (~50% relative humidity, RH) testing conditions. Whilst hydrophobic polymers do not absorb water significantly (so their mechanical properties are unchanged), polar materials in contrast such as biopolymers (for example DNA, elastin, starch and cutin [61,62]) absorb water and can swell significantly at saturation. Their mechanical properties are interlinked with their water content. It can be necessary to understand their properties and behaviour in fluid media so it is highly desirable to test under these conditions rather than to attempt to infer from measurements under normal laboratory testing conditions.

Nanoindentation is fast becoming a popular technique but hitherto commercial nanoindentation systems have not operated in fluid conditions. Recently, the testing capability of one commercial nanomechanical testing instrument has been extended by the development of a fluid cell allowing nanoscale testing of samples fully immersed in fluids see Figure 3.7. The cell works with the instrument's pendulum design and the horizontal loading has certain benefits for testing in fluid.

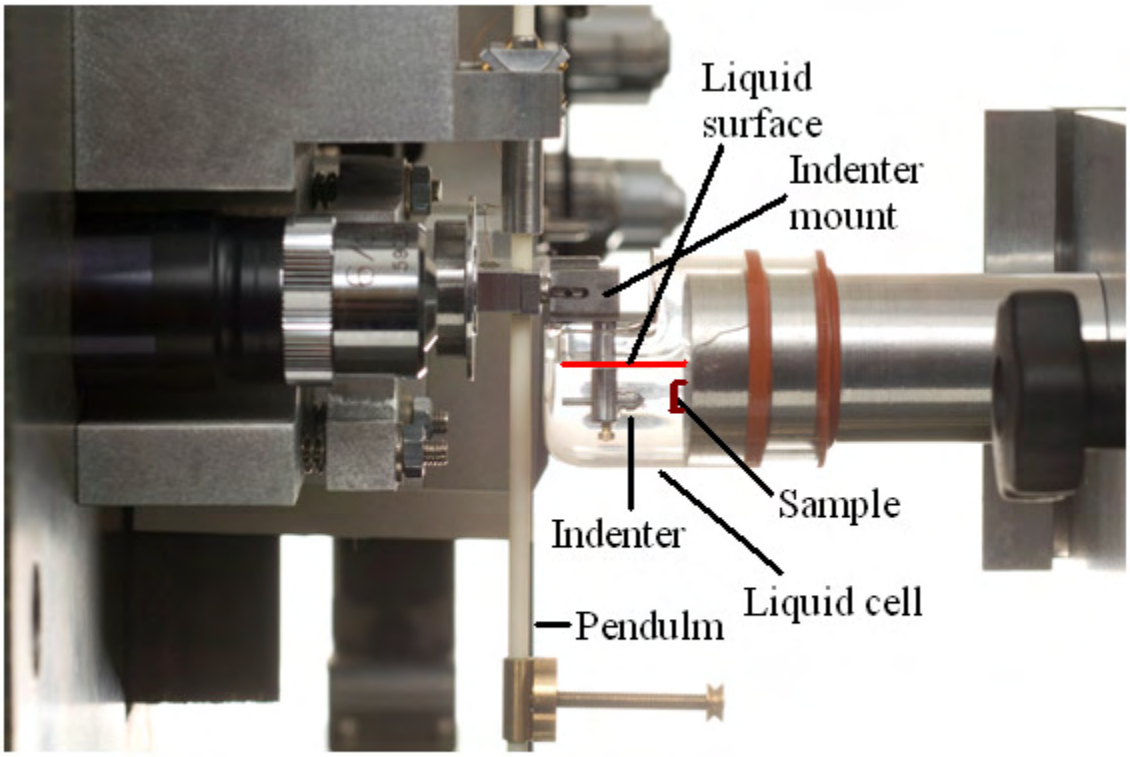

Figure 3.7 Schematic of NanoTest fluid cell.

In this chapter the fluid cell has been used to investigate the influence of water on the nanomechanical properties of commercial Nylon 6 materials. Nylon was selected as a reliable benchmark test sample as it is already well known from testing by Tabor and others that water adsorption has a significant impact on many of its properties at the macroscale [63–69]. Nylon 6 can absorb a surprising amount of water, either by immersion or simple exposure to high humidity. The effect on the glass transition and mechanical properties is an important consideration in the use and suitability of the material for specific applications. With its polar nature and open microstructure nylon is readily plasticized by water. Plasticization decreases specific interactions such as hydrogen bonds in the amorphous regions of the polymer. Tabor and

Cohen [63], and later Amuzu [64], have shown that the friction and shear strength of Nylon is a strong function of humidity. Tabor and Cohen showed that friction of Nylon on glass is increased in water due to the increased contact area when wet [63]. More recently Stuart and Briscoe [65] suggested that the observed increase in wet friction with load on nylon was also due to this increasing contact area. Newman and co-workers have reported that water immersion resulted in a greater reduction in elastic modulus on Nylon 7 than Nylon 11, presumably because of the higher intermolecular interactions of the former [66].

In addition to changes in the hardness and elastic properties on immersion we were interested in the influence of absorbed water on the indentation creep behaviour of nylon. In contrast, we have previously concentrated on the exact fitting of the initial phase of nanoindentation creep data to a simple logarithmic equation originally developed for soft metals. [34,43,51] (Equation 3-12)

$$\text{Increase in depth} = A\ln(Bt + 1) \qquad \text{Equation 3-12}$$

The quality of fit to the creep deformation during this initial phase is excellent in practice. The approach has been recently adapted (normalising by the initial penetration depth) and the sensitivity of a dimensionless creep parameter, A/d(0), has been investigated recently as a measure of time-dependent deformation during indentation at constant force at room temperature [7,30,60], and also at elevated temperature [60] as shown in Equation 3-13.

$$d/d(0) = [A/d(0)]\ln(Bt + 1) \qquad \text{Equation 3-13}$$

It has been shown by dynamic mechanical analysis (DMA) measurements that water absorption alters both the magnitude of the tan delta peak and the glass transition temperature [69]. The tensile strength of dry Nylon 6 at 20 °C is typically 76-97 MPa. The properties are highly dependent on water content. Water will behave as a plasticizer, i.e. the glass transition process moves to a lower temperature upon exposure to moisture. The effect of plasticization is easily shown with polyamides by immersing of dry material in water. Within a very short time scale, this material can absorb between 6 and 9 % by weight of water and this will lower the glass transition to about 20 °C affecting both modulus and tan delta. Once a polymer is at or above its glass transition temperature, it will tend to creep when any applied load occurs. It is of interest to investigate whether the nanoindentation creep analysis could show a similar effect at a more highly localised scale.

3.3.1.2 Experimental

3.3.1.2.1 Materials

Two commercial Nylon 6 materials were tested. Tarnamid T30 (hereafter designated “T30”) was obtained from Zaklady Azotowe, Poland and a comparative sample (hereafter designated “N6”) was obtained from Polysciences Inc., USA. Specimens were prepared by injection moulding under comparable processing conditions. Physical characteristics of the samples studied are given in

Table 3.2.

Table 3.2

Physical Characteristics of the Materials Studied

Material	Symbol	M_w[a] (g/mol)	X_c (wt %)	Density (g/cm^3)	T_m (°C)	η_{rel}[a]
Tarnamid T30	T30	31,000	35.2	1.105	224	3.8
Polysciences M_w 35,000	N6	35,000	32.1	1.100	222	4.1

[a] According to the producer: M_w, molecular weight; X_c, degree of crystallinity (DSC; 10°/min); T_m, melting temperature (DSC; 10°/min); η_{rel}, relative viscosity ($H2SO_4$/25°C).

2.2 Nanoindentation conditions

A NanoTest system (Micro Materials Ltd) fitted with a fluid cell was used for the nanoindentation testing. The fluid cell consists of a pyrex cell which is then fitted to a sample stub prepared with o-ring seals. An indenter mount/adapter is then fitted to the normal indenter holder of the NanoTest. A software calibration is needed to be performed after you have fitted the fluid cell because the position of the indenter to the normal indenter holder has been changed. The reason for this change is so that the indenter is able to be submerged in the fluid of choice. The indentation test temperature was 25ºC. In what follows “dry” is taken to mean testing in ambient laboratory conditions (~50% RH). On immersion in deionised water, the samples were left for >24 hr to equilibrate (saturate). Repeat indentations were performed to 0.5, 5 and 10 mN. 5-20 indentations were performed on each sample at each force dry and a similar number were performed wet. Loading conditions for the 0.5 mN indentations were 0.05 mN/s loading rate, 50 s hold at peak load and unloading at 0.05 mN/s to 90% unloading where an additional hold of 120s allowed measurement of the rate of creep recovery. A linear fit was performed through the last 70 s of the creep recovery data to determine the apparent (close to) linear creep recovery rate. This

creep recovery data was not used to correct the indentation data for thermal drift, which itself is orders of magnitude smaller. For the 5 and 10 mN indentations the conditions were the same except the loading and unloading rates were set to 0.2 mN/s, producing the load history shown in Figure 3.8 for the 5 mN indentations. A diamond indenter with the tip radius function $A_c = 6000h + 22\ h^2$ (essentially a Berkovich with a rounded spherical end cap) was used. The tip radius function was defined by performing a series of indents into a sample of fused silica.

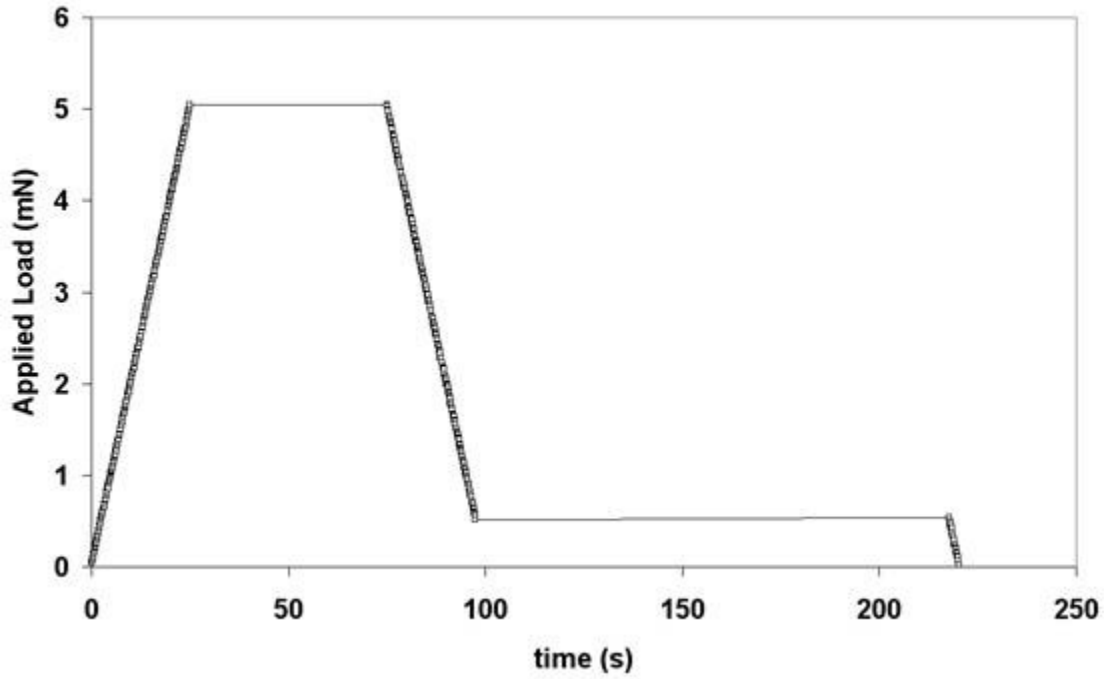

Figure 3.8 Loading history for indentation to 5 mN.

3.3.1.3 Results and discussion

Illustrative indentation curves for T30 dry and wet are shown in Figure 3.9. Similar curves (not shown) were obtained on N6. Significant indentation creep (Figure 3.9 and

Table 3.3) and creep recovery (

Table 3.3) effects are observed during the hold periods on N6 and T30 both wet and dry.

Table 3.3 Creep Parameters

Creep Parameters

	A (nm)	B (s^{-1})	$d(0)$ (nm)	$A/d(0)$	Creep recovery rate (nm/s)
T30 dry 0.5 mN	23.1 ± 2.8	0.45 ± 0.15	346 ± 35	0.067 ± 0.006	0.07 ± 0.01
T30 wet 0.5 mN	26.4 ± 3.5	1.07 ± 0.38	764 ± 58	0.034 ± 0.007	0.12 ± 0.02
T30 dry 5 mN	61.7 ± 4.9	0.31 ± 0.08	1339 ± 33	0.046 ± 0.003	0.28 ± 0.02
T30 wet 5 mN	48.1 ± 7.9	0.49 ± 0.11	2403 ± 156	0.020 ± 0.003	0.67 ± 0.11
T30 dry 10 mN	82.8 ± 3.3	0.18 ± 0.02	2116 ± 30	0.039 ± 0.002	0.50 ± 0.02
T30 wet 10 mN	68.2 ± 6.8	0.27 ± 0.05	3539 ± 122	0.019 ± 0.001	0.85 ± 0.05
N6 dry 0.5 mN	20.8 ± 1.9	0.58 ± 0.13	343 ± 28	0.061 ± 0.006	0.09 ± 0.02
N6 wet 0.5 mN	8.7 ± 1.0	3.3 ± 0.8	567 ± 29	0.015 ± 0.001	0.35 ± 0.04
N6 dry 5 mN	57.6 ± 2.3	0.30 ± 0.07	1422 ± 42	0.041 ± 0.002	0.39 ± 0.02
N6 wet 5 mN	38.7 ± 3.1	0.56 ± 0.13	2093 ± 40	0.018 ± 0.002	0.51 ± 0.07
N6 dry 10 mN	83.7 ± 7.9	0.18 ± 0.03	2129 ± 86	0.039 ± 0.003	0.60 ± 0.06
N6 wet 10 mN	51.7 ± 2.2	0.29 ± 0.05	3181 ± 110	0.016 ± 0.001	0.75 ± 0.07

Creep parameters from eq. (1) using the data during the 50 s hold at peak load.

The appreciable creep recovery indicates the behaviour is viscoelastic/viscoplastic. Figure 3.12 shows the increase in depth during the 50 s hold at peak load for the two indentations in Figure 3.9.

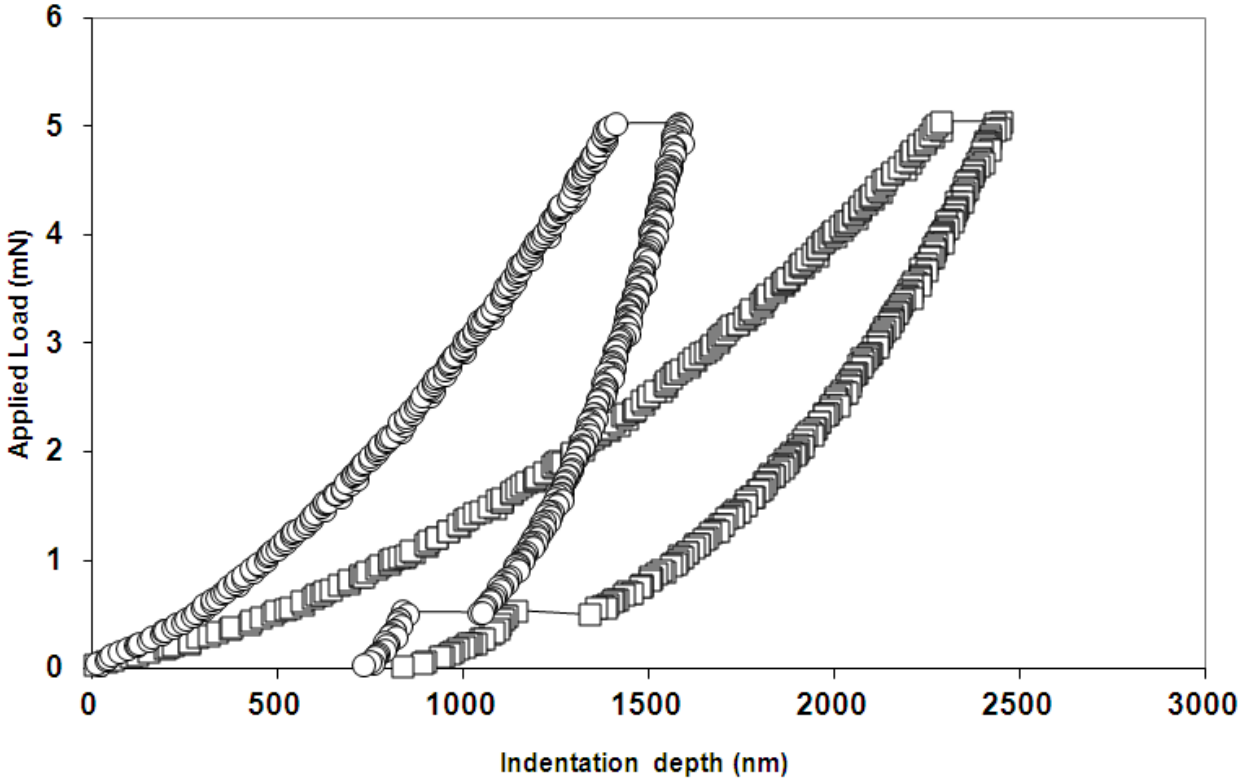

Figure 3.9 Typical dry (circles) and wet (squares) indentation curves for T30. Berkovich indenter loading at 0.2 mN/s to a peak load of 5 mN. Fifty seconds hold at maximum load for creep. One hundred twenty seconds hold at 90% unloading for creep recovery.

Hardness and elastic modulus were determined from unloading curves using the procedure of Oliver and Pharr [12].

Although the reliability of absolute values has been questioned due to the accuracy in determining the contact depth (and hence area) on viscoelastic materials the unloading slope approach should be sufficient to determine the relative changes due to the change in environment for this particular application.

Table 3.4 shows how the hardness and reduced modulus vary with applied force and test medium. Dry data show only minimal difference in mechanical properties between the two Nylon 6 samples. Hardness and elastic modulus determined from the Oliver and Pharr procedure are

almost invariant with load, increasing by ~ 10% for the lowest indentation load compared to the largest. Although the loading rate was reduced the loading time for the smaller indentations was lower and this may have contributed to the slight effect rather than any particular existing gradient in mechanical properties.

Table 3.4 Hardness and Reduced Modulus

	H (GPa)	E_r (GPa)
T30 dry 0.5 mN	0.123 ± 0.016	1.70 ± 0.18
T30 wet 0.5 mN	0.046 ± 0.007	0.39 ± 0.04
T30 dry 5 mN	0.117 ± 0.009	1.87 ± 0.04
T30 wet 5 mN	0.052 ± 0.006	0.58 ± 0.06
T30 dry 10 mN	0.111 ± 0.002	1.67 ± 0.07
T30 wet 10 mN	0.055 ± 0.002	0.60 ± 0.05
N6 dry 0.5 mN	0.122 ± 0.016	1.79 ± 0.15
N6 wet 0.5 mN	0.089 ± 0.017	0.70 ± 0.10
N6 dry 5 mN	0.113 ± 0.014	1.72 ± 0.13
N6 wet 5 mN	0.070 ± 0.030	0.70 ± 0.03
N6 dry 10 mN	0.113 ± 0.012	1.60 ± 0.13
N6 wet 10 mN	0.065 ± 0.006	0.67 ± 0.04

Hardness and elastic modulus determined from analysis of unloading segments of indentation curves.

Testing wet shows some difference between the two materials, with greater decreases in hardness and modulus for T30 than N6, particularly for the smaller load indentations (see also Figure 3.10). The data imply that T30 is more effectively plasticized than N6 and water is more effective at plasticizing the surface layers on T30 which may be due to the slightly lower molecular weight of T30.

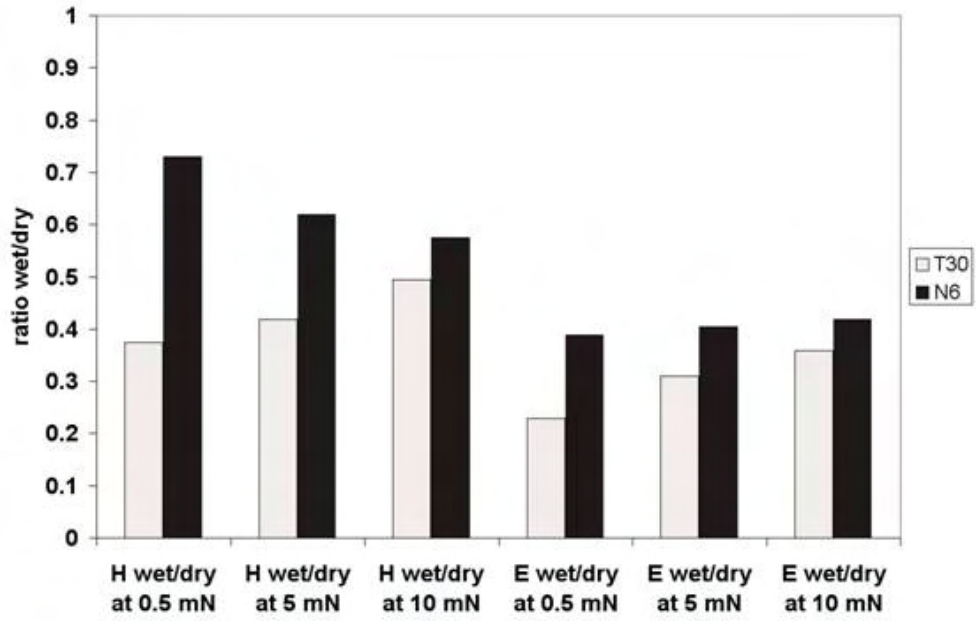

Figure 3.10 Ratios of hardness (wet/dry) and modulus (wet/dry)

There were no observable changes in indentation behaviour in leaving the samples immersed in fluid for longer periods. It is reasonable to assume that 24 hr immersion is more than adequate for saturation of the surface layers of the polymers, consistent with Tabor's original microindentation data [63].

Including hold periods in the load history (see Figure 3.11) allows investigation of creep and creep recovery processes. As mentioned earlier, we have recently investigated equations 1 and 2 and the use of A/d(0) [27,69], as a measure of time-dependent deformation occurring during the hold segment at peak load in an indentation test. The fit is good and both samples show similar A/d(0) values dry. Figure 3.12 shows that there is a small increase in indentation creep in water. Despite this, the proportion of time-dependent deformation compared to the total deformation (A/d(0)), decreases significantly in water on N6 and more notably on T30.

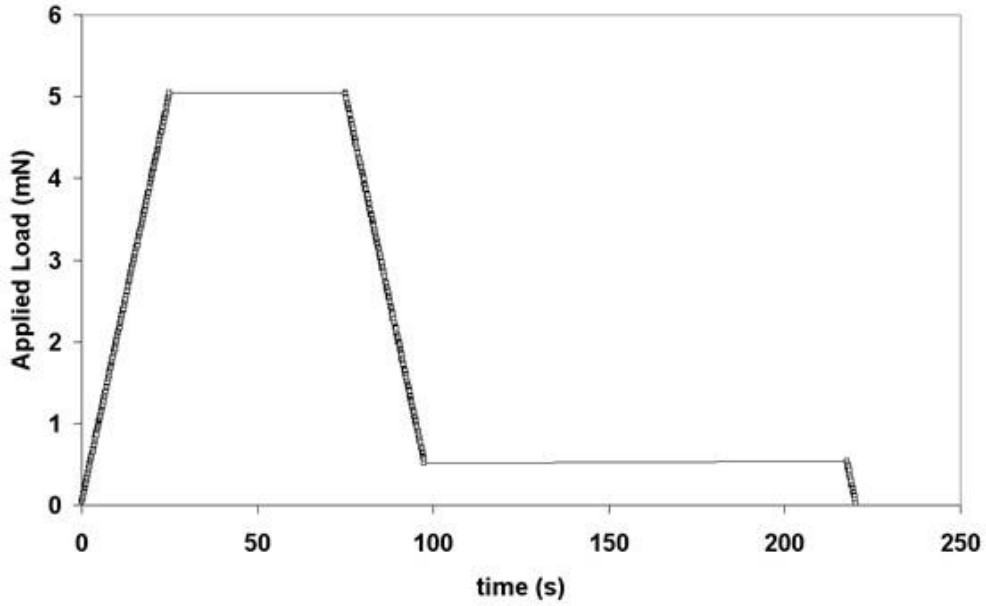

Figure 3.11 Loading history for indentation to 5 mN.

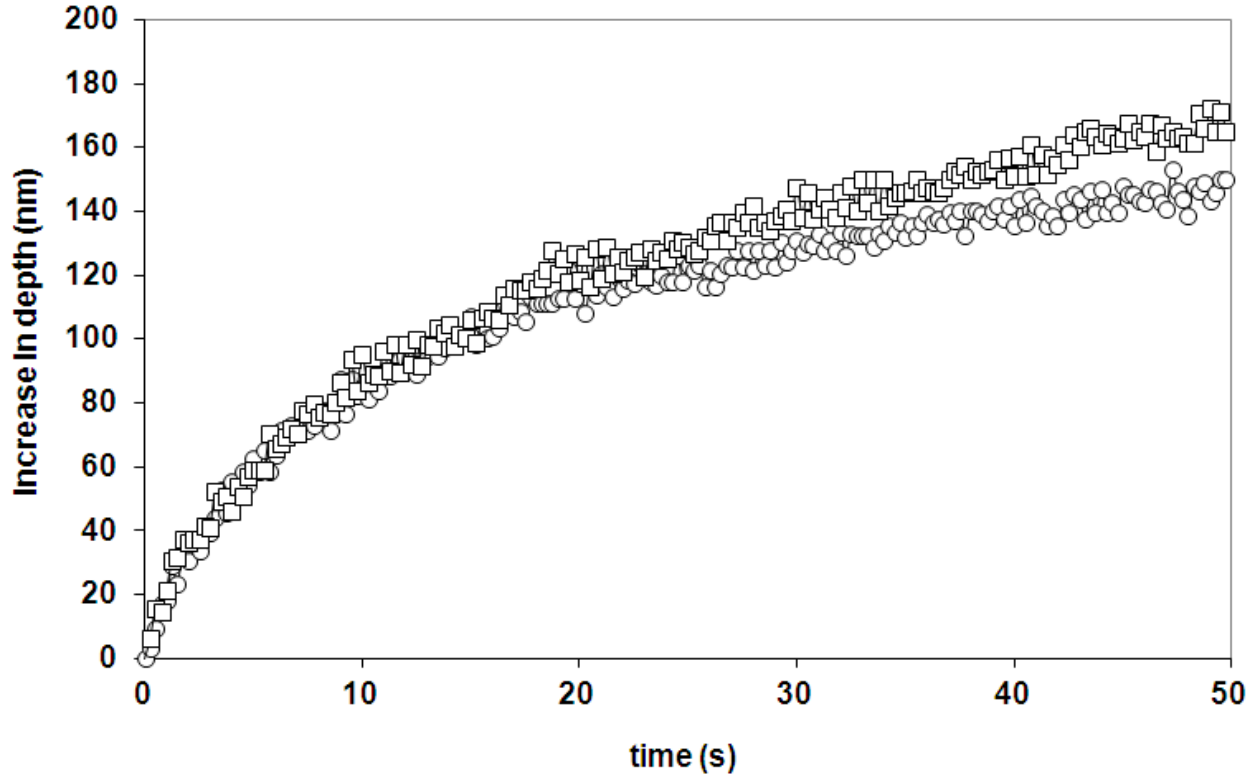

Figure 3.12 Nanoindentation creep during 50 s hold at 5 mN on T30 after loading at 0.2 mN/s with a Berkovich indenter; wet, (Squares); dry,(Circles).

Based on evidence from nanoindentation data at ambient and elevated temperatures Beake et al have suggested that A/d(0) correlates with tan delta [7,30,60]. The decrease in A/d(0) when wet would then be explained by a decrease tan delta at the testing temperature due to a decrease in magnitude of the tan delta peak and a shift in the glass transition temperature region. Absorption of 1% water has been shown to reduce the α–peak (Tg) by 30°C in Nylon 6,12 [69]. A pronounced reduction in glass transition temperature on water absorption has similarly been reported by Grunina and co-workers for a range of biopolymers, such as DNA and elastin, using differential scanning calorimetric methods [61]. It has been suggested that addition of water influences the molecular packing in amorphous polymers such as Nylon [69]. Bonded water molecules lower the amount of interchain H-bonds enabling closer interchain packing density. Decreased cohesive forces resulting from breaking the H-bonds could be responsible for the shift in Tg. The free-volume concept of the glass transition breaks down, as it might otherwise be assumed that the peak would shift to higher temperatures with increasing density [69].

The reduction in the creep parameter A/d(0) when wet has an influence on hardness and modulus determined from unloading slope analysis after the hold at peak load. It is known that the altering the extent of creep by changing the hold time influences hardness and to a lesser extent elastic modulus on polymeric materials. Altering the creep by changing the test medium should have a related effect. From the data in

Table 3.4 it is possible to determine the relative change in hardness and modulus on immersion and saturation in water. The ratios of hardness and modulus when wet compared to when dry [H

(wet/dry) and E (wet/dry)] are shown for each indentation force in Figure 3.10. Although there is a decrease in elastic modulus of about 60-70% on immersion the corresponding decrease in hardness is only ~50%. The influence of creep on hardness is lesser when testing nylon in water, which is consistent with the lower relative creep when wet. Figure 3.10 also emphasizes the differences in mechanical behaviour between the samples when wet due to the more effective plasticization of T30.

3.3.1.4 Conclusions

1. Results with a fluid cell fitted to a commercial nanoindenter are presented in this publication. Measurements on Nylon 6 samples immersed in water for >24 hr were compared to tests under usual ambient (~50% RH) conditions. As expected water absorption caused clear differences in the mechanical properties of the polymers.

2. The creep parameter A/d(0) - a measure of the proportion of time-dependent deformation compared to the total deformation - decreases significantly in water. We have suggested elsewhere that A/d(0) correlates with tan delta. The observed reduction in A/d(0) when wet is consistent with a decrease in the tan delta peak due to a shift in the glass transition temperature when wet.

3. Changes to the indentation creep response when wet influence the hardness and modulus determined from analysis of the unloading curve; with hardness decreasing by around 50% and elastic modulus by around 65% on immersion. The difference may be related to the role of creep. The smaller effect of creep on hardness is consistent with the lower relative creep when wet.

4. The use of a fluid cell in conjunction with a humidity control chamber (also possible in commercial nanoindentation systems) would extend the range of nanomechanical testing to cover virtually the entire range of possible moisture content (~5-100% RH) and is expected to have applications in testing biological samples and polymeric materials at highly localised scale inaccessible to other testing techniques.

Chapter 4 Sub - ambient instrumentation development

4.1 Introduction

There is a lack of commercially available low temperature instrumentation for tribological and nanomechanical property measurement. In the present research the Peltier effect will be employed to provide the localised low temperature environment. The Peltier thermoelectric module is a solid-state device that operates as a heat pump cooling the indenter and sample surface. This will result in a unique low temperature chamber which will be fitted to an existing NanoTest instrument at the University of Birmingham thus facilitating nanomechanical property testing at temperatures as low as –30 ^{o}C.

4.1.1 Cryotechnical systems and challenges

Materials are needed to work under extreme conditions the rapid development of space technology, cryogenic machining, superconductivity and hydrogen technology has meant that materials need to function in low-temperature application conditions. For instance liquid gases (e.g. hydrogen and natural gases) are used for environmentally friendly energy supply and in energy transportation systems. It has been reported that BMW has started producing cars with hydrogen combustion engines and the Deutsche Aerospace Airbus is developing a prototype of an aircraft with hydrogen engines [70]. Large marine cargo systems are being built using stainless steel valves for the transportation of liquid natural gas (about -160^{o}C). In addition, current superconducting materials and devices must work below their critical transition temperatures (95k or -178^{o}C for high-temperature superconducting ceramics). With the increasing applications of cryotechnical systems, new demands are arising concerning the functionality and reliability of

materials under such low temperature conditions, which presents challenging tasks for material scientists and engineers.

4.1.2 The need for low-temperature mechanical properties

An important aspect of the use of liquid gases (hydrogen and oxygen) is the safety of the equipment. Leakage of liquid hydrogen and/or oxygen can cause violent fire and even tragic explosion. However, it is known that the mechanical properties of materials are highly temperature-dependent, and the main technical problem is the embrittlement of materials at low-temperatures. Therefore, for cryogenic applications materials must have adequate mechanical properties (strength/hardness, ductility and toughness) so that equipment and vessels can be designed against catastrophic failure.

In many applications, surface engineering is used to improve mechanical and tribological properties of surface materials. Under cryogenic temperatures, the mechanical and tribological properties of these materials may be different from at room temperature. For example, conventional lubricants (oils and greases) are not effective in lubricating cyrotechnical tribo-systems because of the high changeability of their rheological properties [71]. Therefore, surface coatings (especially self-lubricating coatings) are used to protect the surfaces in relative motions under force. However, low temperature could introduce high interface stresses in surface engineered materials due to the difference in thermal properties between the surface coating and the substrate, thus again increasing the operation risk. Moreover, low-temperature may cause phase transformation for metastable surface engineered materials. For example S-phase formed in austenitic stainless steels (ASS) by plasma surface alloying can contribute to combined

improvement in corrosion and wear resistance. S-phase technology could be used with ASS valves for liquid natural gas. However, there could be the possibility of potential martensite transformation under the synergetic action of low-temperature and mechanical stressing and degradation of surface properties and this has to be addressed before practical use of S-phased materials. Surface engineering of titanium alloys are also cryogenic candidate materials.

Finally, the deformation behaviour and tribological properties of polymers and rubbers are greatly affected by changes in temperature. For instance, the coefficient of friction between footwear sole/tyre and ice is temperature dependent and slipping on ice in winter causes slipping injuries and traffic accidents [72]. Clearly there is an urgent need to investigate the mechanical and tribological properties of these materials (especially surface engineered materials) at low temperatures for the development of new safe cryotechnical systems and to prevent slipping injuries and road accidents.

4.1.3 The need for the cryo-nanoindentation instrument

As discussed above, the properties of materials are strongly temperature dependant. This means that if a material or surface engineered system provides safe contact at one temperature it can be unsafe if it is used at another. Unfortunately, to date such data has been available only at room temperature and advanced temperatures up to 500^{o}C. However, the micro/nano mechanical properties at low temperatures have not been tackled.

Because of the lack of a commercially available low temperature instrument for tribological testing, researches often resort to using a home-made simple device. Such simple devices cannot be used to produce accurate basic material properties such as harness (H), Young's modulus (E)

and H/E for the design and property prediction of advanced micro/nano composite coatings. Therefore, it is essential to develop novel sub ambient temperature nanoindentation instrument to facilitate the investigation into the mechanical and tribological properties of polymeric and surface engineered materials at below ambient temperatures and in the future cryogenic temperatures.

4.2 Instrument development

4.2.1 Initial prototypes –

4.2.1.1 Purging designs

A number of prototypes where considered and further developed to reach the final design for the purging of the cryogenic cooling system. The purpose of the purging is to remove or reduce the moisture content around the diamond indenter enough to allow testing of the sample materials without the formation of ice or water vapour on the sample surface.

4.2.1.2 Overall Design Brief

- Local purging around the diamond indenter, to provide a reduced volume to be purged.
- The design must be able to be easily incorporated with other modules of the NanoTest, namely impact and scratch and high resolution microscope.
- It should be easy for a user to be able to assemble and disassemble the cryogenic purging kit to be able to use other types of modules on the NanoTest.

- This is in contrast to purging the whole instrument which would have a large volume to purge and also a vast quantity of materials to outgas.

4.2.1.3 Prototype design 1

4.2.1.3.1 Design brief

An easy to incorporate method of reducing the moisture content in the atmosphere around the diamond indenter in order to achieve below ambient testing of samples. The sample stage will have a thin PVC sleeve reinforced with steel wire, so that it will be able to be purged without risk of it breaking under pressure.

4.2.1.3.2 Design

An aluminium shield placed over the diamond indenter. A small box was constructed out of Perspex in front of the indenter on the shield to allow the user to be able to see the contact with the indenter tip and sample (this is a requirement of the NanoTest instrument in the first instance to set up the experimental parameters.).

A sample plate with a flexible thin PVC sleeve attached was then linked and secured on to the aluminium shield. The PVC sleeve was reinforced with wire for the reasons mentioned above in the design brief.

The purging gas was then fed into the Perspex box at a height so that it was directly in line with the height of the indenter.

4.2.1.3.3 Results

The gas feeds into the small box worked well.

However on visual inspection it was not enough to prevent frosting on the sample surface (Sample under test was fused silica).

The flow rates were increased, but this had a detrimental effect on the balance of the pendulum.

4.2.1.3.4 Discussion

The hole in the shield for the indenter was too large and therefore the purging gas rushed through this and did not sufficiently protect the surface of the sample. Therefore as the temperature of the sample was reduced to zero degrees Celsius, ice formed on the surface of the sample.

The purging gas was also flowing directly on to the capacitor plates and as a result causing the system to drift significantly because the distance between the perpendicular plates was increased.

4.2.1.3.5 Conclusion

- Water vapour was not being significantly removed from the atmosphere using this method.
- Purging gas flowing out of the gap between the indenter and the shield caused the system to drift.
- A method was needed to seal the gap between the indenter and the shield.

4.2.1.4 Prototype design 2

4.2.1.4.1 Design brief

Reduce the moisture in the vicinity of the diamond indenter and the sample stage. The method employed should not cause significant drift on the depth signal of the indentation equipment (NanoTest). The sample stage will retain the PVC reinforced sleeve as used in the previous prototype.

4.2.1.4.2 Design

The second prototype design had to be significantly changed, so that the purging gas would not flow into the system and then be exhausted directly onto the capacitor plates of the NanoTest. A thin gold sheet was considered to be a perfect solution to be flexible enough to seal the gap between the indenter and the shield. Thus the gas entering the system would be contained in the system and exhausted out of an exit hole on the opposite side to where it had been purged into the system. To assist the prototype development cycle a thin plastic cling film was used as a temporary solution until a final design had been reached and then this would be exchanged for the thin gold sheet.

The shield was placed onto the instrument with the cling film in place directly covering the indenter mount on the NanoTest. A Berkovich indenter was then inserted into the indenter holder by piecing the cling film with the indenter shaft. This provided an integral seal between the shield and the indenter holder. The PVC sleeve was then linked and sealed against the front of the shield.

Two flow meters where used in the system. The first flow meter controlled the incoming purge gas and the second flow meter was place on the exhaust of the system.

4.2.1.4.3 Results

The purging worked well and the sample was able to be cooled below zero degrees without frosting appearing on the sample surface.

However with the gas flowing into the system it was impossible to balance the pendulum. The flow meters were used to regulate the gas through the system. However this had no benefit on being able to balance the NanoTest pendulum.

4.2.1.4.4 Discussion

Using the two flow meters proved to be an effective way of removing the moisture and an argon or nitrogen shielded atmosphere was able to be produced. The small volume enabled the moisture to be rapidly removed.

The delicate thin cling film seal proved to be an effective barrier preventing exhausting the cold purging gas directly onto the capacitor plates of the NanoTest. However, when the gas was purged into the system the cling film expanded and changed the balance of the pendulum. This was detrimental to obtaining any nanoindentation data. This method was not going to provide a solution to effectively purge the area around the sample and indenter. It was decided not to trial the thin gold sheet and look to another approach to purge the system.

The PVC sleeve with wire reinforcement was not providing an adequate seal to be able to prevent

the moisture in the ambient air from penetrating back into the system

4.2.1.4.5 Conclusion

- Water vapour was being purged from the system to allow cooling of the system to -5 ^{o}C. To enable a useful tool for use by materials scientists a range of 20 ^{o}C to -30 ^{o}C would be preferable.
- Purging gas was causing an expansion of the cling film seal between the shield and indenter mount. This therefore rendered the measurement part of the NanoTest inoperable.
- A different approach was needed to enable successful purging of the system.
- PVC sleeve would have to be replaced with a more robust method to seal between the sample stage and the indenter of the system.

4.2.1.5 Prototype design 3

4.2.1.5.1 Design brief

The design needs to be able to purge the system including the NanoTest parallel capacitator plates, so that they are at a constant temperature with the purging gas shield. The seal between the sample stage and the indenter needs to be robust and be able to be easily disconnected so that additional samples can be tested.

The whole of the purging design needs to be able to be removed easily so that other options on the NanoTest can be used for different experiments in the future.

4.2.1.5.2 Design

The third prototype design involved encapsulating the whole of the NanoTest pendulum and magnet. This had been avoided in the past to try and simplify the setup of the purge when switching between other operating modes on the NanoTest. The NanoTest also incorporates system damping to enable low force measurements to be performed; therefore this had to be included when purging the system as it fits at the bottom of the pendulum.

A Perspex chamber was designed so that all the parts above could be contained in the purged environment. A PVC bellows was specifically design and this was then outsourced to KMK Compensators, UK to construct. The bellows was convoluted and had flange seals at both ends. These where attached to the Perspex purging chamber by means of a flange bolted to the front of the chamber. This can be seen in more detail in Figure 4.1. Stainless steel rings could also be placed inside the bellows to prevent them from contacting the sample cooling stage, if in the future a pump was used in order to remove the air in the chamber and backfill it with the purge gas (argon or nitrogen). This would enable to achieve a faster purge time to the desired dew point level. Rings could also be fitted to the outer side of the bellows so that the system can be pressure purged without the x-axis motor on the NanoTest system being forced out of its holdings when the system was pressurised.

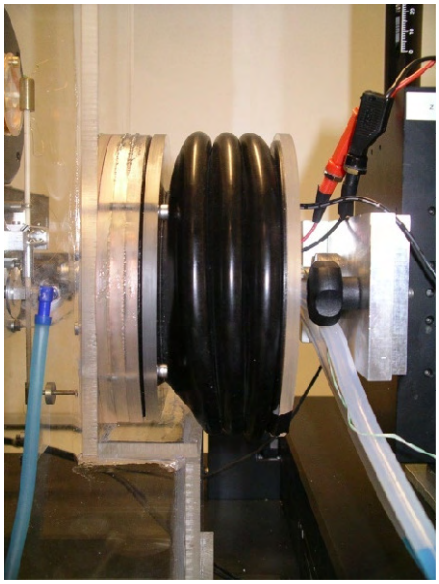

Figure 4.1 Bellows and flange arrangement

To enable the purge chamber to be quickly removed a magnetic seal would be used to attach it to the frame of the NanoTest. Magnetic strips where bonded onto the NanoTest and then a similar strip was attached directly onto the purge chamber. This provided an easy method for users to attach the chamber to carry out sub-ambient measurements.

Figure 4.2 shows the prototype purge chamber with the cold sample stage installed.

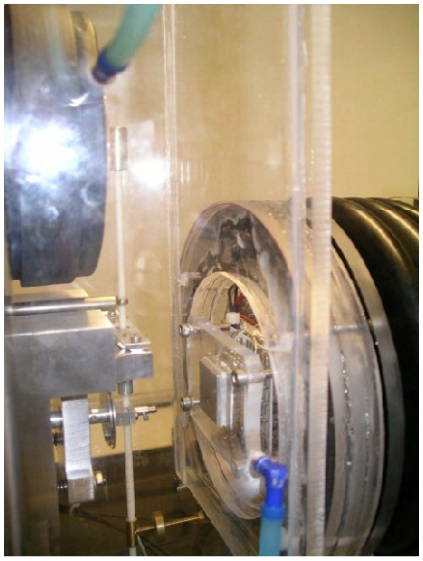

Figure 4.2 Prototype purge chamber with sample cooling stage

4.2.1.5.3 Results

The magnetic seal was poor and leaked heavily around the base. The inlet and outlet pipes worked well, however having the inlet directly aimed at the indenter meant that at high flow rates vibrations could be seen on the pendulum. At low flow rates the chamber worked well and cooling to -10^{o}C without frosting was possible.

The bellows achieved an excellent seal and were able to be purged at a high flow rate without bursting.

4.2.1.5.4 Discussion

The purging system was easy to setup and the bellows could be perfectly sealed against the face of the purge chamber. This method was excellent however the design was let down by the magnetic seal of the chamber to the frame of the NanoTest system. In order to be able to pressure purge the system a better method of sealing the chamber to the NanoTest frame would be needed.

The main issues occurred at the corners between the base of the NanoTest and its back plate. O-ring seals would be used in order to be able to achieve the moisture levels to cool to -30 ^{o}C. Also the chamber should only seal on one face of the NanoTest system, which would mean that the damping assembly would have to be adjusted in the next design.

The clear Perspex chamber enabled full view to make the initial contact of the experiment and ensured easy visual verification of any potential frosting on the sample surface. (See Figure 4.3)

The new bellows were very flexible and enabled full movement of the X-Y-Z axis stage.

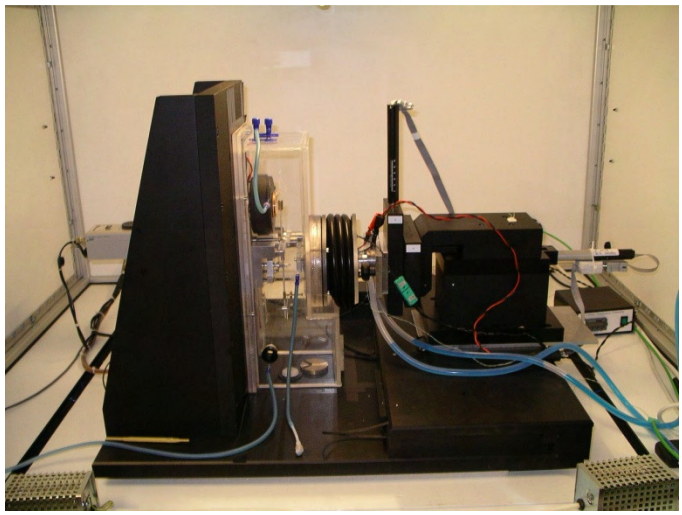

Figure 4.3 NanoTest fitted with Perspex purging chamber

4.2.1.5.5 Conclusion

- A further iteration will be necessary to enable a working prototype to a temperature of -30 ^{o}C
- The custom bellows worked well to give full movement of the sample stage.

- The seal to the chamber with a flange was a reliable method of joining the bellows to the purge chamber.

4.2.2 Final design

4.2.2.1 Design and fabrication

The sub-ambient temperature instrument has been designed especially to be compatible with a commercial nanomechanical test instrument (NanoTest platform from Micro Materials). The purpose of this chapter is to describe the development and implementation of the new validated test capability.

The design comprises of three main areas; (i) electronics for the cooling of the samples and the indenter, (ii) a purging chamber for eliminating condensation problems arising during the in-service condition testing, and (iii) low vibration cooling loop to enable vibration free measurements.

4.2.2.1.1 Electronics for the cooling of the samples and the indenter.

4.2.2.1.1.1 I.1. Peltier coolers

The cooling was provided by multistage thermo electric coolers (TEC) otherwise known as Peltier coolers [73]. The 3 stage TEC enables a greater temperature gradient between the top

surface and base of the TEC so that lower temperatures can be achieved. In recent years miniature multistage TEC's have been developed for laser diode applications in physics, these enable a TEC to be mounted onto a pendulum operated nanoindenter. A similar design with single stage TEC was proposed by Asif and Pethica for a vertical loading nanoindenter, in their study they heated and cooled the sample from 17 ^{o}C to 60 ^{o}C [26].

A miniature TEC was employed to cool the diamond indenter. This was extremely lightweight, and attached behind a (pyramidal) Berkovich indenter. The cooling setup for the indenter side cooling (Figure 4.4*)* consists of a Berkovich diamond, with a K type thermocouple attached close to the tip, for accurate temperature feedback. This is then attached to a TEC, using a two part cement. The full cooling setup is then bonded to an aluminium heat-sink, which has a pin machined on the reverse. This pin is used to mount the cooler into the holder of the nanoindenter. The heat-sink is cooled via convection of argon gas being passed over it during the tests.

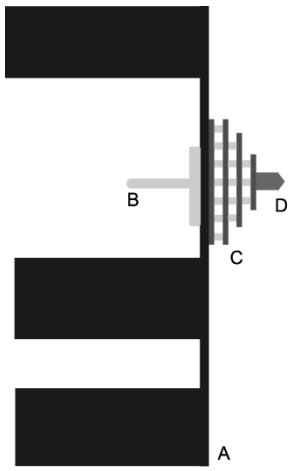

Figure 4.4 Indenter cooling Stack

The side for cooling the test samples has a larger TEC to aid in cooling of multiple samples. The cooling unit for the sample side is a stack design as shown in Figure 4.5. It consists of a 20x20 mm aluminium sample holder, which is sandwiched on top of the TEC, with a Perspex cover to hold it in place. Behind the TEC is a copper water-cooled heat-sink. An aluminium rod is then attached to the reverse of the heat-sink with a M3 tapped centred hole in its base to enable it to be attached to a standard holder of the NanoTest platform.

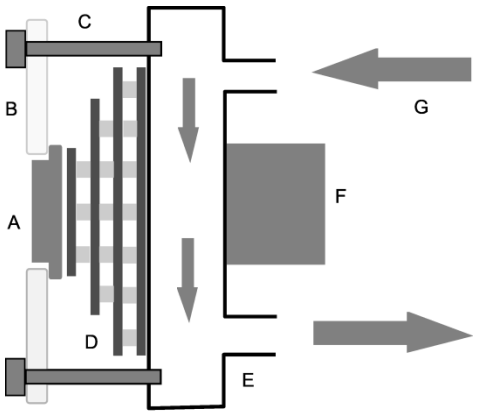

A. Sample Plate
B. Perspex Clamp
C. Clamp Blots
D. TEC
E. Water Cooled Heat Sink
F. Stub
G. Water Flow Direction

Figure 4.5 Sample cooling Stack

4.2.2.1.1.2 Temperature control

The TEC's used for this development are both multistage TEC's as referred to earlier. The indenter TEC is a miniature 3 stage TEC manufactured by Marlow Inc (Dallas,USA) with a ΔT of 96 ^{o}C. The sample TEC consists of 3 stages and is manufactured by Laird Technologies (Missouri, USA) (formerly known as MELCOR).

The TEC's are both powered from a temperature controller custom designed at the University of Birmingham. This has two channels, with each channel controlling a separate TEC, enabling them to be operated independently of each other. This increases the flexibility to tailor the experiment design. For example in other nanomechanical test techniques nano-scratch and impact testing it might be useful to set different temperatures to the indenter and samples in order to simulate different contact conditions. Having two channels was also beneficial in testing and when verifying the instrumentation during its design and development.

The custom temperature controller consists of a power circuit with two PID loop controllers (Eurotherm (Worthing, UK)). Each channel has a dedicated Eurotherm which controls the power output to its individual TEC. The Eurotherms have an "autotune" feature to enable a temperature to be tuned using the PID features of the Eurotherm. [74] This autotune enables a temperature to be easily set and regulated. Once the temperature has been reached and stabilised, the value of the power output can be read from the Eurotherm and then manually programmed into the Eurotherm ignoring the PID control.

K type thermocouples are used to measure the temperature of the TEC's; the readings are then fed back to the temperature inputs of the Eurotherms so that the testing temperature can be reached and regulated, and finally a manual power setting programmed.

4.2.2.1.2 Purging chamber for eliminating condensation problems at below ambient conditions.

A purging chamber (Figure 4.6) is used to prevent water condensing on the sample surface,

during the cooling of the samples. This fully encloses the pendulum indenter system of the NanoTest shown in Figure 4.7. The aluminium purging chamber was designed to encapsulate the whole pendulum system of the NanoTest platform while leaving the bulk of the electronics for the measurement un-purged. The chamber was designed to a bulk head specification, with o-ring seals machined into the flange which are sealed onto the NanoTest.

Windows were also incorporated into the design to:-

1. enable the users to observe the initial contact of the indenter with the surface
2. ensure that different samples could be located for testing.
3. provide access, for routine maintenance, changing samples, and changing indenters.

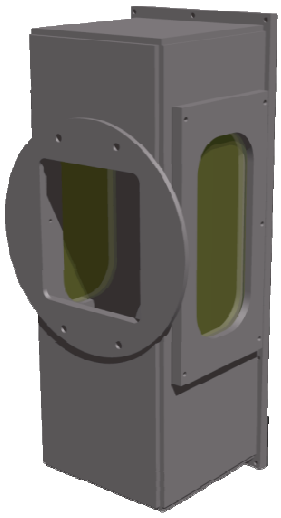

Figure 4.6 Purging Chamber

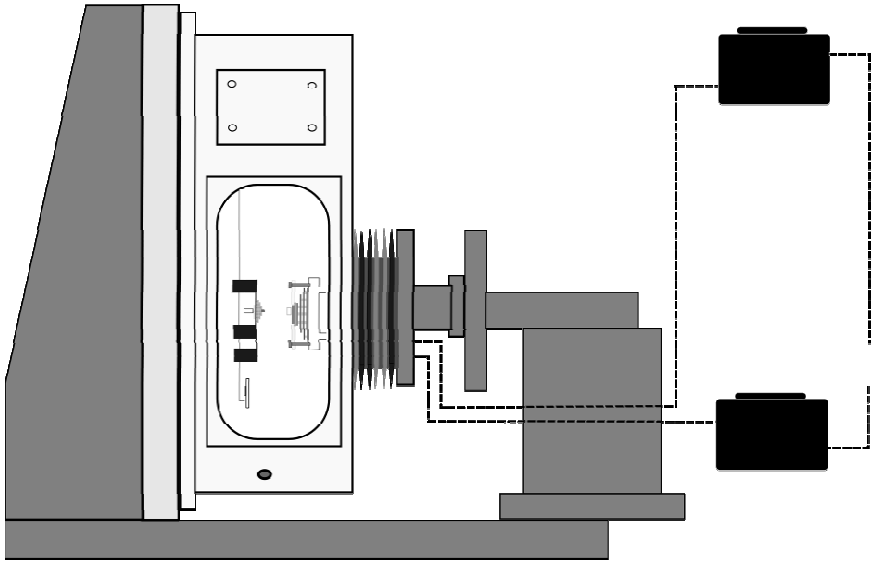

Figure 4.7 Sub-ambient temperature stage chamber encapsulating pendulum and water loop to cool sample TEC

Borosilicate (Pyrex) windows were used, so that the system could be baked out to remove any water vapour that may be stuck to the surfaces.

The damping plate of the NanoTest system (a design feature to enable improved low load performance) had to be raised off the baseplate onto a 30 mm solid aluminium shelf. This provided a place to securely mount the nano-impact module providing capabilities in the future for sub-ambient temperature impact test measurements to be obtained Figure 4.8. A removable plate was added to the left hand side of the purging chamber to enable a gas outlet valve to be attached. This plate was made purposely larger than necessary in order that it could be taken off and have additional holes machined. This was essential for any extra measurement or electronic fittings that may have required to be added to the purging chamber during the initial prototyping of the system.

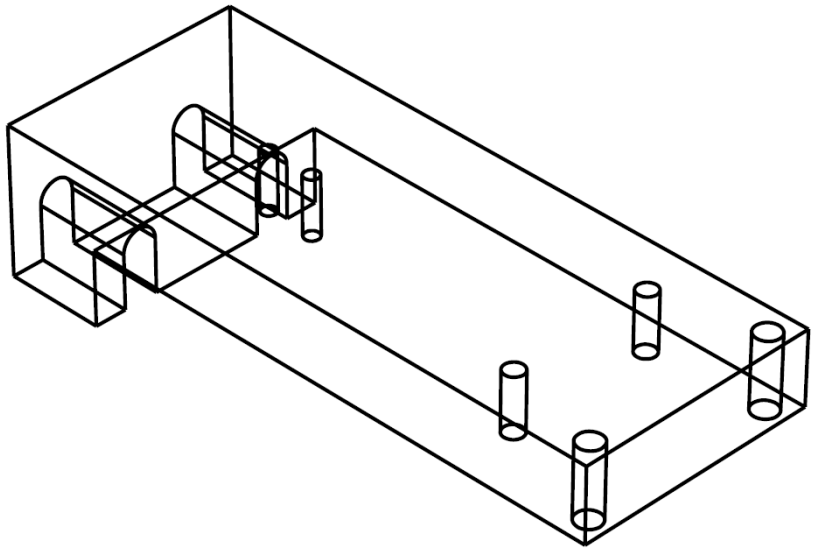

Figure 4.8 Damping Plate

A cylindrical cover was designed for the limit stop of the nanoindenter and this was secured to the reverse of the NanoTest plate, along with a small cover to seal the large M8 bolt that holds the NanoTest magnet in position. The hole for the coaxial cable leading to the capacitor plate was sealed permanently with epoxy resin. Figure 4.9 and Figure 4.10 respectively.

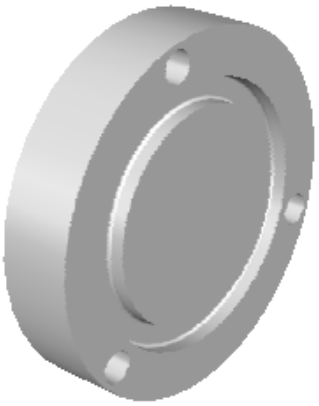

Figure 4.9 Magnet bolt cover

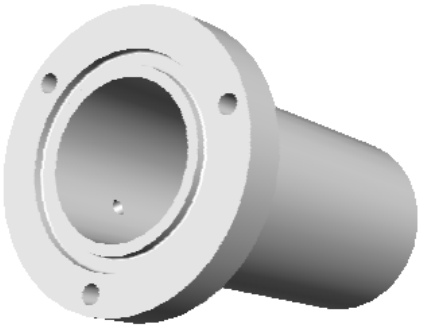

Figure 4.10 Micrometer limit stop cover

The gas inlet was positioned on the left hand side face of the chamber, near to the base, this enables argon to be purged on an open loop, into the chamber and expelled at the top, through the outlet valve to create a positive purge.

As detailed in Figure 4.7, a PVC bellows forms a perfect seal between the front of the chamber and the XYZ stage of the nanoindenter allowing for full movement of the motorised stages. It is connected to the purging chamber using an Al flange, which is closed tight using four M4 nuts that bolt on to studs located at the front of the chamber. The second flange on the reverse of the bellows contains connections for a water-cooling loop, further details on the specification of the water loop will be given in the next section. Electrical connections for the thermocouples and power for the sample side cooling are also integrated into this flange.

4.2.2.1.3 Low vibration water cooling loop to enable vibration free measurements.

The TEC for the indenter cooling is relatively small and so can be cooled via gas convection.

However higher demands are placed on the TEC used to cool the samples. This must be cooled with a cooling loop [75] i.e. forced cooled. For this a gravity-fed water loop was developed to provide vibration-free water to the heatsink of the sample cooling stack. Water is fed to the heatsink as shown in Figure 4.7 via 8mm ID hoses. The heat is then dissipated to a large tank of water and mechanically pumped to a second tank of water placed above the system to provide fresh cold water to repeatedly cool the stack for vibration-free measurements.

4.3 Validation of the system

4.3.1 Validation

Validation tests were carried out on a calibration sample of fused silica, which was obtained from the instrument manufacturer (Starna Scientific Ltd. Essex UK). Tests were carried out on fused silica over the temperature range to show that the machine was calibrated, and capable of testing over the set range.

The cold indenter had a tip radius function ($A_c = 6800\ h + 29\ h^2$), equivalent to a Berkovich diamond indenter with a rounded cap tip. Figure 4.11 shows the Youngs modulus (E) of the fused silica sample. The E was determined by unloading curve analysis using the Oliver and Pharr procedure [12].

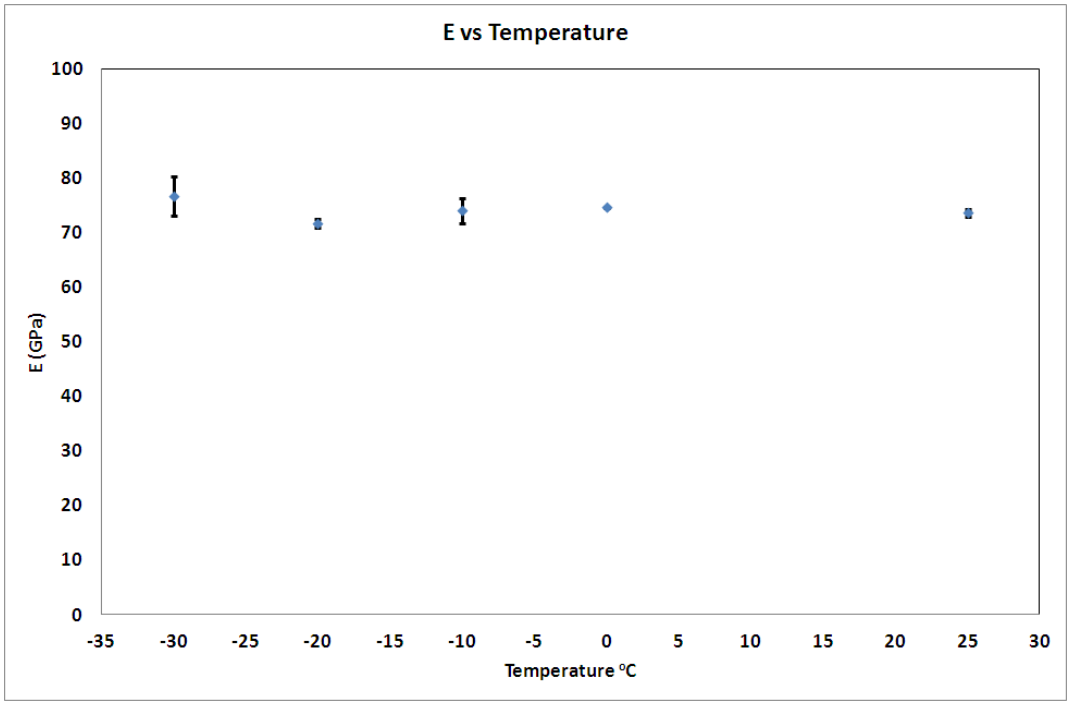

Figure 4.11 E (GPa) of fused silica taken at range of sub ambient temperatures.

When cooling, the system must be purged so to avoid water condensation on the sample surface, and secondly to enable the TEC's to perform more efficiently [76]. Figure 4.12 shows the results of the atmosphere contained in the purged chamber. This was measured using an MKS environmental quadrapole. (MKS Instruments UK Ltd, Crewe, UK)

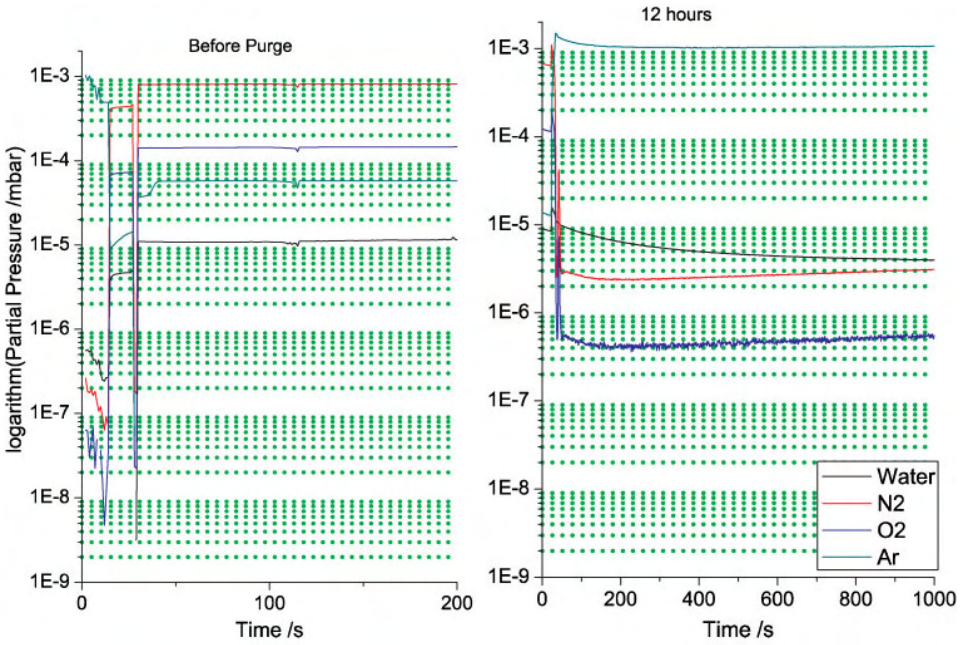

Figure 4.12 Results before and after purging measurements taken with an environmental quadrapole manufactured by MKS.

To extract reliable mechanical data from the load displacement curve the data must be free from environmental effects.

Figure 4.13 demonstrates the minimal effects that the argon purging gas and cooling water loop had on the tests carried out in this paper.

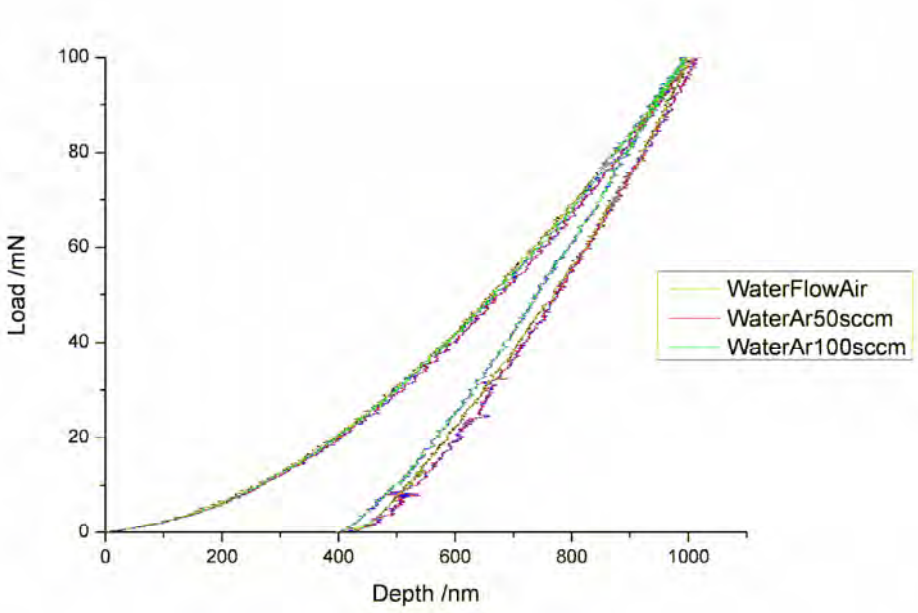

Figure 4.13 Figure 6 Water and Argon flowing while performing nanoindentation curves show minimal effects to the obtained curves.

Further tests were carried out using the 'auto tuning' features of the Eurotherms [74] to provide automatic temperature control and using manual tuning to keep the current temperature using a fixed power output. Figure 4.14.

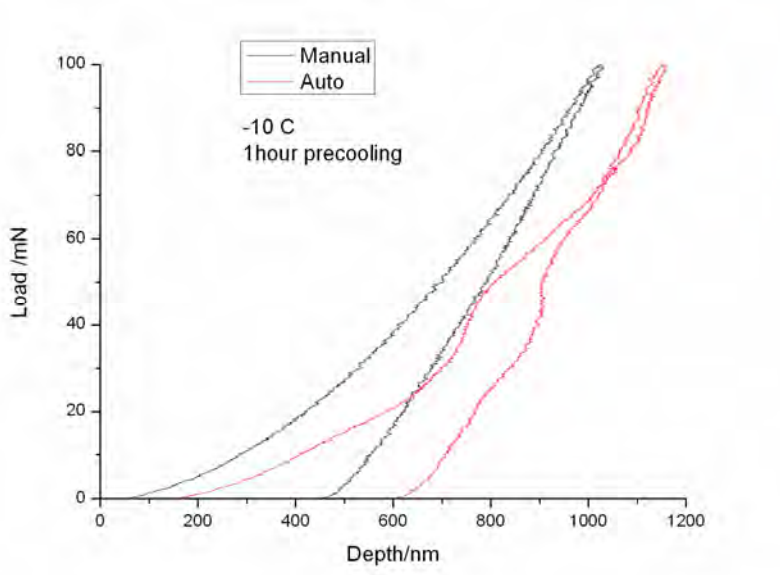

Figure 4.14 Manual and auto tuning of the temperature and the effects on the unloading/ loading curves of the instrument.

4.3.2 Case studies

Application studies have been successfully carried out on Polypropylene using the developed instrumentation to demonstrate the nanomechanical behaviour through the glass transition temperature -18 ^{o}C [77].

Interesting studies on the mechanical and tribological properties of DLC at sub-ambient temperatures have also been carried out to reveal significant changes with temperature on this metastable material, this is a research area which has not yet been explored by utilising nanomechanical probing of the mechanical properties [78].

4.3.2.1 Discussion

The inlet of Argon is located at the bottom of the front plate, while the outlet is at the top of the front plate. As the Argon possess a higher molecular weight (39.948 amu) than most major gases in the air including O_2 (31.999 amu), N_2 (28.013 amu) and water vapour (18.015 amu). With the controlled flow rate, the chamber can be filled with pure argon gradually. Even though the pendulum has a relatively small mass, it has been found that the argon flow up to 250 sccm shows no effect on the movement of the pendulum. The gravity water loop has been shown to remove the heat from the TEC effectively. The water flow can be well-controlled to reduce the noise to the depth signal.

Dual side cooling is needed because of the experimental drift on the indentation curves if measurements are performed without both the indenter tip and sample being cooled. This follows findings during nanoindentation at the high temperatures [5,60,79,80]. An example Finite Element model in Figure 4.15 illustrates the need for a cold diamond has been produced. Individual temperature values have been plotted vs. time for positions above and below the diamond as shown in Figure 4.16. As expected, the diamond initially cools and the sample initially heats up. Since the diamond holder is thermally connected to the outside world only via the specimen and the surrounding air, there is no heat being conducted downwards from the instrument frame. Therefore in practice the temperature gradient would be even more pronounced than that shown. Measurements were taken with the new sub-ambient instrumentation.

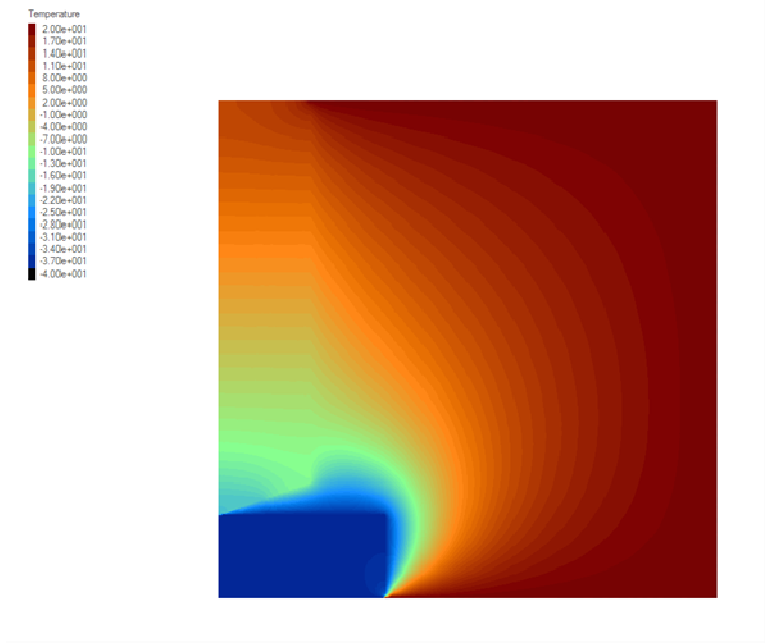

Figure 4.15 Temperature distribution for Fig. 4a after 5 s

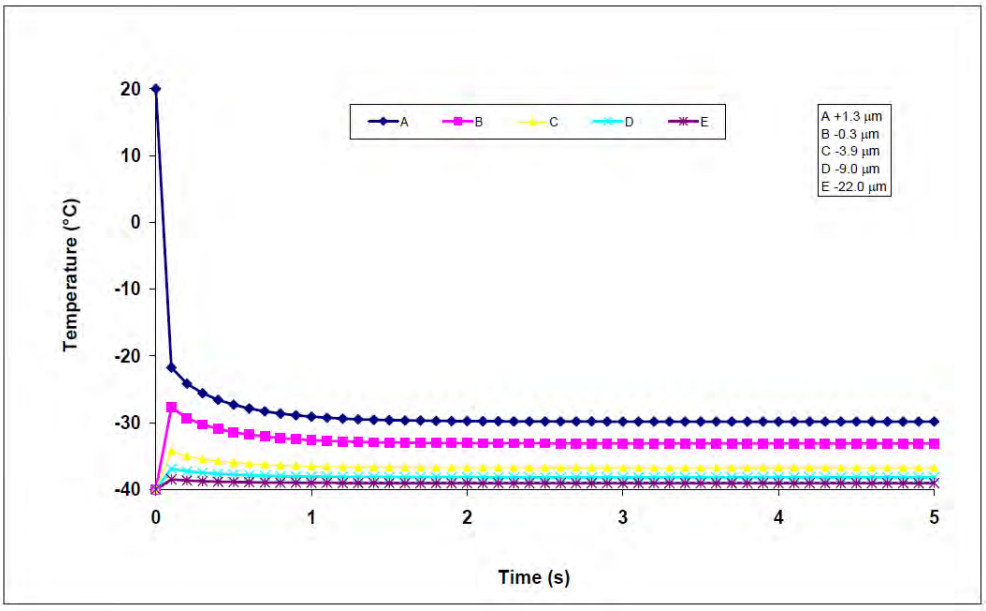

Figure 4.16 Change in temperature with time at different points along the diamond axis. The legend refers to locations relative to the diamond tip.

With suitable indenter cooling, the Elastic modulus results from the tests over the sub ambient temperature range on fused silica compare well to those reported by NIST [81] over the same temperature ranges using another technique, ultrasonic resonance.

The results clearly show that the addition of cooling water and an argon purging loop had minimal effects on the overall fused silica curves. It was established that a purging of 50 sccm of argon gave the optimum results without affecting the pendulum mechanism of the instrument as demonstrated in

Figure 4.13.

Aluminium was chosen for the final prototype chamber as it provided effective purging combined with a reduction in overall weight. This enabled the chamber to be removed quickly and easily to perform other nanomechanical tests when required. Subsequently flexible heaters could be used to bake out the system, which further reduced the moisture content. If users required to use this method to rapidly purge or to reach lower ppmV levels of moisture Pyrex windows were specifically required to withstand bake out temperatures

The MKS results show that the levels of oxygen and water dramatically reduce after the chamber has been purged. Two measurements were taken using the MKS instrumentation; these are presented in Figure 4.12 which shows the pressures inside the MKS versus time. The initial measurement with a time period of 200 s shown on the LHS of Figure 4.12 was taken as the purge chamber was fully sealed. The positive purge was not started until this measurement had

been taken. The second measurement, (plotted on the RHS of Figure 4.12), shows the gaseous environment contained in the purging chamber after positive purging with argon at a rate of 100 sccm for 12 hours. The duration for the second measurement was 1000 s. The extended measurement time indicated that the purge environment had stabilised after the initial12 hours and that further purging with argon gas would not improve the water vapour levels. The pressure drops indicated by the two plots in Figure 4.12 show that the purge has been successful. The TEC's on the indenter and sample stage were only turned on after the 12 hour purge. During the first 30 s the MKS has not been flushed with the environment contained in the purge chamber so measurements are the residual gas remaining in the MKS instrumentation indicating the high pressure levels and sudden pressure drops as the MKS initialises.

The amount of water vapour was also verified using a Michell moisture monitor as 300 ppmV. A normal user would not require the sophistication of the MKS instrument. A hygrometer such as the Michell moisture monitor would be sufficient to enable users to perform nanoindentation measurements at sub-ambient temperatures. During the development it was beneficial having the MKS to be able to carefully calibrate the purging system to refine the amount of argon flow and length of time needed for an optimum purge.

It was discovered that auto tuning using the Eurotherms alone would not provide a stable temperature for nanoindentation results to be achieved. A temperature could be programmed using the auto tune, and then a manual power lock setting was inputted into the Eurotherm, to provide stability when performing the actual measurements. If auto tuning was used without a further manual power lock measurement curves obtained on fused silica tended to have (1)

increased depths and (2) non-uniform loading and unloading curves that result in unrealistic values for reduced modulus and hardness if they were to be analysed Figure 4.14 demonstrates curves resulting from a manual power lock and auto-tuning.

In the future it would be beneficial to expand the work by integrating computer controls via Labview (National Instruments) for the purging of the system, and design a multi gas purging system, to test samples in different atmospheres.

The option to use state of the art JT Cooling devices, to extend the testing temperature range and achieve temperatures down to -150 ^{o}C could also be explored.

4.3.2.2 Conclusions

In conclusion, a sub-ambient temperature instrument has been appropriately designed, developed and successfully tested. The design consist of three main areas; (i) electronics for the cooling of the samples and the indenter, (ii) a purging chamber for eliminating condensation problems arising during the in-service condition testing, and (iii) low vibration cooling loop to enable vibration free measurements.

The results follow NIST data provided for fused silica. An important ultra low vibration cooling has been designed which will benefit users. A purging system and optimum parameters have been developed and tested for a horizontal loading system. A significant finding is that purging and cooling has no effect on the operation of the instrument.

After extensive testing a combination of auto and manual tuning is best for controlling the cooling at the nanoscale. The instrument has the potential to be utilised in testing of surface

engineered systems and polymeric materials for applications in aerospace and electronic industries. There is the possibility of developing the work further by exploring the use of computer controls and to increase the testing temperature ranges to as low as -150 ^{o}C which will expand the possibilities for exploitation.

In conclusion a sub-ambient temperature testing instrument has been designed and a working prototype constructed and developed. This instrumentation will enable researches to carry out various nanomechanical and nanotriboloical testing from ambient to -30 ^{o}C.

Tests have been carried out on fused silica, with results matching those obtained through other techniques reported by NIST [81]. It is demonstrated how to build a sub-ambient prototype and case studies are presented of experiments carried out on surface engineered materials and bulk polymers.

4.4 Applications

4.4.1 Polymers

4.4.1.1 Abstract

Mechanical properties and creep behaviour of an atactic-polypropylene (aPP) have been studied in the vicinity of its glass transition temperature (-18ºC) via a nanoindentation platform integrated with a sub-ambient temperature capability. All low temperature tests were validated by measurements on a fused silica reference sample from 25ºC to -30ºC. The fused silica results showed virtually invariant elastic modulus with temperature over this range consistent with literature measurements by sonic resonance. Hardness and elastic modulus of aPP increased as

the test temperature decreased and the amorphous regions went through the glass transition. The creep behaviour was analysed using two approaches: (i) a logarithmic method, and (ii) the Boltzmann integral method. The results showed that the creep extent decreased as the temperature was reduced, and for the time constants obtained there were upper-limit values at -10ºC, about 8ºC above the quoted glass transition temperature. The strain rate sensitivity obtained by the logarithmic method also showed a maximum at -10ºC.

4.4.1.2 Introduction

A popular engineering polymer, polypropylene, is in the rubbery state at room temperature. Its mechanical properties are expected to vary strongly with reducing temperature as it transforms to the glassy state [82–85] i.e. when the material passes through its glass transition temperature. Moreover, polypropylene shows temperature-dependent viscoelastic behaviour under loading. Thus its time-dependence around the glass-rubber transition temperature is also of interest in this study.

In light of the above comments, a newly-developed sub-ambient temperature capability based on the commercial NanoTest platform^{TM} (Micro Materials Ltd. Wrexham, UK) was therefore utilized to investigate the mechanical properties and creep behaviour of polypropylene around its glass-rubber region. Likewise, there are other researchers [86–89] analysed the creep data assuming the steady-state creep strain rate follows a power law. Of particular significance in this study, two different approaches were adopted to analyze the temperature-dependent creep behaviour of the polypropylene.

4.4.1.3 Experimental

The test materials were fused silica and atactic-polypropylene (aPP). The fused silica was obtained from the instrument manufacturer (Starna Scientific Ltd. Essex UK) with a quoted Young's modulus of 72 GPa. The aPP was obtained from ENSINGER Ltd, Mid Glamorgan, UK [90] with a quoted glass transition temperature of approximately -18ºC. A Berkovich indenter was used for all tests. Indentations were load-controlled to different peak loads at various loading rates as shown in

Table 4.1. The loading history included a hold at peak load before unloading in order to minimize the influence of viscoelastic deformation during subsequent unloading. For aPP, this hold period was set to 20s, and displacement data at constant load was collected during this period to analyse the creep response of the aPP. The Oliver and Pharr method [12] was used to extract hardness and elastic modulus values from the unloading data. Unloading rates were set equal to the loading rates. The separation distance between indentations was 35μm and each test was repeated 5 times.

Table 4.1 Nanoindentation test conditions

No.	Sample	Peak Load (mN)	Loading rate (mN/s)	Loading time (s)	Hold period (s)	Temperatures (ºC)
1	FS	100	5	20	5	RT (25)
2	aPP	50	25	2	20	0
3	aPP	50	10	5	20	-10
4	aPP	50	2.5	20	20	-20
5	aPP	50	1	50	20	-30

To study the time-dependent behaviour of aPP at different temperatures, the creep data were analysed and fitted using two approaches: (i) the logarithmic method discussed in Refs. [29] and [30] , and (ii) the Boltzmann integral method discussed in Refs. [27,31–33] The logarithmic equation can be expressed as

$$d = A\ln\left(\frac{t}{\tau_L}+1\right) \qquad \text{Equation 4-1}$$

where d is the increase in depth at maximum load, t is the time at peak load, A and τ_L are termed the extent parameter and the time constant, respectively. Equation 1 can also be expressed as the creep strain

$$\frac{d}{d(0)} = \frac{A}{d(0)}\ln\left(\frac{t}{\tau_L}+1\right) \qquad \text{Equation 4-2}$$

4.4.1.4 Results

Fused silica was used as a reference sample and tested from room temperature (25ºC) down to -30ºC. To ensure isothermal contact conditions, prior to indentation the diamond was held at the specimen surface for 5 to 30s under minimal load. The recorded loading-unloading curves show good repeatability. The elastic modulus (E) is found to be (72 ± 2) GPa over the temperature range +25 to –30ºC which agrees with the data in Ref [81].

The hardness (H) and elastic modulus (E) results of aPP were measured at different loading rates and temperatures. Indentation tests with the highest loading rate 25mN/s (corresponding to only

2s loading time) resulted in approximately 10% higher modulus for all temperatures studied. There was no clear difference in H and E between the three slowest loading rates, 10mN/s, 2.5mN/s and 1mN/s (loading time 5s, 20s and 50s, respectively). The average values of H and E of aPP were therefore determined from these and are shown in Figure 4.17. It is clear that the hardness and elastic modulus increased as the testing temperature decreased. The scattering of data can be attributed to the relatively high surface roughness of aPP (Ra ~0.67 μm). To minimize the effect of the roughness, a high testing load of 50mN was used. The corresponding maximum depth was about 4000 nm, significantly higher than the Ra value.

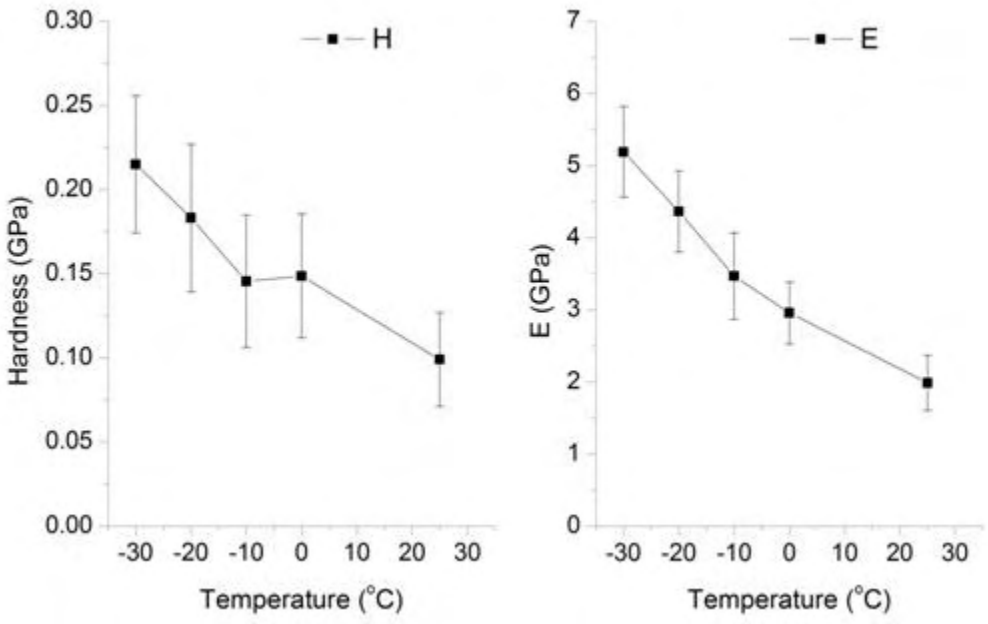

Figure 4.17 Averaged hardness and elastic modulus of aPP tested at different temperatures.

Figure 4.18 illustrates a typical quasi-logarithmic creep curve. The curves obtained at all test temperatures were of this conventional continuous form, with no discrete relaxation events such as those reported by Ngan on PE [91].

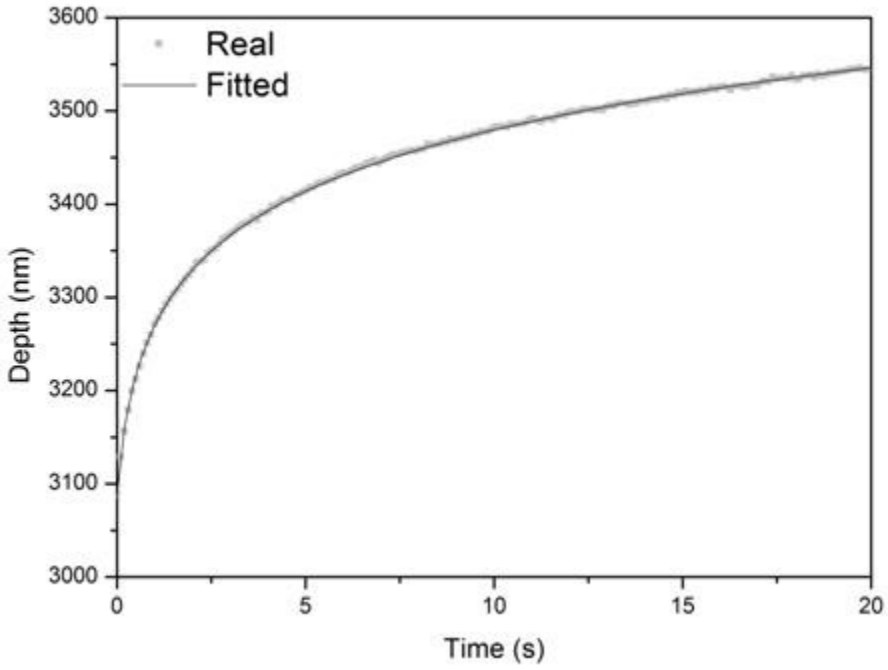

Figure 4.18 Superimposed experimental creep data and logarithmic expression. Testing conditions: (i) load 50 mN, (ii) loading rate 25mNs−1, (iii) temperature −10 ◦C; fitting parameters: A = 97.47 nm, B = 5.46 s−1; d(th = 0) = 3088.1 nm.

Figure 4.19 shows typical creep curves at different temperatures after constant loading at a rate of 25mN/s. It can be seen that the initial depth before the hold period has been reduced upon decreasing the temperature. The creep depth measured at different conditions (temperature and loading rate) is shown in Figure 4.b. It can be seen that the total creep depth during the hold period decreased with decreasing temperature and loading rate.

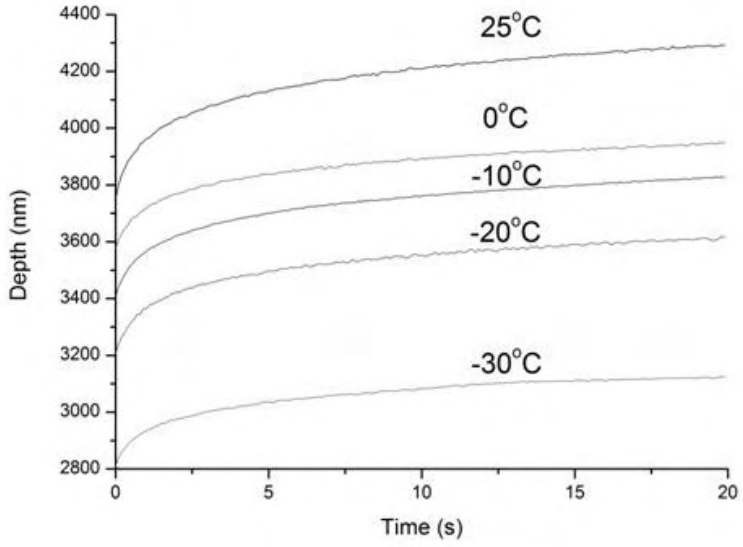

Figure 4.19 (a) Illustrative penetration depth during hold period for the loading rate = 25mNs−1; (b) increase in penetration depth during hold period at different testing temperatures.

4.4.1.5 Discussion

4.1 Hardness and elastic modulus on aPP

The elastic modulus values for the fused silica reference sample were essentially independent of the test temperature over the range studied. This result is in agreement with studies using sonic resonance reported by NIST [81], which also show virtually invariant properties of the fused silica over this range. These results provided validation of the performance of the nanoindentation test capability to -30ºC.

Figure 4.17 shows that the hardness and elastic modulus of aPP exhibited the expected strong dependence on the testing temperature. The increase in H and E can be attributed to the transition of the amorphous regions in the semi-crystalline aPP from a 'rubbery' state at room temperature

to a ‘glassy’ state as the temperature was decreased to its glass transition temperature (-18ºC).

The scatter in the measured H and E values of aPP (Figure 4.17) can be attributed to the high level of surface roughness. This effect was alleviated by employing relatively high loads (and hence penetration depths). At 50mN the maximum depth at peak load decreased from ~4800nm at 25ºC to ~3000nm at -30ºC. Tweedie et al. have recently reported that contact loading may increase the glass transition temperature, so that polymers below their bulk glass transition temperature may exhibit significantly higher than expected stiffness, particularly when the penetration depth is under 200 nm [92], consistent with other reports of increasing elastic modulus on polymeric materials as the indentation depth is reduced. Brostow et al.[2,93] also found densification inside the scratching groove for polypropylene, resulting in increased hardness. Tweedie et al. suggest that the contact loading creates an interfacial region of confined molecular mobility, adjacent to the probe, either via intermolecular interactions or via stretching or alignment of macromolecular chains. Nevertheless, the contribution of this modified region to the overall mechanical response of the bulk polymer decreases with increasing contact depth. To exclude this possibility, a series of comparative indentations at the testing load 25mN was also carried out; the resultant values of E were essentially identical to those at 50mN within the experimental error. The measured increase in E at sub-ambient temperatures does not appear therefore to be overestimated due to the decreasing indentation depths at 50mN.

It has been suggested elsewhere that the combination of a slow loading rate, long hold and fast unload can minimize artefacts in modulus determination on viscoelastic materials. The constant hardness and modulus observed on aPP for indentations at 1, 2.5 and 10mN/s suggests the

presence of the 20s hold period was effective in minimizing the influence of viscoelasticity on the measured hardness and modulus for these slower loading rates. The hold period was sufficiently long to avoid the presence of any 'nose' shape – as observed by Ngan and others for shorter holding periods [88,89,94,95] – even with the slowest unloading rate, 1mN/s.

In contrast, at the highest load rate of 25mN/s, the peak load was reached in only 2 s and the resultant modulus values were about 10% higher than at the other loading rates for all temperatures. The influence of visco-deformation on the measurement of the unloading contact stiffness has been discussed in [29,94] and the applicability of the Feng & Ngan compliance correction equation (Equation 4-3) [94] has been investigated.

$$\frac{1}{S} = \frac{1}{S_u} + \frac{\dot{D}_h}{\left|\dot{P}\right|} \qquad \text{Equation 4-3}$$

where S is the contact compliance, S_u is the elastic contact stiffness at the onset of unloading, $\dot{D}_h$ is the indenter displacement recorded at the end of the hold period, and $\left|\dot{P}\right|$ is the unloading rate at the onset of unloading.

However, after application of this equation the calculated modulus (Ec) showed a much stronger dependence on the loading/unloading rate with a minimum in Ec at 10mN/s - about 40% less than at 1mN/s. It appears that this correction may not be suitable for our testing conditions as (1) our hold period 20s is ten times higher than that used in [95], (2) our tests also involved different loading rates and Equation 4-3 does not allow for that. The higher E at 25 mN/s is a result of the smaller depth at the end of loading period (D_{max}). At room temperature, the maximum depth for

the loading rate of 25mN/s (~4200 nm) was much less than for the other loading rates of 1 to 10mN/s (4480-4750 nm). The depth after creep for the 25 mN/s tests was extrapolated to 70s using the logarithmic equation to investigate whether the apparently higher E was simply a result of a shorter total loading time before unloading. The corresponding maximum penetration depth was about 4350 nm - considerably less than those from the tests using the slower loading rates. It is possible therefore that the indentation behaviour of polypropylene shows a more complex dependence on loading rate. It could be explained by an increase in yield strength of polypropylene with the strain rate [83]. Thus extra energy could be required for plastic deformation during indentation. Similar behaviour has been observed on uniaxial PET previously[51].

4.2 Creep analysis

As described in the Experimental section, the creep behaviour was studied using the logarithmic method and Boltzmann integral method. All hold periods were fitted well using the logarithmic equation (Figure 4.18).

The variation in the creep extent parameter (A) with temperature from indentations with a loading time of 20s is shown in Figure 4.20. The dimensionless parameter (A/d(0)) has been considered as a measure of stain rate sensitivity [37], which enables meaningful comparisons of different testing conditions. Our results are shown in Figure 4.21. It can be seen that the value of A/d(0) is between 0.028 and 0.032 over the entire temperature range, with the highest A/d(0) at -10ºC . The creep time constant (τ_L) from the loading time 20s has been plotted against the testing temperatures in Figure 4.20b. It is clear that there is also a maximum τ_L value at -10ºC.

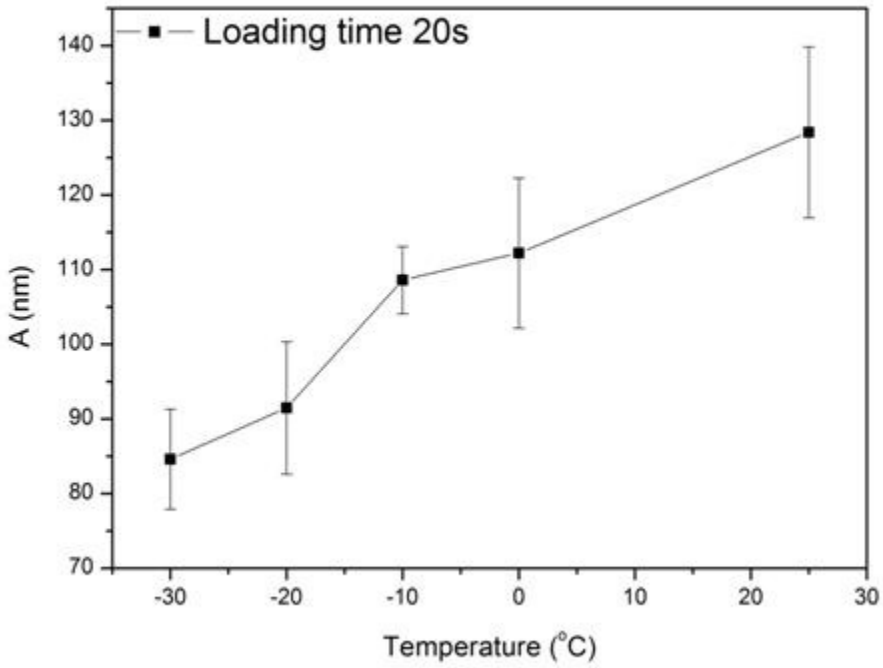

Figure 4.20 Creep extent parameter (*A*) versus test temperature fitted using logarithmic equation.

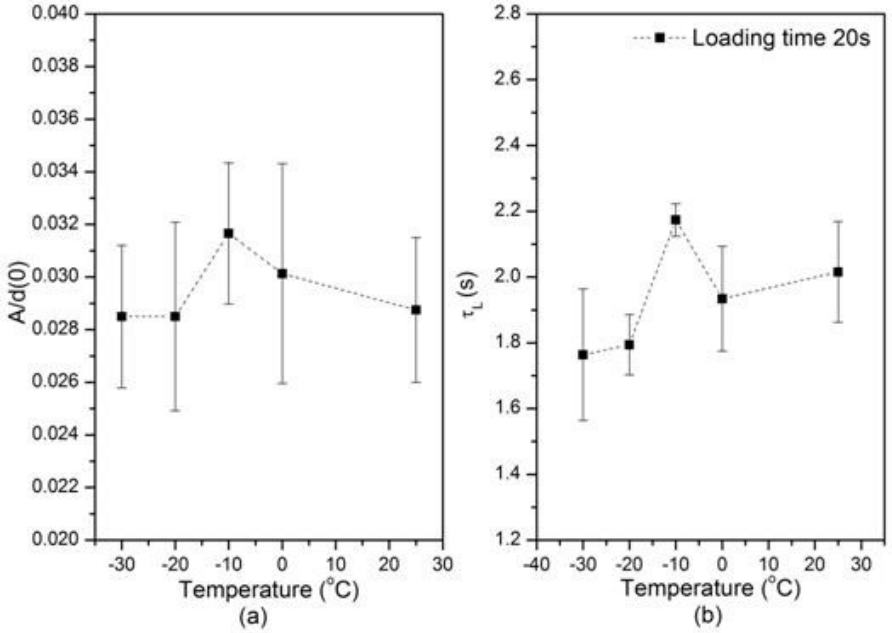

Figure 4.21 (a) Creep strain rate sensitivity (A/d(th = 0)) versus test temperature and (b) creep

time constant (τL) versus test temperatures fitted using logarithm equation.

It has been shown previously that the actual time to reach the maximum load influences the creep kinetics dramatically [30]. When a constant loading rate was considered for each particular temperature, it was found that τ_L increased with increased loading rate, exhibiting a power law relationship as shown in Figure 4.22.

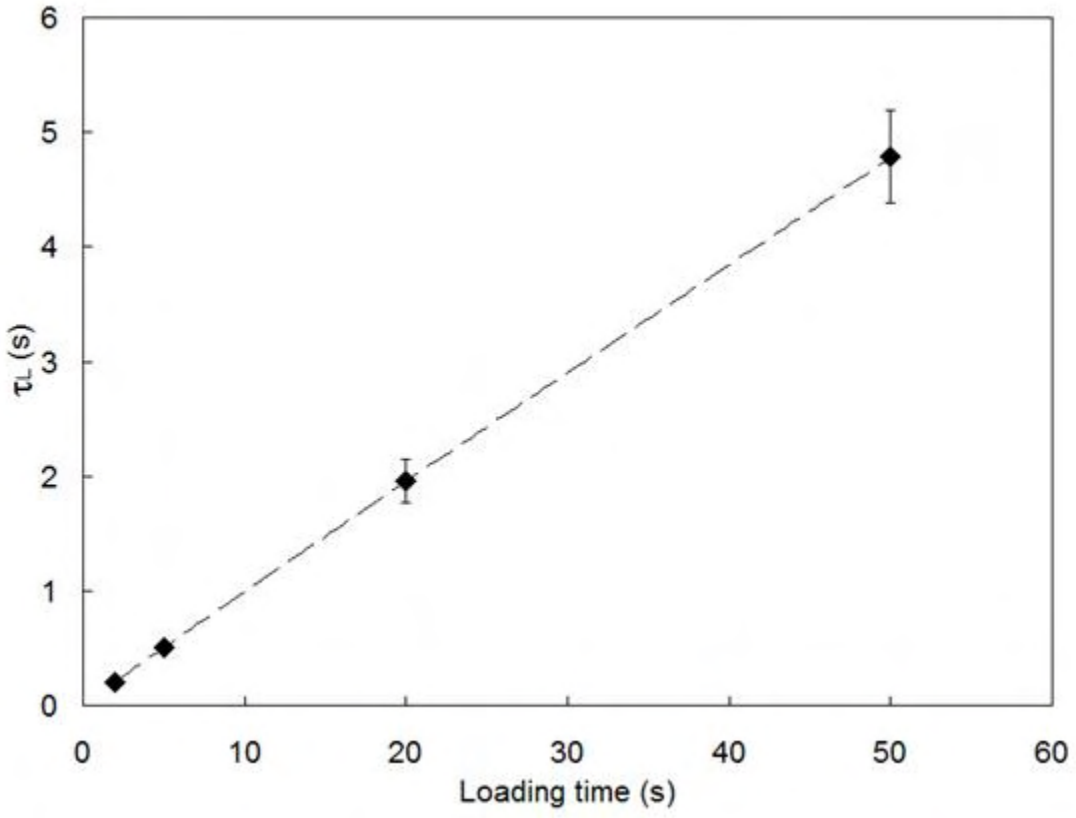

Figure 4.22 Superimposed experimental creep time data (τ_L) and the power-law fitted dash curve (y = 0.105x0.976, R2 = 1).

Clearly, the correlation coefficient (and Figure 4.22) indicates that the experimental creep data is extremely well described by the logarithmic equation. The fitted creep extent parameter, A,

decreased with decreasing the test temperature. The dimensionless creep strain sensitivity, A/d(0), and the creep time constant, τ_L, showed upper-limit values appearing at -10ºC. At the same time, the creep time constant, τ_L, showed a power law relationship with the loading time.

The creep data has also been fitted using the Boltzmann integral method. The adjusted square of the correlation coefficient (R^2) is shown in Figure 4.23. We can see that the quality of fit is improved upon decreasing the loading rate.

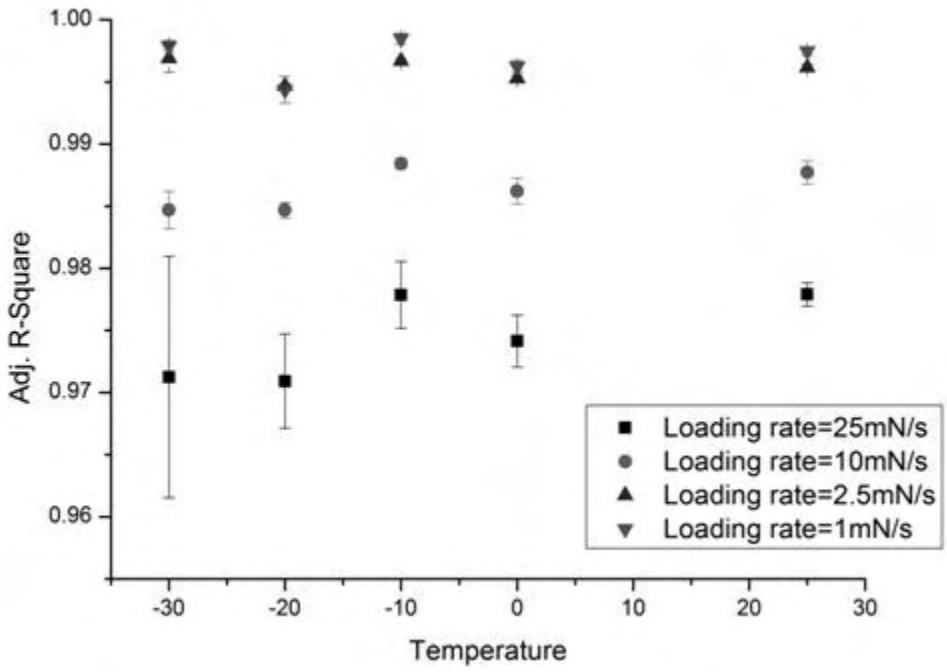

Figure 4.23 The results of adjusted R-square for the Boltzmann integral fitting.

As shown in Figure 4.24a, the time constant (τ_B) also reached a maximum at -10ºC. This indicated that both methods are effective for revealing the effect of glass transition on creep. The time constant also strongly depended on the loading rates. Figure 4.24b shows that the time

constant (τ_B) at -10ºC exhibited a power-law relationship with the loading rates, which agree the results of Figure 4.22.

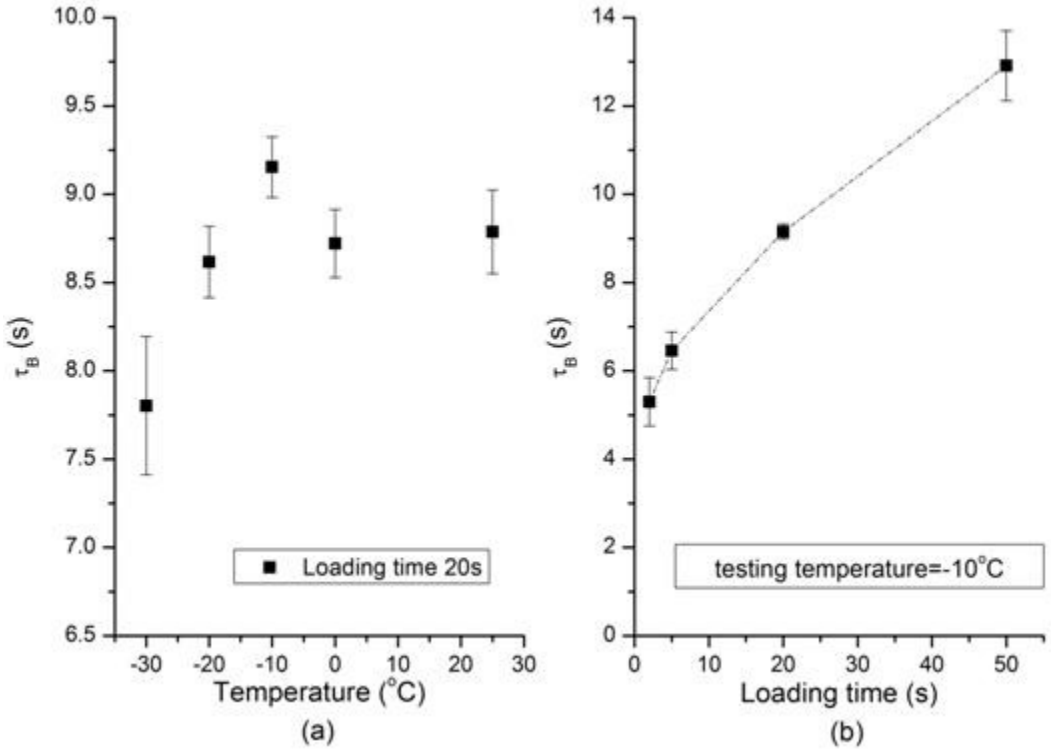

Figure 4.24 (*a*) Creep time constant (τB) versus test temperatures and (*b*) Superimposed experimental creep time data (τB) versus loading time fitted using Boltzmann integral equation and the power-law fitted dash curve ($y = 4.105x0.271$, $R2 = 0.962$).

The fitted variables c_0' and c_1' are shown in Figures 10.a and 10.b. We can see that c_0' decreases with the temperature. As c_0' is proportional to the instantaneous elasticity, this is consistent with the measured E (Figure 4.17) increasing as the temperature decreases. The creep extent (c_1') showed strong dependence on temperature and loading rate, as agreed by the fitted creep extent (A) in Figure 4.20 obtained using the logarithmic equation. More creep occurred for higher

loading rates and temperature.

The creep mechanism in polymers is explained by the Eyring theory as proposed by Berthoud et al. and Tweedie et al. [53,55]. For a creep event to occur, the polymer chains must overcome a potential barrier by thermal activation at a particular reaction rate. At higher temperatures, the thermal barrier is easier to be overcome and thus the movement of the polymer chains, such as translation and rotation becomes easier than at lower temperatures. Therefore, the creep extent parameter (c_1) would be expected to decrease with a decrease in testing temperature. As the viable (c_1') is proportional to c_1, it decreases with decreasing temperature as shown in Figure 10.b.

An assumption is made the creep extent (c_1) obeys an Arrhenius relationship:

$$creep\_extent = k \exp\left(\frac{-Q}{RT}\right) \qquad \text{Equation 4-4}$$

where k is constant, R is the gas constant, T is the Kelvin temperature and Q is the activation energy. After taking logarithms, the activation energy Q_B (Boltzmann integral method) can be obtained from the slope (-Q/R) of the ln(c') vs. 1/T curve as shown in Figure 11. The calculated Q_B is 11.0±2.9kJ/mol.

As shown in Figure 4.21 and Figure 4.24a, in the temperature range considered there were maximum values of A/d(0) and τ_L using the logarithmic method, and τ_B for the Boltzmann integral method, at -10ºC. In reference [55], the creep stain sensitivity (A/d(0)) for a range of

amorphous and semi-crystalline polymers was related to the difference between their glass transition (T_g) and testing temperatures. Similarly for the present work, these parameters indicate a property change around T_g.

The peak values of A/d(0), τ_L and τ_B were found at -10ºC, 8ºC above the supplier quoted T_g (-18ºC) of the studied aPP. As described in reference [84], reported glass transition temperatures for polypropylene are influenced by a wide range of factors, such as sample tacticity, sample crystallinity and chain length, as well as the measurement technique used. As an example, in Dynamic Mechanical Analysis measurements (DMA),the peak in tan delta is typically offset to a few degrees higher than the T_g determined from the inflexion point in the storage modulus versus temperature graph [7,30]. It has been suggested previously that, based on previous ambient and elevated temperature measurements on semi-crystalline and amorphous polymers, changes in A/d(0) are correlated with changes in the tan delta peak [96]. It is notable that the offset in A/d(0) (and the time constants) from the glass transition appears the same (typically ~8-10ºC) for elevated temperature, ambient temperature and sub-ambient nanoindentation measurements for a wide range of polymers.

The peak values of A/d(0) and τ_L for the logarithmic method at -10ºC are about 9% and 16% higher, respectively, than the average of the others. The greater increase in τ_L is consistent with the data in [8] that the parameter τ_L was more sensitive than A/d(0) to changes in the glass transition region. As mentioned above, the average value of τ_L from all the tested temperatures can be fitted well to a power law relationship vs. loading time. This agrees with the finding [96] that the power law fit for aPP is a better fit than a linear relationship and it is not possible to

determine a measurable creep cut-off time from the indentation measurements.

4.4.1.6 Conclusions

The hardness and elastic modulus of atactic-polyprolythene increased as the testing temperature decreased through the glass transition range and the polymer changed from rubbery to glassy.

The indentation creep behaviour of atactic-polyprolythene can be fitted well using both the logarithmic method and Boltzmann integral method.

- The creep extent (A and c'_1) decreased with decreasing test temperature.
- The time constants (τ_L and τ_B) increased with the loading time with a power-law relationship.
- A/d(0), τ_L and τ_B indicated a creep rate change at -10ºC, which is around the glass transition temperature;
- The fit for the Boltzmann integral method was better at lower loading rates.

4.4.2 DLC

4.4.2.1 Abstract

Previous work on low temperature tribological investigations was limited to macro-scale studies due to the lack of suitable instrumentation. This limitation has been overcome using a newly developed low temperature nanoscratch tester capable of characterizing the scratch resistance of coatings down to -30 ºC. The scratch resistance and mechanical properties of a functionally graded a-C:H(Ti)/TiCN/TiN/Ti coating have been investigated from 25 ºC to –30 ºC. It has been found that the a-C:H(Ti)/TiCN/TiN/Ti coating failed at high load by cracking and spallation in

the room temperature scratch tests. Fractography suggests these failures originate from or close to the interface between the top a-C:H(Ti) layer and the TiCN layer. Decreasing the test temperature from 25 ºC to 0 ºC, resulted in an increase in H, H/E_r and H^3/E_r^2, consistent with improved crack resistance and wear resistance, with smaller further improvements on decreasing temperature further to -30ºC.

4.4.2.2 Introduction

Scratch tests are widely used to study the mechanical properties, tribological behaviour and adhesion strength of coatings [97–99]. The scratch response is not an intrinsic property and depends on the testing system, including the physical properties of the testing materials and the indenter, loading mode and sliding velocity, and the environment such as the medium and temperature [100–102]. When materials are operated at low temperatures, their physical properties such as hardness and ductility can vary greatly from those at room temperature due to phase transition, thermal effect, etc. Low temperature scratch instruments have been developed to characterize the tribological behaviour at low temperatures [103,104]. These instruments are generally test at the macro-scale and are not suitable to micro- or nano-scale measurement. Recently, a nanoindentation instrument with a low temperature capacity (down to –30 ºC) has been developed [77]. The design aims to minimize/eliminate thermal drift and water vapor condensation problems. Both samples and indenter probe are cooled by two thermal-electrical coolers (Peltier elements). The whole system is encapsulated in a sealed chamber which is purged with pure dry argon to avoid water condensation. Following the similar philosophy, a nanoscratch system with low temperature capacity was developed and a schematic diagram of the nanoscratch system is shown in Figure 4.25.

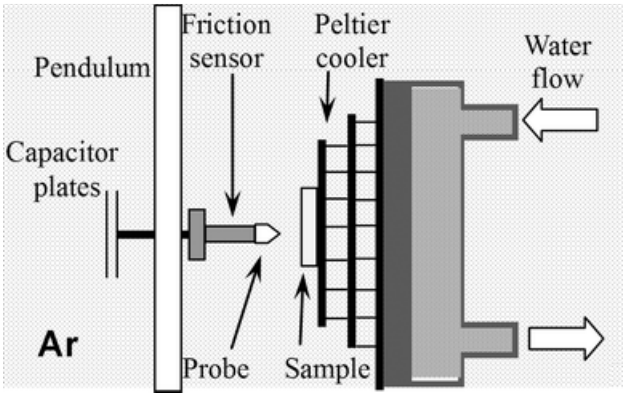

Figure 4.25 Schematic diagram of nanoscratch design

Carbon-based coatings such as DLC (Diamond like Carbon) are widely used for wear protection and friction reduction purpose due to their excellent mechanical and tribological properties (e.g. high hardness, wear resistance and low friction) [105–108]. However, the tribological properties of carbon-based coatings show strong environmental dependence. The effect of the test medium (water, oil, air or vacuum) on the tribological properties of DLC coatings has been extensively studied. In aqueous conditions, the wear resistance of the hydrogenated DLCs became worse [109,110] while the friction is reduced [110,111]. In oil conditions, the wear resistance of DLC coatings can be improved [110,112]. Velkavrh et. Al [113] reported that the oils with higher viscosity can reduce friction only in the high velocity range. Hydrogenated DLC exhibits ultra-low friction in vacuum in contrast to non-hydrogenated DLC coating which has high friction [114]. Oxidation was reported for a hydrogenated DLC by Eun et. Al [115] in a vacuum sliding test which resulted in an unstable low friction behaviour. Reduced wear resistance was found in vacuum for both non-hydrogenated DLC [116] and hydrogenated DLC [117]. Tribological tests were also carried out in humid air and it was found that the higher relatively humidity can increase wear resistance and the friction [116,118].

Since DLC coatings are essentially metastable, temperature can also play an important role. At elevated temperature, the sp^3 diamond bonds in DLC will transform to the sp^2 graphite bonds, thus deteriorating its tribological properties [119–123]. Increasing applications of coatings in aerospace, deep-sea environments require that these coatings possess the good low temperature properties and to ensure their suitability it is important to test their mechanical integrity at these temperatures rather than infer from the results room temperature tests.

It is widely reported that the DLC coatings can have a high residual stress that results in failure at high load [124,125]. The graded Ti/TiN/TiCN/Ti interface was designed to improve the interface shear strength [125,126] and the load bearing capacity. a-C:H coatings alloyed with Ti shows not only good self-lubricating properties in dry sliding conditions but also little sensitivity to relative humidity and independence of counterpart material and test atmosphere [127,128]. The a-C:H-Ti/TiCN/TiN/Ti may potentially be a good candidate coating system combining lubrication with good wear resistance in various conditions. Due to the absence of suitable nano-scale instrumentation its low temperature properties have not previously been investigated, so the recently developed instrumentation has been used in this study to investigate the temperature dependence of the mechanical and tribological behaviour of the graded DLC coating over the temperature range 25 ºC to –30 ºC.

4.4.2.3 Experimental

4.4.2.3.1 2.1 Materials

The substrate is M2 high speed steel with approximately 25x20 mm^2 in area and 2 mm thickness.

These samples were ground and polished with 6μm diamond paste prior to the deposition process. The a-C:H(Ti)/TiCN/TiN/Ti multilayer coating was produced using an unbalanced magnetron sputtering system (Teer 450/4 UDP system), described in detail elsewhere [129]. Initially, a layer of Ti of ~0.1 μm was deposited, then nitrogen was introduced to produce a ~1 μm layer of TiN. C_2H_2 was added gradually to produce TiCN layer ~1.2 μm thick. Finally the C_2H_2 flow was increased further to reduce the sputtering of Ti atoms due to the formation of compounds on the Ti target, so that a small percentage of Ti and hydrocarbon are sputtered simultaneously to produce the Ti-C:H layer (~1.2 μm).

4.4.2.3.2 2.2 Nanoindentation testing

Nanomechanical properties were measured at three different temperatures, room temperature (25ºC), 0ºC and -30ºC, using a NanoTest 600 platform (Micro Materials Ltd.) integrated with the sub-ambient temperature capacity. The experimental configuration is described in detail in reference [77,130]. The sample was attached to an aluminium block cooled by a Peltier cooler. The Berkovich diamond indenter was cooled by another Peltier cooler. The peak loads were 5 mN, 20 mN, 100 mN and 400 mN with a fixed loading and unloading time of 20 seconds and a 30 s dwell time at peak load. The mechanical properties including hardness (H) and reduced elastic modulus (E_r) were calculated from the unloading slope of the load-displacement curves using the Oliver and Pharr method [12].

4.4.2.3.3 2.3 Nanoscratch testing

The nanoscratch tests were performed at constant temperature with the test sample cooled by a thermal-electrical cooler. The indenter probe was attached to a tangential force transducer without

additional cooling. In order to establish the isothermal contact between the scratch probe and the cooled sample, the probe was kept at a distance about 5 μm away from the sample surface until a minimised heat flow is obtained. Prior to the scratch, the probe slid on the surface with a very low load to reach thermal equilibrium. The entire scratch assembly was encapsulated within an argon-purged chamber.

At room temperature, the nanoscratch test was carried out without purging. A spheroconical diamond indenter of 8 μm end radius was used. Prior to the test, the tangential force sensor was calibrated with sensitivity about 180mN/V. Machine compliance was calibrated at room temperature. The nanoscratch tests were carried out in the multi-pass mode at a constant speed of 1 μms^{-1} over a 100 μm track with (1) pre-scratch topographic scan, (2) a levelling distance followed by a ramped scratch and a constant scratch (3) a post-scratch low load scan. In the pre- and post-scratch scans, the applied load was sufficiently low (0.01 mN) that no appreciable deformation occurs ('off-load scans'). In the 'on-load' scratch scan, the low load (0.01 mN) was used for the first 20 μm to provide a baseline for subsequent leveling of the surface for contact pressure analysis. Then the load gradually increased up to the peak load (400 mN) at 8 mN/s, this stage covers the distance from 20 μm to 70 μm. In the last 30 μm, the load was kept constant at the peak load. The probe depth and tangential force were collected simultaneously during all the scans. Nanoscratch tests at each temperature were repeated five times.

4.4.2.3.4 Post-test examination

The groove volume in the whole track at 400mN was measured using a confocal microscope (Olympus OLS3100) to evaluate the wear resistance. The scratch marks and the cross-sectional

morphology of the fractured samples were studied using a JOEL 7000 scanning electron microscope.

4.4.2.4 Results

Three illustrative scratch tracks tested at 25 ºC, 0 ºC and –30 ºC are shown in Figure 4.26. At the ramped scratch stage (from 20 µm to 70 µm scan distance), the width of the tracks increased gradually but there was no clear failure of the coating observed for the range of temperatures tested at. In the constant load region of the scratch track (400 mN; 70 µm to 100 µm scan distance), tensile cracks and spallation appeared in the 25 ºC scratch tracks as demonstrated in Figure 4.26a. At lower testing temperatures, the occurrence of these failure modes decreased significantly.

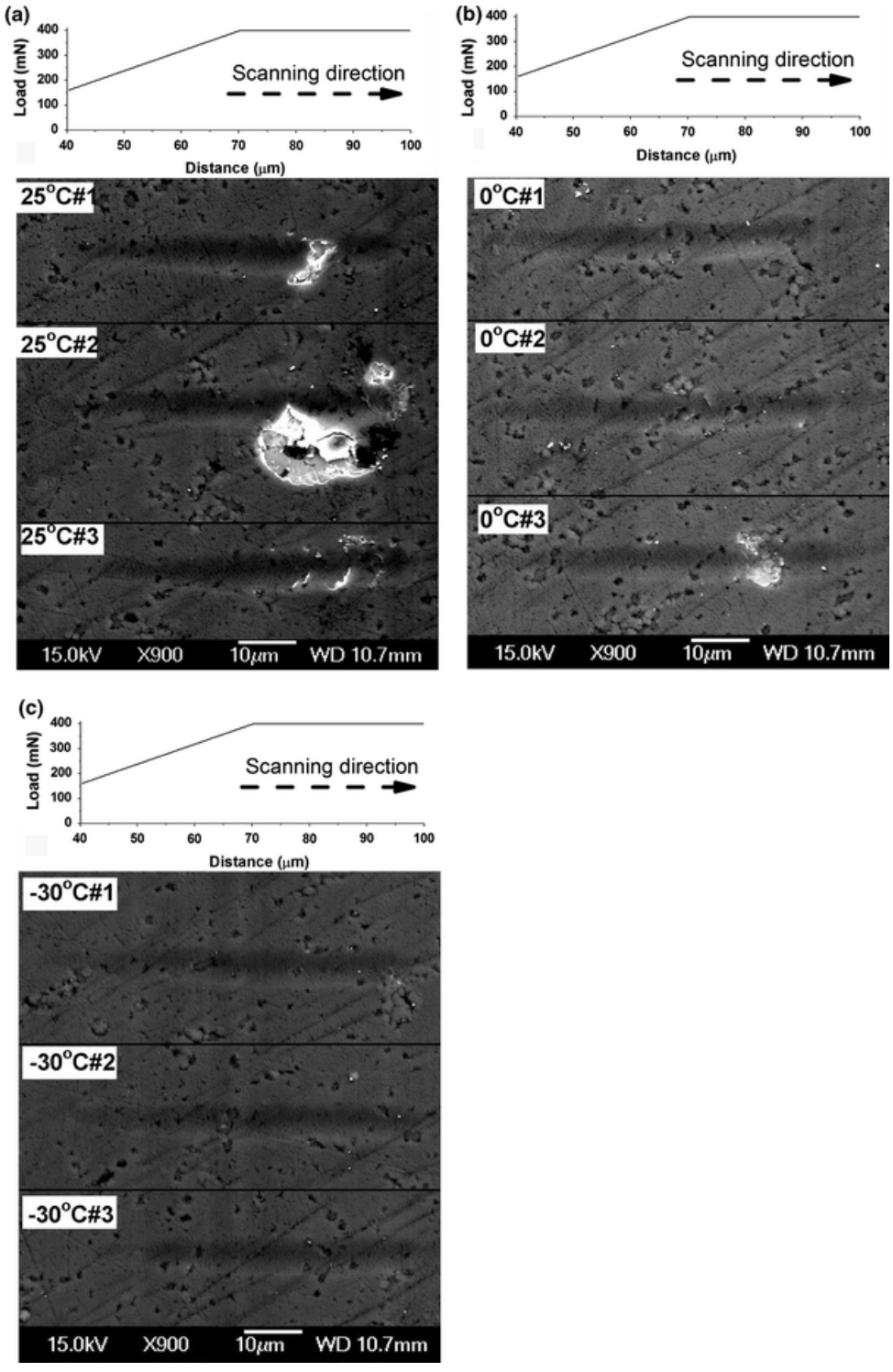

Figure 4.26 SEM Morphology of the scratch tracks produced at **a** 25 °C, **b** 0 °C, **c** –30 °C

A simple statistical analysis of the occurrence of the coating failures has been carried out for all the scratches (figure 3.a). The total number of the crack and spallation areas observed at each test temperature decreased from 7 and 2 at 25ºC respectively, to 1 and 1 at 0ºC respectively. The spallation area is also much larger at 25ºC (Figure 4.26b). At -30ºC, the coating shows good integrity and no cracks or spallation can be found as shown in Figure 4.26c.

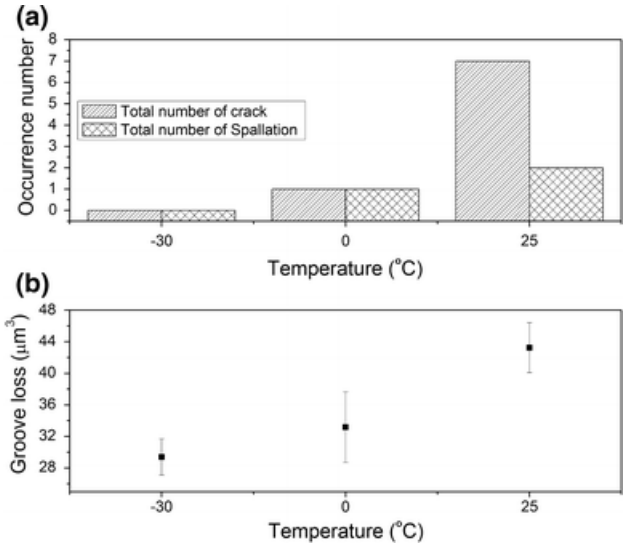

Figure 4.27 **a** Statistical results of the occurrence number of crack and spallation in the scratch tracks at different temperatures. **b** Groove volume in the scratch tracks at different temperatures

The scratch tracks at -30ºC also appeared shallower in Figure 4.26c. The groove volume in the whole track measured using the confocal microscope is shown in Figure 4.27b. It is clear that the groove volume decreases with the decrease of the testing temperature (the spallation area was not counted into the groove volume as it was dramatically increased when the spallation occurred).

During the ramped scratch region, the friction coefficient increased with the load. The top-layer carbon coating is still intact over the surface (Figure 4.26). There is only plastic deformation of

the coating without the failure, so the increase in friction coefficient is ascribed mainly to the greater ploughing at higher load. The recorded friction coefficient at the constant scratch stage is shown in Figure 4.28. It can be seen that the average friction coefficient of this coating at different temperatures are similar, at about 0.15. For the scratches tested at 25ºC and 0ºC, several big step changes were observed corresponding to the spallation failures. The fluctuation of the friction coefficient is caused by the rough surface, R_a = (46 ± 13) nm.

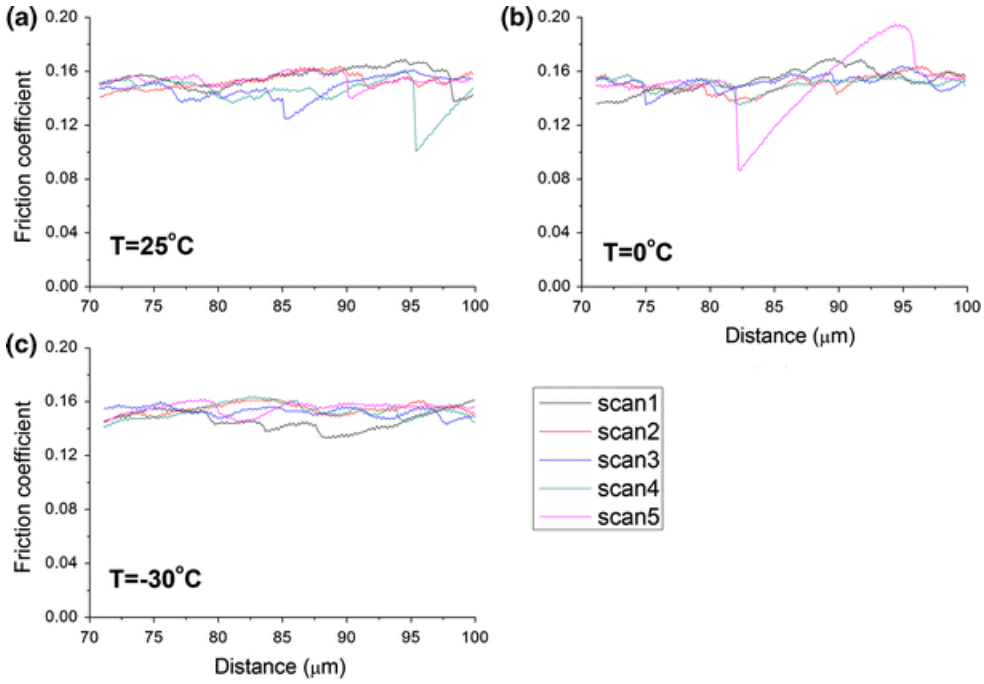

Figure 4.28 Friction coefficient at the constant scratch stage tested at different temperatures **a** 25 °C, **b** 0 °C, **c** –30 °C

Figure 4.29 shows the mechanical properties measured using the nanoindentation platform at different temperatures. It can be seen that the hardness (Figure 4.29a) was increased when the temperature reduced from 25ºC to 0ºC. With further reduction in the test temperature to -30ºC, the hardness does not increase further. The reduced elastic modulus (Er) in Figure 4.29b does not

show clear change against temperature under all loads. The H/E_r and H^3/E_r^2 ratios (Figure 4.29c and Figure 4.29d) also prove the clear increase when the testing temperature decreased from 25ºC to 0ºC, the further decrease in temperature brings slightly increase in the H/E_r value.

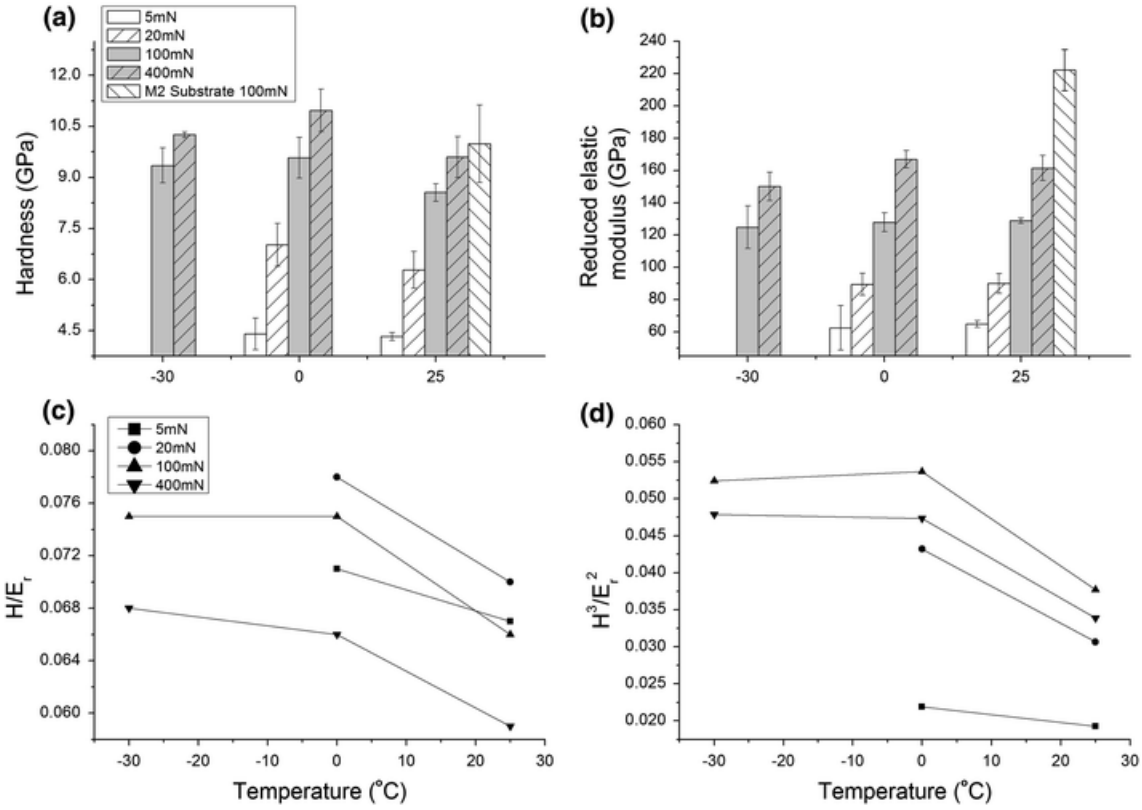

Figure 4.29 The mechanical properties of a-C:H(Ti)/TiCN/TiN/Ti coating at different temperatures **a** hardness, **b** elastic modulus, **c** H/E_r, **d** H^3/E_r^2

4.4.2.5 Discussion

The a-C:H(Ti)/TiCN/TiN/Ti coating has a lower hardness (Figure 4.29) than most reported DLC coatings whose hardness is commonly over 10GPa [125]. The ratio of sp^3 to sp^2 bonding was measured by Raman spectroscopy analysis and the sp^3 fraction was found to be as low as 50%. Such relatively low content of sp^3 bonds may be attributed to the relative low deposition energies

as discussed in references [105,131]. Pei et. al. [132] also reported that the hardness of a nc-TiC/a-C:H coating without bias during deposition is about 5.5GPa which is similar to our result. The ceramic sub-layers, TiCN and TiN, normally possess higher hardness (>20 GPa) and elastic modulus (>350 GPa) [133–137], which were significantly higher than the carbon coating. The M2 high speed steel substrate also possess higher hardness (9.9 ± 1.1 GPa) and reduced elastic modulus (222.2 ± 12.8 GPa) than the carbon coating. Therefore, the subsequent hard coating layers provide strong loading support. The coating system can be described as a soft lubricant coating on a hard substrate, instead of a hard coating on a soft substrate.

As shown in Figure 4.29, both H and E_r increase with the increase of the peak load reflecting the increasing contribution of the harder and stiffer ceramic sublayers and the substrate. The maximum penetration depth (δ_m) was around 160 nm, 310 nm, 660 nm and 1300 nm at 5 mN, 20 mN, 100 mN and 400 mN, respectively. It is known that the measured H and E_r of the coating using the Oliver and Pharr [12] method can be misleading, especially for a thin film. It is often suggested that the relative indentation depth (RID), the depth of indentation divided by the coating thickness, should be less than 10% of the coating thickness to obtain coating hardness independent of the substrate [138]. However Chen and Bull [139] found that the critical relative indentation depth where coating hardness can be obtained independent of the substrate, depends on the coating system. For a soft coating on hard substrates, the plastic deformation zone in the substrate may occur when the RID is much higher than 10% depending on the mechanical properties of the coating and the substrate [139]. Thus the coating can be assumed to behave as a bulk material before the substrate is plastically deformed. The radius of the plastic zone (R_p) can be estimated using the method proposed by Chen and Bull [139,140] as shown in Equation 4-5

for an ideal Berkovich indenter.

$$\frac{R_p}{\delta_m} = -12.907\frac{H}{E_r} + 4.5451 \qquad \text{Equation 4-5}$$

The calculated R_p is about 0.6 μm, 1.2 μm, 2.5 μm and 5.0 μm, corresponding to the peak load, 5 mN, 20 mN, 50 mN and 400 mN. At 5mN the plastic zone is well within the top a-C:H(Ti) layer so no plastic deformation occurs in the sublayers or substrate. With the increase of the RID, the plastic deformation zone extends into the sublayers, the hardness increased rapidly because both elastic and plastic deformations of the sublayers tend to increase the hardness of the composite [139]. When the peak load reached 400 mN, the influenced volume in sublayers increased and the substrate M2 steel started to deform plastically which also contributes to the increase in measured hardness. Thus the hardness increases gradually with an increase of RID.

As shown in Figure 4.26a, the a-C:H(Ti)/TiCN/TiN/Ti coating is more susceptible to cracks and spallation during highly load scratching at 25 ºC than at lower temperatures (0 ºC and –30 ºC). The depth information for the scratch mark (25ºC#2) as shown in Figure 4.26a was analysed using a 3D-confocal microscope. It has been found that the maximum depth at the spallation area is about 1 μm, which is close to the interface between the top a-C:H coating and the TiCN sub-layer. The maximum shear stress appeared below the surface according to the Hertz theory [141]. Thus, the cracks can initiate from the weak area such as the interface between these sub-layers.

Drees et al. [109] have found the catastrophic failure of a-C:H coatings in water-lubricated tests.

Similar findings were reported by Ronkainen et al [128]. However, the dramatic failures of a-C:H coatings were attributed to different explanations. Ronkainen et al. claimed that it is due to a rapid increasing wear process, while Dress et al. attribute to the adhesive failure at the coating/substrate interface. For a-C:H alloyed Ti coating, it has been found that the interface can endure in the aqueous environment [128]. Thus the interface strength depends on the composition and structure at the interface. In this study, although the nanoscratch at room temperature was carried out at ambient conditions with relatively higher humidity than those at lower temperatures, the dramatic failure of the coatings at the interface is not affected by the different humidity but the mechanical properties of the interface.

It was found by Uhure et. al. [142] that the surface roughness shows no clear effect on the critical load for the coatings on the 220 grit, 1000 grit and 1 micron finished substrates during ramped load scratch tests. Similar findings were reported in [143] that the critical scratch normal load (L_c) stays as constant when the surface roughness R_a >500nm. However, the film adhesion is related to the angle between the scanning direction and the grinding marks [143]. When the scratch is orientated parallel with the grinding marks, the adhesion is better. In this current study, care was taken to ensure that the orientation of the grinding and polishing marks relative to the scratch direction did not change between the tests at different temperatures, as confirmed in Figure 4.26, where the angles between the scanning direction and the original grooves are the same. The reduced failure of the top coating at lower temperature cannot be attributed to a surface roughness effect.

A fractography study was carried out by breaking the sample with a prefabricated crack at room

temperature. The fracture section was then investigated by SEM. The coating was buckled resulting in the detachment from the substrate as shown in Figure 4.30a. A lateral crack was found at the point A in Figure 4.30a. The distance from the crack to the surface is about 1.38-1.5 μm which is close to the nominal thickness of the a-C:H top layer. The radial crack below point B appears with the bending of the sublayers TiCN/TiN and this resulted in the decrease of the distance from B to the surface (about 1.8 μm). Figure 4.30b shows another area where the coating was fractured in both lateral and radial directions. A comparative fracture experiment was also carried out at 0ºC. The morphology of the fracture section is shown in Figure 4.31. The whole coating adhered to the substrate after fracture. No buckling and lateral cracks can be identified within the whole fracture section.

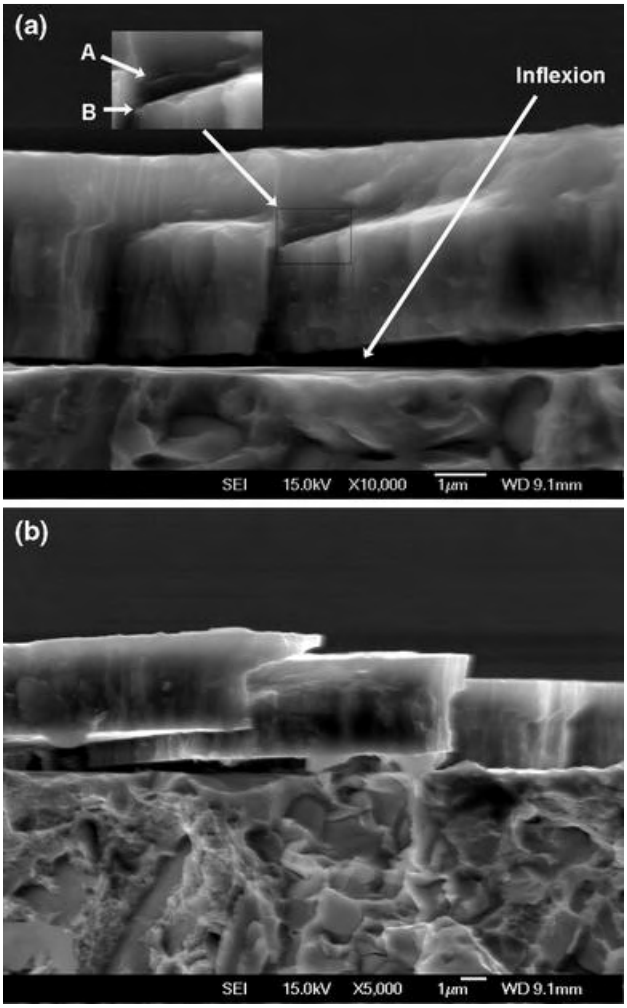

Figure 4.30 Fracture section of the a-C:H(Ti)/TiCN/TiN/Ti coating on M2 substrate prepared at room temperature: **a** Site 1. **b** Site 2

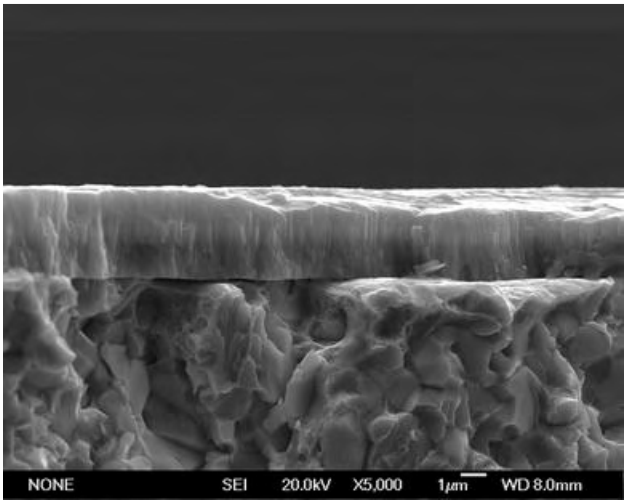

Figure 4.31 Fracture section of the a-C:H(Ti)/TiCN/TiN/Ti coating on M2 substrate prepared at 0 °C

It is of interest to investigate the stress and strain distribution at the failure of coating. A numerical approach by Beake et. al. [144] has been used to estimate the contact pressure (P_m) (scratch hardness) at the failure region of the coatings. The contact depth (h_p) for the spherical indenter is expressed the average value of the on-load scratch depth (h_t) and the residual scan depth (h_r). Thus the contact radius can be expressed as

$$a = \sqrt{2Rh_p - h_p^2} \qquad \text{Equation 4-6}$$

where R is the radius of indenter, and the pressure P_m can be calculated by

$$P_m = \frac{L}{\pi a^2} \qquad \text{Equation 4-7}$$

where L is the load.

The contact radius and the pressures at the failure of coating during scratches have been estimated as (3.2 ± 0.2) μm and (12.8 ± 1.3) GPa respectively for 25ºC tests. The value of the contact radius is approximately half of the width of the scratch tracks shown in Figure 4.26. Assuming it obeys the Hertz contact conditions, the maximum shear stress is at 0.48*a*, about 1.7 μm, which is slighter higher than thickness of the top carbon layer. The variation can be attributed to the influence of the tangential force which can alter the position of the maximum shear stress [145–147], reaching the surface when it increases to ~0.3. When the tangential force is low, the contact is very close to Hertzian. Increasing friction at higher load causes the actual position of the maximum shear strength to be nearer the surface than predicted byEquation 4-6. The friction coefficient during the constant scratch is about 0.15 (Figure 4.28) so the maximum shear strength may be close to the interface between the a-C:H(Ti) toplayer and the TiCN sublayer.

The groove volume comes from plastic deformation (non-wear) and micro machining effect (wear). Williams [97] reported that for micro-machining to be a preferred mode of deformation, the attack angle of the indenter, that is the angle between its leading edge or face and the direction of sliding, must exceed some critical value. In this study, the scratch probe is a conical probe with a round end cap of radius 8 μm. For the penetration depths obtained at up to 400 mN the contact angle with surface is estimated as about 23.5º. The depth of the residual scratch groove is due to plastic deformation. As shown in Figure 4.26, there are no clear abrasive marks and debris within the scratch tracks.

H/E, the resistance against elastic strain to failure, and H^3/E_r^2, the resistance against plastic

deformation, are tribologically important parameters [148,149]. Leyland and Matthews [150,151] indicated that coating elasticity and toughness are important factors in wear, particularly in abrasion, impact, and erosive wear. The elasticity effect can be evaluated using *H/E* ratio and it has shown some merits by various researchers [152–154]. In this paper, H/E_r is used instead of *H/E* assuming the ν can be treated as a constant.

As shown in Figure 4.29, the *H*, H/E_r and H^3/E_r^2 of these coatings increased clearly from 25 ºC to 0 ºC, but the change with further decrease in temperature is minimal. The extent of elastic recovery in nano-scratch testing is known to correlate strongly with *H/E* [136,154]; higher *H/E* materials show enhanced recovery in scratch as they do in an indentation contact. Measurements of significantly reduced groove volume at 0 ºC, with a much smaller increase at –30 ºC, are consistent with the trend in *H/*E at 400 mN observed in the nanoindentation tests. The improved *H* can be attributed to the increased hardness of the top DLC layer. The DLC coating is metastable while the ceramic sublayers (TiCN/TiN) are insensitive to temperature. Therefore, the hardness difference between these layers is reduced which may help the stress transfer at the interface during loading. The increased H/E_r at low temperature - high elastic strain to failure - may also have contributed to the improved bonding strength. These H/E_r values are less than 0.08. As mentioned in [144], the scratch resistance can be improved with the increase of H/E_r when H/E_r is lower than 0.08-0.1. Both critical loads and wear resistance in nanoscratch tests can be improved.

Considering the fracture toughness, an analytic expression was reported by Leyland and Matthews [150] which suggested that it can be improved by both a high critical stress for fast

fracture (which implies a need for high hardness) and low elastic modulus. Musil [155] also indicated that the toughness of a coating system (resistance to crack) increase with the increase of H^3/E_r^2. It has been reported in [132], the critical indentation load at which the radial cracks start to propagate are presented correlating with H^3/E_r^2 of the coatings as determined by nanoindentation. These agree with the findings in this paper as cracks are not formed in the first place.

It has also been found that the penetration depth in the second 'off-load' scan is less than 10% of the depth in the 'on-load' scan, indicating that elastic-plastic deformation in sliding of the a-C:H(Ti)/TiCN/TiN/Ti coating is dominated by elastic deformation when using the 8 μm probe. The improvement of interface strength and wear resistance and can be attributed to the reduction in the H difference between different layers, and the higher H/E_r and H^3/E_r^2 at low temperature (0 ºC and –30 ºC). The mechanism of the increased mechanical properties at low temperatures is unclear. One possible explanation is the metastability of DLC coatings that might undergo graphitization under high strain and high temperature resulting in the mechanical property deterioration. Neville and co-workers have reported that a contact pressure of 1.5 GPa was sufficient to induce graphitisation in wear experiments at room temperature [156]. As the contact pressure stress can be as higher than 10 GPa in this study, graphitisation may occur at room temperature and low temperature as well. As a thermally activated process, the transformation may be reduced by lowering the temperature. To fully understand the mechanism, further work including cross-sectional TEM of the indented area will be carried out.

The novel low temperature nanoscratch capability described in this paper has demonstrated its

ability to investigate the local tribological properties of coating at sub-ambient temperatures. With further development and testing, it is feasible to apply this technology to many low temperature applications. For example, the temperature of aircraft tyres can be lower than –50 ºC during the aviation cycle and when landing, extremely heavy loads can be applied. Similarly some spacecraft instruments have to be cooled to obtain an improved performance and the materials utilized in the assembly of these electronic circuits can be subjected to mechanical loading and relative movement.

4.4.2.6 Conclusions

It has been found that the failure of a-C:H(Ti)/TiCN/TiN/Ti coating in highly loaded sliding contact is in the form of cracks and spallation in the room temperature scratch tests. Fractography and contact pressure analysis suggest the failures originate at or close to the interface between the top a-C:H(Ti) layer and the TiCN layer. Decreasing temperature from 25 ºC to 0 ºC, increases both H/E_r and H^3/E_r^2, consistent with improved crack resistance, with smaller further improvements on the decreasing temperature further to –30 ºC.

Chapter 5 Summary and conclusions

5.1 Sub-ambient temperature equipment

The main body of research in the thesis was focused to develop sub-ambient temperature nanoindentation equipment. There is a clear lack of instrumentation dedicated to the application of sub-ambient temperature in service mechanical property determination. It is envisaged with this new novel equipment, that it will inspire researches to use this budget method to adapt their existing nanoindentation apparatus to perform the new type of measurements.

The main use of the equipment is foreseen to be in polymer engineering. There is scope for testing in principle for other lower temperature applications (as proof of concept). The thesis gives a general overview of nanoindentation and its principles. The theme is then carried on to explore materials with time dependence properties before moving towards non-ambient testing.

It is important to have a clear understanding of the material responses at the different regimes before embarking on the challenging task of designing and developing prototype instrumentation. Clearly without having the experiences of testing a wide range of materials which response change over time or with their environments; it would have been difficult to understand the necessary requirements of a sub-ambient nanoindentaion equipment.

5.2 Established peer reviewed literature

Building on the experiences of testing materials primarily polymers at ambient and in a liquid environment. A solid basis for the preparation of developing the new kit was established. The early research and application research after the validation of the novel equipment has led to the

publication of a series of papers. Even though the papers are young they have begun to be established as a credible body of literature cited by peers. And the citation list is continuing to grow.

5.3 Glass transition determination and expansion of testing regimes

Through the initial testing of the polymers a method was established to work out the T_g through nanoindentation testing.

This research has expended the testing temperature range of nanoindentation instrumentation from ambient to - 30 ^{o}C

5.4 Full product lifecycle prototype to commercial realisation

The research is being commercialised into a new product for Micro Materials Ltd and in the spirit of the Engineering Doctorate research programme the intellectual property is providing the company with an expanding product and application range. It is already installed and being used experimentally in four of the leading research institutions globally.

Appendices

1.1 Overview

This section shows the diversity of the modern engineer. First most the researcher must achieve and participate in a key series of projects to show his ability of the understanding in his current field and how he can expand on the ideas of past and present research.

Secondly the Researcher must be able to network, especially if they are embarking on a professional doctorate, to organise effective conferences have good communication skills.

Another growing role in industry is to be able to pass on this knowledge, through training and educational lectures, using the available technology of the day.

Being part of the societies in his/her research area. Participate in the running of Journals and publishing new findings.

1.1.1 International Federation of Heat Treatment and Surface Engineering (IFHTSE)

An organisation can no longer function without a website, but more importantly an up to date website, the research engineer (RE) took part in development of the federation's website and bringing it in line with other websites. It is based on a CMS Content management system, run by Interactive Dimensions, based in Preston, UK.

The website is now managed by the RE with input from the secretariat general Robert Wood. It is continually growing and it has the means to be able to evolve with IFHTSE as the global community expands. It has a members section that in due course will be a rich source of

information for the new and also the established members of the IFHTSE.

1.1.2 Innovate

A European project setup to bring surface engineering into 21st century teaching for vocational training.

This was one of the first projects that entailed transforming regular lectures to an e-learning platform. It was based round a consortium of European university and companies, Bodycote International, and SME's Ad.Surf.Eng, Ltd and Micro Materials Ltd.

A framework was established between two open learning platforms IBM learning environment called learning space and a French based bespoke learning environment platform called Sollan.

It was agreed that the two systems held the key to providing the perfect learning space for the vocational surface engineering course.

Micro Materials Ltd was a partner of the project who as we have discussed through the thesis are a manufacture of nanoindentation equipment.

The researcher of this thesis was tasked with producing technical instruction videos which provide users of the NanoTest with an insight into the instrument. The purpose of the videos where to reinforce the training that is given when the new customer who's primary language is not always English receives there instrument. They had to provide information on a wide range of topics.

Training videos

Instrument calibration

Instrument setup procedures

Instrument Experiment quick setups for each of the modules of the NanoTest.

The videos were standalone modules recorded to DVD, they were a mixture of screenshots with a voice over, and explained to the user how to setup both hardware and experimental software for the NanoTest platform.

The videos were a vital teaching and reference aid to the company whose sales were to academic establishments stretching all over the world. The researcher had the opportunity to join a colleague in China for a training visit in 2007 and experienced how vital it was to have more than a few days of hands on training and an instrument manual.

Every few years research teams change and evolve. The trouble with having a specialist instrument is that supporting the instrument can be a costly task. Having to pay for an engineer to retrain users every few years was not something that suited the company's business model or the customers of the Nanotest. The videos aimed to provide a visual guide to be left with the users so that new users could hopefully learn the basics from watching the videos and being able to see hands on how different parts of the instrument interlocked and functioned.

1.1.3 Maney 2008

Assistant to the editors for the Journal International Heat Treatment and Surface Engineering.

Liaising between Maney and the journal editors to prepare material ready for publication. This

involved making final editorial changes to papers, ensuring the content and figures were managed between the partners. Adapting figure ready for publication retyping documents from pdf format so that they could be then typeset by the publisher Maney.

1.1.4 China Xian Jiatong University

Nanomechanical workshop.

The workshop was organised by the researcher of the thesis. It was setup by late Professor Tom Bell to promote the activities of Xian Jiantong University. It was to be the first of a series of workshops.

The first workshop was themed around nanoindentation. Its guest speaker was Dr Anthony Fisher-Cripps. The workshop brought together the 5 major instrument manufactures from across the globe. It featured a diverse audience attracting researches from Malta University, Birmingham University, and other institutions from around the world. Its themes were nanoindentation and modelling of surface engineering systems . Investigating changing the black art of surface engineering by introducing a combination of the techniques to enable surface engineering systems to advance. And build on duplex surface systems.

A conference report from IHTSE, vol1, No.3

Nano-mechanical property characterisation

Workshop and seminar, Xi'an, China July 2007

As part of a general strategy for an increased level of international communication and

collaboration, a series of workshops or small conferences based on materials engineering developments at Xian Jiao Tong University is planned. The first of these – 'Nano-mechanical property characterisation' was organised on 10-13 July 2007 by the XJTU International Surface Engineering R&D Centre which is part of the State Key Laboratory for the Mechanical Behaviour of Materials sited at the university.

The Laboratory for Mechanical Behaviour of Materials at XJTU was established on the basis of a Research Institute for Strength of Metals founded in Xi'an Jiao Tong University in 1963. Later it was supported with funding by the State Education Commission and in 1994 became open to the outside world as a State Key Laboratory.

Ever since its formation, close attention has been paid in the State Key Laboratory to the correlation of mechanical properties with processing, composition and microstructure. This is still true today. The Laboratory now recognises that Nano Mechanical property measurements are crucial in the design of innovative surface engineered systems, and thus provides a real focus for this Workshop and International Seminar on Surface Engineering and Nano Mechanical properties.

The current high standing of this State Key Laboratory is reflected in the 120 post graduate students enrolled to pursue degrees in the Lab. These young researchers are regarded as the backbone of the Laboratory.

The principal overseas academic partner in the Workshop and Seminar was the Surface Engineering Group within the Department of Metallurgy and Materials at the University of

Birmingham. This Department enjoys the highest possible UK 5* research rating. The Surface Engineering Group was the first multidisciplinary research group internationally to be committed to the subject of surface engineering and in particular to plasma surface modification. The Birmingham Surface Engineering Group (BSEG) has made a substantial contribution to wealth creation, competitiveness and growth via scientific development and subsequent industrial awareness and acceptance of advanced surface engineering processes. In addition, during the past two decades, the BSEG has established close relationships with many Chinese universities and research institutions. The BSEG has received more than 10 Chinese Delegations, about 20 individual short-term Chinese visitors and about 20 long term visiting scholars supported by Chinese government and many Chinese PhD students have been funded by UK sources at Birmingham University.

Collaborators in the planning of the workshop were:

China State Key Laboratory for Mechanical Behaviour of Materials

Xi'an Science and Technology Bureau

Xi'an Jiao Tong University

University of Birmingham, UK

International Federation for Heat Treatment and Surface Engineering (IFHTSE)

The timing of this event marked 25 years since the introduction of techniques for the measurement of mechanical properties at the nanometre scale and revealed how rapidly techniques, equipment, and scientific understanding are developing. In addition to the presentations on XJTU work, contributions came from Australia, Malta, Switzerland, UK and USA and elsewhere in China including Beijing, Chengdu, Changchun, Chongqing, Hong Kong, Shenyang and Shanghai. Most of the world's nano mechanical property equipment manufacturing companies in this field were represented.

The first day of the workshop was devoted to presentations by five international suppliers of nano-mechanical property instrumentation and started with a keynote lecture by Dr Tony Fischer Cripps on the fundamentals of nano-mechanical property measurements. This truly remarkable lecture captured in a succinct manner the thoughts of a world authority on the subject. This lecture was followed by talks from, Bin Zhang – CSM Instruments, Jun Xiao – Center for Tribology Inc – USA, Adrian Harris – Micro Materials Ltd - UK and Lance Kuhn – Hysitron Incorporated – USA. Each speaker naturally explained the advantages of their own companies techniques but the presentations were given at a high technical level, reflecting the key theme of the day – bringing nano-mechanical properties into the real world. Each presentation stimulated lively discussion from an expert audience of circa 50 participants from 6 countries. The Conference Chairman Prof. Tom Bell summarised the day's Workshop with the following statement and question:

Nano-mechanical property characterisation is clearly now an essential design aid for innovative surface engineered systems.

Will the day come when nanomechanical testing replaces traditional mechanical property testing?

Over the next two days seminar sessions covered the fundamentals and practicalities of property measurement and evaluation, the science base, modelling and surface engineering design.

Keynote papers covered:

Fundamentals of nano-mechanical property measurements – Dr Tony Fischer Cripps

Atomic scale nano-mechanics of one-dimensional nano-materials by in situ TEM – Academician Zhang Ze & Prof. Han Xiaodong

Study of the mechanical behaviour of advanced materials by multi-scale mechanical experiment and simulation – Prof. Lu Jian

Super-hard nano-composite coatings and mechanical properties – Prof. Xu Kewei

Modelling based design of surface engineered systems – Dr. Luo Jiaming

Nano Surface Engineering and Remanufacturing – Academician Xu Binshi & Prof. Xu Yi

Invited papers covered:

Nanothermodynamics of nanophase diagrams – Prof. Jiang Qing & Dr. Lang Xingyou

Nanoindentation studies on the initial plasticity and indentation creep of CU single crystals. –

Academician Lu Ke & Prof. Wang Wei

Contact mechanics of coated systems under sliding conditions. – Prof. Ma Lifeng

Microscopic characterisation of nano-indentation tested materials. – Dr. Li Xiaoying

Nanoindentation of freestanding chip/film and embedded second phase particles: Effect of target fixing/constraint on measurement scatter. – Prof. Cai Xun & Prof. Shen Yao

Investigation on nanofretting. – Prof. Qian Linmao & Prof. Zhou Zhongrong

Nano mechanical characterisation of ion beam and plasma surface modified polymeric materials. – Dr Dong Hanshan

Nanotesting techniques-based micromechanical properties characterisation for coating/substrate system. – Prof. Zhang Jin & Mr. Wang Zhenlin

There were also a series of interesting current research presentations from XJTU and Birmingham University postgraduate students.

A high level of communication and interaction was achieved, substantially aided by the ability of the Chinese contributors to make their presentations and hold discussions in English.

Significant points and questions emerging from discussion were:

Definition of hardness – will a different approach be needed for different materials

What training is needed to produce a supply of competent workers in the field, and how much will be 'black box'

What about market development and ROI for the pioneers

What about the development of standards and best practice

The plan now is to start work on the production of a volume of proceedings to be published in 2008 by XJTU. This will be a fully edited volume yielding a state of the art statement by including various added-value elements, e.g.:

Selected key papers from the literature in this field

A comprehensive listing of papers concerning nano-mechanical property characterisation over the past 25 years

Robert Wood and Gerard Bell

IFHTSE University of Birmingham

1.1.5 MinSE

Testing out the new e-learning platform for a Modern Masters in surface engineering. This would be the first Master's course for surface engineering. Part traditionally taught and part taught using the moodle e-learning platform. It went on to be accredited by IOM3.

Training for tomorrow The lack of thermal processing training available on a global basis has been noticed and I am aware of two initiatives intended to fill this gap. Masters degree in heat treatment and surface engineering (MinSE) B. Birch IHTSE

References

1. Roy MJ, Klassen RJ, Wood JT. Evolution of plastic strain during a flow forming process. Journal of Materials Processing Technology. 2009 Jan;209(2):1018–25.

2. Brostow W, Chonkaew W, Rapoport L, Soifer Y, Verdyan A, Soifer Y. Grooves in scratch testing. Journal of Materials Research. 2007 Jan 31;22(09):2483–7.

3. Beake BD, Liskiewicz TW, Pickford NJ, Smith JF. Accelerated nano-fretting testing of Si(100). Tribology International. 2012 Feb;46(1):114–8.

4. Beake BD, Smith JF. Nano-impact testing—an effective tool for assessing the resistance of advanced wear-resistant coatings to fatigue failure and delamination. Surface and Coatings Technology. 2004 Nov;188-189:594–8.

5. Everitt NM, Davies MI, Smith JF. High temperature nanoindentation – the importance of isothermal contact. Philosophical Magazine. 2011;91(7-9):1221–44.

6. Altaf K, Ashcroft IA, Hague R. Investigation of the effect of relative humidity on polymers by depth sensing indentation. Journal of Materials Science. 2011 Jul 9;46(23):7551–7.

7. Beake BD, Bell GA, Brostow W, Chonkaew W. Nanoindentation creep and glass transition temperatures in polymers. Polymer International. 2007 Jun;56(6):773–8.

8. Bell GA, Bieliński DM, Beake BD. Influence of water on the nanoindentation creep response of nylon 6. Journal of Applied Polymer Science. 2008 Jan 5;107(1):577–82.

9. Mott BW. Micro indentation Hardness Testing. London: Butterworth; 1956.

10. Newey D, Wilkins MA, Pollock HM. An ultra-low-load penetration hardness tester. Journal of Physics E: Scientific Instruments. 1982 Jan;15(1):119–22.

11. Doerner MF, Nix WD. A method for interpreting the data from depth-sensing indentation instruments. Journal of Materials Research. 1986;1(04):601–9.

12. W.C. Oliver, Pharr GM. An improved technique for determining hardness and elastic modulus using load and displacement sensing indentation experiments. J Mater Res. 1992;7(6):1564–83.

13. Tabor D. The Hardness Of Metals. London: Oxford University Press; 1951.

14. Berkovich. Three-faceted diamond pyramid for microhardness testing. Industrial Diamond Review. 1951;11(127):129–32.

15. Fischer-Cripps AC. Nanoindentation. New York: Springer; 2011.

16. Boussinesq m. J. Application des potentiels à l'étude de l'équilibre et du mouvement des solides élastiques, principalement au calcul des deformations et des pressions que produisent, dans ces solides, des efforts quelconques exercés sur und petite partie de leur surface ou de leur intérieur;memoire suivi de notes étendues sur divers points de physique mathématique et d'analyse. Paris: Gauthier-Villars; 1885.

17. Sneddon. The relationship between load and penetration in the axisymmetric Boussinesq problem for a flat punch of arbitrary profile. International Journal of Engineering Science. 1965;(3):47–57.

18. Loubet J, Georges J, Marchesini O, Meille G. Vickers indentation curves of magnesium oxide(MgO). Journal of Tribology. 1984;(106):43–8.

19. Pethicai JB, Hutchings R, Oliver WC. Hardness measurement at penetration depths as small as 20 nm. Philosophical Magazine A. 1983 Apr;48(4):593–606.

20. Indicoat Final Report Determination of hardness and modulus of thin films and coatings by nanoindentation. NPL Report MATC(A)24; 2001.

21. Schuh CA, Packard CE, Lund AC. Nanoindentation and contact-mode imaging at high temperatures. Journal of Materials Research. 2006;21(03):725–36.

22. Trenkle JC, Packard CE, Schuh CA. Hot nanoindentation in inert environments. Review of Scientific Instruments. 2010;81(7):073901.

23. CSM instuments brochure [Internet]. CSM Instruments; 2012. Available from: http://www.csm-instruments.com

24. Temperature control stage [Internet]. Hysitron; Available from: www.hysitron.com

25. Heating and cooling for nanoindentation [Internet]. Surface; Available from: www.surface-tech.com

26. Syed Asif SA, Pethica JB. Nano-Scale Indentation Creep Testing at Non-Ambient Temperature. The Journal of Adhesion. 1998;67(1/4):153–65.

27. Fischer-Cripps AC. A simple phenomenological approach to nanoindentation creep. Materials Science and Engineering: A. 2004 Nov;385(1-2):74–82.

28. Cheng L, Xia X, Scriven LE, Gerberich WW. Spherical-tip indentation of viscoelastic material. Mech. Mater. 2005 Jan;37(1):213–26.

29. Chudoba T, Richter F. Investigation of creep behaviour under load during indentation experiments and its influence on hardness and modulus results. Surface and Coatings Technology. 2001 Dec;148(2-3):191–8.

30. Beake B. Modelling indentation creep of polymers: a phenomenological approach. Journal of Physics D: Applied Physics. 2006 Oct 21;39(20):4478–85.

31. Odegard GM, Gates TS, Herring HM. Characterization of viscoelastic properties of polymeric materials through nanoindentation. Experimental Mechanics. 2005 Apr;45(2):130–6.

32. Menčík J, He LH, Swain MV. Determination of viscoelastic–plastic material parameters of biomaterials by instrumented indentation. Journal of the Mechanical Behavior of Biomedical Materials. 2009 Aug;2(4):318–25.

33. Oyen ML. Analytical techniques for indentation of viscoelastic materials. Philosophical Magazine. 2006 Nov 21;86(33-35):5625–41.

34. Beake BD, Zheng S, Alexander MR. Nanoindentation testing of plasma-polymerised hexane films. J. Mater. Sci. 2002;37(18):3821–6.

35. Oyen ML. Spherical Indentation Creep Following Ramp Loading. Journal of Materials Research. 2005;20(08):2094–100.

36. Oyen ML, Cook RF. A practical guide for analysis of nanoindentation data. Journal of the Mechanical Behavior of Biomedical Materials. 2009 Aug;2(4):396–407.

37. Oyen ML. Sensitivity of polymer nanoindentation creep measurements to experimental variables. Acta Materialia. 2007 Jun;55(11):3633–9.

38. Ferry JD. Viscoelastic properties of polymers. New York: Wiley; 1980.

39. Brostow W, Corneliussen RD. Failure of plastics. Munich; New York: Hanser Pub.□: Distributed in the United States of America by Macmillan Pub.; 1986.

40. Nielsen LE, Landel RF. Mechanical properties of polymers and composites. New York: M. Dekker; 1994.

41. Gol'dman AI, Shelef M, Dickie RA. Prediction of the deformation properties of polymeric and composite materials. Washington, DC: American Chemical Society; 1994.

42. Mazur S. Coalescence of polymer particles. Polymer powder technology. Chichester; New York: J. Wiley; 1995.

43. Beake BD, Chen S, Hull JB, Gao F. Nanoindentation Behavior of Clay/Poly(Ethylene Oxide) Nanocomposites. J. Nanosci. Nanotechnol. 2002 Feb 1;2(1):73–9.

44. Brostow W. Time-stress correspondence in viscoelastic materials: an equation for the stress and temperature shift factor. Materials Research Innovations. 2000 Oct 27;3(6):347–51.

45. Brostow W. Performance of plastics. Munich [u.a.]: Hanser; 2001.

46. Rau K, Singh R, Goldberg E. Nanoindentation and nanoscratch measurements on silicone thin films synthesized by pulsed laser ablation deposition (PLAD). Materials Research Innovations. 2002 Feb 1;5(3-4):151–61.

47. Tho KK, Swaddiwudhipong S, Liu ZS, Zeng K, Hua J. Uniqueness of reverse analysis from conical indentation tests. Journal of Materials Research. 2004;19(08):2498–502.

48. Alkorta J, Martínez-Esnaola JM, Sevillano JG. Absence of one-to-one correspondence between elastoplastic properties and sharp-indentation load–penetration data. Journal of Materials Research. 2005;20(02):432–7.

49. Beake BD, Leggett GJ. Nanoindentation and nanoscratch testing of uniaxially and biaxially drawn poly(ethylene terephthalate) film. Polymer. 2002 Jan;43(2):319–27.

50. Beake BD, Leggett GJ, Alexander MR. Characterisation of the mechanical properties of plasma-polymerised coatings by nanoindentation and nanotribology. Journal of Materials Science. 2002;37(22):4919–27.

51. Beake BD, Goodes SR, Smith JF, Gao F. Nanoscale repetitive impact testing of polymer films. Journal of Materials Research. 2004;19(01):237–47.

52. Juliano TF, VanLandingham MR, Tweedie CA, Vliet KJ. Multiscale Creep Compliance of Epoxy Networks at Elevated Temperatures. Experimental Mechanics. 2006 May 12;47(1):99–105.

53. Tweedie CA, Van Vliet KJ. Contact creep compliance of viscoelastic materials via nanoindentation. Journal of Materials Research. 2006;21(06):1576–89.

54. Beake BD, Shipway PH, Leggett GJ. Influence of mechanical properties on the nanowear of uniaxially oriented poly(ethylene terephthalate) film. Wear. 2004 Jan;256(1-2):118–25.

55. Berthoud P, G'Sell C, Hiver J-M. Elastic-plastic indentation creep of glassy poly(methyl methacrylate) and polystyrene: characterization using uniaxial compression and indentation

tests. Journal of Physics D: Applied Physics. 1999 Nov 21;32(22):2923–32.

56. Painter PC, Coleman MM. Fundamentals of polymer science□: an introductory text. Lancaster, Pa.: Technomic Pub. Co.; 1994.

57. Selected Works of Paul J. Flory Volume III [Internet]. Stanford University Press; 1995. Available from: http://books.google.co.uk/books?id=y-ueAAAAIAAJ

58. Young RJ, Lovell PA. Introduction to polymers. Second. Boca Raton; London: CRC Press; 1991.

59. Hartmann B, Haque MA. Equation of state for polymer solids. Journal of Applied Physics. 1985;58(8):2831.

60. Gray A, Beake BD. Elevated temperature nanoindentation and viscoelastic behaviour of thin poly(ethylene terephthalate) films. Journal of nanoscience and nanotechnology. 2007;7(7):2530–3.

61. Grunina NA, Belopolskaya TV, Tsereteli GI. The glass transition process in humid biopolymers. DSC study. J. Phys. Conf. Ser. 2006 May 1;40:105–10.

62. Round A, Yan B, Dang S, Estephan R, Stark RE, Batteas JD. The Influence of Water on the Nanomechanical Behavior of the Plant Biopolyester Cutin as Studied by AFM and Solid-State NMR. Biophys. J. 2000 Nov;79(5):2761–7.

63. Cohen SC, Tabor D. The Friction and Lubrication of Polymers. Proceedings of the Royal Society A: Mathematical, Physical and Engineering Sciences. 1966 Apr 5;291(1425):186–207.

64. Amuzu JKA. The effect of humidity on friction and shear strength of nylon. J. Mater. Sci. Lett. 1984 Apr;3(4):291–2.

65. Stuart B, Briscoe B. Surface plasticisation of nylon 6,6 by water. Polym. Int. 1995 Sep;38(1):95–9.

66. Newman BA, Kim KG, Scheinbeim JI. Effect of water content on the piezoelectric properties of nylon 11 and nylon 7. J. Mater. Sci. 1990 Mar;25(3):1779–83.

67. Hahn MT, Hertzberg RW, Manson JA. Effects of rubbery phase and absorbed water on impact-modified nylon 66. J. Mater. Sci. 1986 Jan;21(1):31–8.

68. Ashida M, Noguchi T, Mashimo S. Effect of absorbed water on dynamic modulus for short fiber–CR composites. J. Appl. Polym. Sci. 1984 Dec;29(12):4107–14.

69. McCrum NG, Read BE, Williams G. Anelastic and dielectric effects in polymeric solids. Anelastic and dielectric effects in polymeric solids. New York: Dover Publications; 1991. page 478–97.

70. Hübner W, Gradt T. Cryotribology. Tribology International. 2001 Apr;34(4):iii–iv.

71. Wigley D. Materials for low-temperature. Oxford: Oxford University Press; 1978.

72. Gao C, Abeysekera J, Hirvonen M, Grönqvist R. Slip resistant properties of footwear on ice. Ergonomics. 2004 May 15;47(6):710–6.

73. Sales BC. Thermoelectric Devices: Refrigeration and Power Generations With No Moving Parts. In: Buschow KHJ, Cahn RW, Flemings MC, (print) BI, Kramer EJ, Mahajan S, et al., editors. Encyclopedia of Materials: Science and Technology. Oxford: Elsevier; 2001. page 9179 – 9185.

74. Ang KH, Chong GCY, Li Y. PID control system analysis, design, and technology. IEEE Transactions on Control Systems Technology. 2005 Jul;13(4):559–76.

75. Chein R, Huang G. Thermoelectric cooler application in electronic cooling. Applied thermal engineering. 2004;24(14-15):2207–17.

76. Rowe DM. CRC handbook of thermoelectrics. Boca Raton, Fla.: CRC Press; 1995.

77. Chen J, Bell GA, Dong H, Smith JF, Beake BD. A study of low temperature mechanical properties and creep behaviour of polypropylene using a new sub-ambient temperature nanoindentation test platform. Journal of Physics D: Applied Physics. 2010;43(42):425404.

78. Chen J, Bell GA, Beake BD, Dong H. Nano-mechanical and tribological properties of a multilayered DLC coating under sub-ambient temperatures. International Journal of Engineering Systems Modelling and Simulation. 2010;2(4):199.

79. Beake B, Smith J. High-temperature nanoindentation testing of fused silica and other materials. Philosophical Magazine A. 2002;82(10):2179–86.

80. Tang F, Zhang LC. On the Reliability of Nanoindentation on Si Wafer at Elevated Temperatures. Advanced Materials Research. 2011;325:684–9.

81. Munro RG, National Institute of Standards and Technology (U.S.). Elastic moduli data for polycrystalline oxide ceramics. Gaithersburg, MD: U.S. Dept. of Commerce, Technology Administration, National Institute of Standards and Technology; 2002.

82. Zhu Y, Okui N, Tanaka T, Umemoto S, Sakai T. Low temperature properties of hard elastic polypropylene fibres. Polymer. 1991 Jan;32(14):2588–93.

83. Zrida M, Laurent H, Grolleau V, Rio G, Khlif M, Guines D, et al. High-speed tensile tests on a polypropylene material. Polymer Testing. 2010 Sep;29(6):685–92.

84. Cowie JMG. Glass transition temperatures of stereoblock, isotactic and atactic polypropylenes of various chain lengths. European Polymer Journal. 1973 Oct;9(10):1041–9.

85. Wortmann F-J, Schulz KV. Thermomechanics of isotactic polypropylene between −67 and +140°C: investigation of the relaxation behaviour based on literature data. Polymer. 1996 Jan;37(5):819–24.

86. Xu X, Jeronimidis G, Atkins AG, Trusty PA. Stress relaxation behaviour of frozen sucrose solutions. Journal of Texture Studies. 2004 May;35(1):11–32.

87. Dutta AK, Penumadu D, Files B. Nanoindentation testing for evaluating modulus and hardness of single-walled carbon nanotube–reinforced epoxy composites. Journal of Materials Research. 2004 Mar 3;19(01):158–64.

88. Ngan AHW, Wang HT, Tang B, Sze KY. Correcting power-law viscoelastic effects in elastic modulus measurement using depth-sensing indentation. International Journal of Solids and Structures. 2005 Mar;42(5-6):1831–46.

89. Ngan AHW, Tang B. Response of power-law-viscoelastic and time-dependent materials to rate jumps. Journal of Materials Research. 2009 Jan 31;24(03):853–62.

90. Ensinger. Tecafine PP data sheet. Ensinger Ltd, Wilfried Way, Tonyrefail, Mid Glamorgan CF39 8JQ;

91. Li J, Ngan AHW. Nanoscale fast relaxation events in polyethylene. Scripta Materialia. 2010 Apr;62(7):488–91.

92. Tweedie CA, Constantinides G, Lehman KE, Brill DJ, Blackman GS, Van Vliet KJ. Enhanced Stiffness of Amorphous Polymer Surfaces under Confinement of Localized Contact Loads. Advanced Materials. 2007 Sep 17;19(18):2540–6.

93. Brostow W, Chonkaew W, Mirshams R, Srivastava A. Characterization of grooves in scratch resistance testing. Polymer Engineering & Science. 2008 Oct;48(10):2060–5.

94. Feng G, Ngan AHW. Effects of Creep and Thermal Drift on Modulus Measurement Using Depth-sensing Indentation. Journal of Materials Research. 2002;17(03):660–8.

95. Ngan AHW, Tang B. Viscoelastic effects during unloading in depth-sensing indentation. Journal of Materials Research. 2002;17(10):2604–10.

96. Gray A, Orecchia D, Beake BD. Nanoindentation of Advanced Polymers Under Non-

Ambient Conditions: Creep Modelling and Tan Delta. Journal of Nanoscience and Nanotechnology. 2009 Jul 1;9(7):4514–9.

97. Williams JA. Analytical models of scratch hardness. Tribology International. 1996 Dec;29(8):675–94.

98. Bull SJ, Berasetegui EG. An overview of the potential of quantitative coating adhesion measurement by scratch testing. Tribology International. 2006 Feb;39(2):99–114.

99. Beake BD, Bell GA, Goodes SR, Pickford NJ, Smith JF. Improved nanomechanical test techniques for surface engineered materials. Surface Engineering. 2010 Feb 1;26(1):37–49.

100. Hübner W, Gradt T, Schneider T, Börner H. Tribological behaviour of materials at cryogenic temperatures. Wear. 1998 Apr;216(2):150–9.

101. Allsopp D., Hutchings I. Micro-scale abrasion and scratch response of PVD coatings at elevated temperatures. Wear. 2001 Oct;251(1-12):1308–14.

102. Buršíková V, Navrátil V, Zajíčková L, Janča J. Temperature dependence of mechanical properties of DLC/Si protective coatings prepared by PECVD. Materials Science and Engineering: A. 2002 Feb;324(1-2):251–4.

103. Jardret V, Morel P. Viscoelastic effects on the scratch resistance of polymers: relationship between mechanical properties and scratch properties at various temperatures. Progress in Organic Coatings. 2003 Dec;48(2-4):322–31.

104. Hainsworth SV, Kilgallon PJ. Temperature-variant scratch deformation response of automotive paint systems. Progress in Organic Coatings. 2008 Mar;62(1):21–7.

105. Robertson J. Diamond-like amorphous carbon. Materials Science and Engineering: R: Reports. 2002 May 24;37(4-6):129–281.

106. Grill A. Diamond-like carbon coatings as biocompatible materials—an overview. Diamond and Related Materials. 2003 Feb;12(2):166–70.

107. Beake BD, Lau SP. Nanotribological and nanomechanical properties of 5–80 nm tetrahedral amorphous carbon films on silicon. Diamond and Related Materials. 2005 Sep;14(9):1535–42.

108. Charitidis CA. Nanomechanical and nanotribological properties of carbon-based thin films: A review. International Journal of Refractory Metals and Hard Materials. 2009;28(1):51–70.

109. Drees D, Celis JP, Dekempeneer E, Meneve J. The electrochemical and wear behaviour of

amorphous diamond-like carbon coatings and multilayered coatings in aqueous environments. Surface and Coatings Technology. 1996 Dec;86-87:575–80.

110. Statuti RPCC, Radi PA, Santos LV, Trava-Airoldi VJ. A tribological study of the hybrid lubrication of DLC films with oil and water. Wear. 2009 Jun;267(5-8):1208–13.

111. Tokoro M, Aiyama Y, Masuko M, Suzuki A, Ito H, Yamamoto K. Improvement of tribological characteristics under water lubrication of DLC-coatings by surface polishing. Wear. 2009 Dec;267(12):2167–72.

112. Stallard J, Mercs D, Jarratt M, Teer DG, Shipway PH. A study of the tribological behaviour of three carbon-based coatings, tested in air, water and oil environments at high loads. Surface and Coatings Technology. 2004 Jan;177-178:545–51.

113. Velkavrh I, Kalin M, Vižintin J. The influence of viscosity on the friction in lubricated DLC contacts at various sliding velocities. Tribology International. 2009 Dec;42(11-12):1752–7.

114. Andersson J, Erck RA, Erdemir A. Friction of diamond-like carbon films in different atmospheres. Wear. 2003 Oct;254(11):1070–5.

115. Eun KY, Lee K-R, Yoon E-S, Kong H. Effect of polymeric debris on the tribological behavior of diamond-like carbon films. Surface and Coatings Technology. 1996 Dec;86-87:569–74.

116. Jiang J, Zhang S, Arnell RD. The effect of relative humidity on wear of a diamond-like carbon coating. Surface and Coatings Technology. 2003 Apr;167(2-3):221–5.

117. Le Huu T, Zaidi H, Paulmier D, Voumard P. Transformation of sp3 to sp2 sites of diamond like carbon coatings during friction in vacuum and under water vapour environment. Thin Solid Films. 1996 Dec;290-291:126–30.

118. Tanaka A, Nishibori T, Suzuki M, Maekawa K. Characteristics of friction surfaces with DLC films in low and high humidity air. Wear. 2004 Aug;257(3-4):297–303.

119. Kanagawa I, Ogata S, Osaki H. Effect of temperature, humidity and crystal directions on wear of rotary heads. Tribology International. 2003 Apr;36(4-6):433–6.

120. Bremond F, Fournier P, Platon F. Test temperature effect on the tribological behavior of DLC-coated 100C6-steel couples in dry friction. Wear. 2003 Apr;254(7-8):774–83.

121. Ouyang JH, Sasaki S. Friction and wear characteristics of a Ti-containing diamond-like carbon coating with an SRV tester at high contact load and elevated temperature. Surface and Coatings Technology. 2005 May;195(2-3):234–44.

122. Konca E, Cheng Y-T, Weiner AM, Dasch JM, Alpas AT. Elevated temperature tribological behavior of non-hydrogenated diamond-like carbon coatings against 319 aluminum alloy. Surface and Coatings Technology. 2006 Mar;200(12-13):3996–4005.

123. Veverkova J, Hainsworth SV. Effect of temperature and counterface on the tribological performance of W-DLC on a steel substrate. Wear. 2008 Mar;264(7-8):518–25.

124. Taylor CA, Wayne MF, Chiu WKS. Heat treatment of thin carbon films and the effect on residual stress, modulus, thermal expansion and microstructure. Carbon. 2003 Jan;41(10):1867–75.

125. Donnet C, Erdemir A. Tribology of diamond-like carbon films fundamentals and applications [Internet]. New York: Springer; 2008 [cited 2012 Oct 15]. Available from: http://dx.doi.org/10.1007/978-0-387-49891-1

126. Suresh S. Graded Materials for Resistance to Contact Deformation and Damage. Science. 2001 Jun 29;292(5526):2447–51.

127. Zhao F, Li H, Ji L, Wang Y, Zhou H, Chen J. Ti-DLC films with superior friction performance. Diamond and Related Materials. 2010 Apr;19(4):342–9.

128. Ronkainen H, Varjus S, Holmberg K. Friction and wear properties in dry, water- and oil-lubricated DLC against alumina and DLC against steel contacts. Wear. 1998 Nov;222(2):120–8.

129. Monaghan DP, Teer DG, Logan PA, Efeoglu I, Arnell RD. Deposition of wear resistant coatings based on diamond like carbon by unbalanced magnetron sputtering. Surface and Coatings Technology. 1993 Oct;60(1-3):525–30.

130. Bell GA, Chen J, Dong HS, Beake BD, Smith JF. The design of a novel cryogenic nanomechanical and tribological properties instrumentation. International Heat Treatment & Surface Engineering. 2011;5(1):21–5.

131. Zaharia T, Sullivan JL, Saied SO, Bosch RCM, Bijker MD. Fast deposition of diamond-like hydrogenated carbon films. Diamond and Related Materials. 2007 Mar;16(3):623–9.

132. Pei Y, Galvan D, Dehosson J. Nanostructure and properties of TiC/a-C:H composite coatings. Acta Materialia. 2005 Oct;53(17):4505–21.

133. Bienk EJ, Reitz H, Mikkelsen NJ. Wear and friction properties of hard PVD coatings. Surface and Coatings Technology. 1995 Dec;76-77:475–80.

134. Bull S., Bhat D., Staia M. Properties and performance of commercial TiCN coatings. Part 1: coating architecture and hardness modelling. Surface and Coatings Technology. 2003

Jan;163-164:499–506.

135. Randall N., Harris A. Nanoindentation as a tool for characterising the mechanical properties of tribological transfer films. Wear. 2000 Oct;245(1-2):196–203.

136. Beake BD, Ranganathan N. An investigation of the nanoindentation and nano/micro-tribological behaviour of monolayer, bilayer and trilayer coatings on cemented carbide. Materials Science and Engineering: A. 2006 May;423(1-2):46–51.

137. Tricoteaux A, Duarte G, Chicot D, Le Bourhis E, Bemporad E, Lesage J. Depth-sensing indentation modeling for determination of Elastic modulus of thin films. Mechanics of Materials. 2010 Feb;42(2):166–74.

138. Bull SJ. Nanoindentation of coatings. Journal of Physics D: Applied Physics. 2005 Dec 21;38(24):R393–R413.

139. Chen J, Bull SJ. On the factors affecting the critical indenter penetration for measurement of coating hardness. Vacuum. 2009 Feb;83(6):911–20.

140. Chen J, Bull SJ. On the relationship between plastic zone radius and maximum depth during nanoindentation. Surface and Coatings Technology. 2006 Dec;201(7):4289–93.

141. Johnson KL. Contact mechanics. Cambridge [Cambridgeshire]; New York: Cambridge University Press; 1987.

142. Uhure NJ, Fitzpatrick ME, Hainsworth SV. Effect of substrate surface roughness on mechanical properties of diamond-like carbon coatings. Tribology - Materials, Surfaces & Interfaces. 2007 Dec 1;1(4):211–23.

143. Larsson M, Olsson M, Hedenqvist P, Hogmark S. Mechanisms of coating failure as demonstrated by scratch and indentation testing of TiN coated HSS. Surface Engineering. 2000 Oct 1;16(5):436–44.

144. Beake BD, Goodes SR, Shi B. Nanomechanical and nanotribological testing of ultra-thin carbon-based and MoST films for increased MEMS durability. Journal of Physics D: Applied Physics. 2009 Mar 21;42(6):065301.

145. Sackfield A, Hills DA. Some useful results in the tangentially loaded hertzian contact problem. The Journal of Strain Analysis for Engineering Design. 1983 Apr 1;18(2):107–10.

146. Zok FW, Miserez A. Property maps for abrasion resistance of materials. Acta Materialia. 2007 Oct;55(18):6365–71.

147. Arnell RD. The mechanics of the tribology of thin film systems. Surface and Coatings

Technology. 1990 Dec;43-44:674–87.

148. Tsui TY, Pharr GM, Oliver WC, Bhatia CS, White RL, Anders S, et al. Nanoindentation and Nanoscratching of Hard Carbon Coatings for Magnetic Disks. MRS Proceedings [Internet]. 1995 [cited 2012 Oct 16];383. Available from: http://journals.cambridge.org/abstract_S1946427400278196

149. Lin J-F, Fang T-H, Wu C-D, Houng K-H. Nanotribological behavior of diamond surfaces using molecular dynamics with fractal theory and experiments. Current Applied Physics. 2010 Jan;10(1):266–71.

150. Leyland A, Matthews A. On the significance of the H/E ratio in wear control: a nanocomposite coating approach to optimised tribological behaviour. Wear. 2000 Nov;246(1-2):1–11.

151. Leyland A, Matthews A. Design criteria for wear-resistant nanostructured and glassy-metal coatings. Surface and Coatings Technology. 2004 Jan;177-178:317–24.

152. Lin J, Moore JJ, Moerbe WC, Pinkas M, Mishra B, Doll GL, et al. Structure and properties of selected (Cr–Al–N, TiC–C, Cr–B–N) nanostructured tribological coatings. International Journal of Refractory Metals and Hard Materials. 2010 Jan;28(1):2–14.

153. Matthews A, Franklin S, Holmberg K. Tribological coatings: contact mechanisms and selection. Journal of Physics D: Applied Physics. 2007 Sep 21;40(18):5463–75.

154. Shi B, Sullivan JL, Beake BD. An investigation into which factors control the nanotribological behaviour of thin sputtered carbon films. Journal of Physics D: Applied Physics. 2008 Feb 21;41(4):045303.

155. Musil J, Jirout M. Toughness of hard nanostructured ceramic thin films. Surface and Coatings Technology. 2007 Feb;201(9-11):5148–52.

156. Mistry K. et al. 37th Leeds-Lyon Symposium on Tribology. Leeds. 2010;